An organism-wide atlas of hormonal signaling based on the mouse lemur single-cell transcriptome

Shixuan Liu[1, 2, 3], Camille Ezran[2, 3], Michael F. Z. Wang[4], Zhengda Li[1], Kyle Awayan[5], The Tabula Microcebus Consortium[12], Jonathon Z. Long[6, 7], Iwijn De Vlaminck[4], Sheng Wang[8], Jacques Epelbaum[9, 10], Christin Kuo[11], Jeremy Terrien[9], Mark A. Krasnow[2, 3]*, James E. Ferrell, Jr.[1, 2]*

1. Department of Chemical and Systems Biology, Stanford University School of Medicine, Stanford, CA, USA;
2. Department of Biochemistry, Stanford University School of Medicine, Stanford, CA, USA;
3. Howard Hughes Medical Institute, Stanford University School of Medicine, Stanford, CA, USA;
4. Meinig School of Biomedical Engineering, Cornell University, Ithaca, NY, USA;
5. Chan Zuckerberg Biohub, San Francisco, CA, USA;
6. Department of Pathology, Stanford University School of Medicine, Stanford, CA, USA;
7. Stanford ChEM-H, Stanford University, Stanford, Stanford, CA, USA;
8. Paul G. Allen School of Computer Science & Engineering, University of Washington, Seattle, WA, USA;
9. Unité Mécanismes Adaptatifs et Evolution (MECADEV), UMR 7179, CNRS, Museum National d'Histoire Naturelle, Brunoy, France;
10. Unité Mixte de Recherche en Santé 894 INSERM, Centre de Psychiatrie et Neurosciences, Université Paris Descartes, Sorbonne, Paris, France;
11. Department of Pediatrics, Stanford University School of Medicine, Stanford, CA, USA;
12. See the full list of the consortium members and their affiliations at the end of the manuscript.

*Corresponding authors, james.ferrell@stanford.edu, krasnow@stanford.edu

Abstract

Hormones mediate long-range cell communication in multicellular organisms and play vital roles in normal physiology, metabolism, and health. Using the newly-completed organism-wide single cell transcriptional atlas of a non-human primate, the mouse lemur (*Microcebus murinus*), we have systematically identified hormone-producing and -target cells for 84 classes of hormones, and have created a browsable atlas for hormone signaling that reveals previously unreported sites of hormone regulation and species-specific rewiring. Hormone ligands and receptors exhibited cell-type-dependent, stereotypical expression patterns, and their transcriptional profiles faithfully classified the molecular cell type identities, despite their comprising less than 1% of the transcriptome. Cells of similar cell types further display stage, subtype or organ-dependent specification of hormonal signaling, reflecting the precise control of global hormonal regulation. By linking ligand-expressing cells to the cells expressing the corresponding receptor, we constructed an organism-wide map of the hormonal cell communication network. This network was remarkably densely and robustly connected and included a myriad of feedback circuits. Although it includes classical hierarchical circuits (e.g. pituitary → peripheral endocrine gland → diverse cell types), the hormonal network is overall highly distributed without obvious network hubs or axes. Cross-species comparisons among humans, lemurs, and mice suggest that the mouse lemur better models human hormonal signaling, than does the mouse. Hormonal genes show a higher evolutionary conservation between human and lemur vs. human and mouse at both the genomic level (orthology-mapping and sequence identity) and the transcriptional level (cell type expression patterns). This primate hormone atlas provides a powerful resource to facilitate discovery of regulation on an organism-wide scale and at single-cell resolution, complementing the single-site-focused strategy of classical endocrine studies. The network nature of hormone regulation and the principles discovered here further emphasize the importance of a systems approach to understanding hormone regulation.

Introduction

Hormones are chemical messengers that circulate through the bloodstream and control and coordinate functions of both nearby and distant cells. Since the discovery of the first hormone, secretin over a hundred years ago[1], about 100 mammalian hormones have been identified[2]. Over the decades, these hormones have been purified, sequenced, and synthesized, their receptors have been identified, and the intracellular signaling pathways they regulate have been explored[3]. Hormones regulate diverse biological processes ranging from growth and development, reproduction, metabolism, and immune responses, to mood and behavior. Many hormones are also therapeutically significant. For example, the discovery of insulin[4] changed type I diabetes from an inevitably-fatal disease to a manageable one. Likewise, corticosteroids, a class of small molecule adrenal hormones, are used to treat diverse pathological conditions, including the inflammation attendant to COVID-19, where corticosteroids reduce the death rate in severe cases by ~30%[5,6].

The classical endocrine hormones are produced by secretory cells residing in one of the nine endocrine glands. However, it is now clear that other cell types, like fat cells and leukocytes, secrete global regulators into the circulatory system[7]. In addition, some endocrine functions, like menstrual cycles in human females, depend upon interplay and feedback between multiple hormones and cell types[8]. For these reasons, a complete understanding of endocrine physiology requires comprehensive, global approaches. Variations in hormone regulation and function in different species further complicate the situation. Although comparative studies have shown that many hormones are highly conserved across vertebrates[3], the hormone-producing and -receiving cells and their physiological functions are sometimes different[9].

The grey mouse lemur (*Microcebus murinus*) is a small non-human primate with a lifespan of 5-13 years. Because of its small size, rapid reproduction, and close genetic proximity to humans, the mouse lemur is an appealing model organism for studies of primate biology, behavior, aging, and disease[10–14]. As described in detail elsewhere[15,16], we have recently created, using single-cell RNA-sequencing (scRNAseq), a molecular cell atlas of the mouse lemur by profiling mRNA sequences from ~225,000 cells from 27 mouse lemur organs and tissues from 4 individuals (https://tabula-microcebus.ds.czbiohub.org/). Given the ethical concerns of primate studies, tissue samples used in the study were collected opportunistically from aged lemurs. Histopathology was assessed for all organs[17]; many looked histologically normal, although age- or pathology-related changes were detected in certain tissues such as spontaneous tumors in the uteri of two animals and metastasis in the lung of one[16,17]. Presumably, the overall hormone network is still operative in these lemurs, but the age of the animals is both a limitation and an opportunity to study disease-associated changes in hormone profiles. Nevertheless, this extensive, organism-wide dataset provides an unprecedented opportunity to study global hormone regulation at single cell resolution in a non-human primate.

In this study, we present a comprehensive analysis of primate hormone signaling based on the information in the mouse lemur molecular cell atlas[15]. We systematically mapped hormone-producing and target cells for 84 hormone classes, and created a browsable atlas that depicts gene expression of hormone ligands, modulators, and receptors. These systematic analyses detected both canonical and unreported sites of hormone secretion and action. We also analyzed the global expression patterns of hormone ligands and receptors, constructed and characterized

97 an organism-wide cell communication network for hormone signaling, and systematically
98 searched the network for feedback circuits. This analysis revealed a few remarkable principles of
99 hormone signaling and a long list of potentially novel feedback mechanisms. Lastly, we
100 compared hormonal gene expression across humans, lemurs, and mice in selected tissues and cell
101 types, and examined their conservation in expression patterns. This revealed both hormonal
102 genes with a highly conserved expression pattern and ones that show a primate or species-
103 specific expression pattern.

104 The hormone atlas provides a useful resource and a general approach to study hormone
105 regulation and evolution on an organism-wide scale and at single-cell resolution, complementing
106 the more reductionistic strategies typical in classical endocrine studies. The network nature of
107 hormone regulation and principles discovered here further emphasize the importance of a
108 systems approach in understanding hormone regulation.

109

110 Results

111 A comprehensive table of genes involved in the biosynthesis and sensing of human and 112 mouse lemur hormones

113 Although many hormones have been studied for decades, there is not a well-annotated database
114 of hormone ligands, synthases, processing enzymes, and receptors. Therefore, we integrated
115 multiple sources to compile a comprehensive gene table for human hormone signaling (**Table 1**).
116 For the hormone list, we mainly referenced the *Handbook of Hormones*[2], the Wikipedia *List of*
117 *human hormones*, and the *Handbook of Biologically Active Peptides*[18], and added newly
118 discovered hormones including asprosin[19] and the endocrine fibroblast growth factors FGF21,
119 FGF19, and FGF23[20]. To collect the genes involved in hormone production, we assembled the
120 ligand genes for peptide and protein hormones and the hormone synthesis genes for small
121 molecule hormones. Maturation or activation of many hormones requires specific enzymes such
122 as angiotensin-converting enzyme (ACE) for angiotensin, the deiodinases DIO1/2 for thyroid
123 hormones, and prohormone processing enzymes (e.g., PCSK1, PCSK2, CPE) for many peptide
124 hormones[18]. In addition, hormone function may involve endocrine modulators such as IGF
125 binding proteins (IGFBPs) for IGF1 and specific plasma binding proteins for most steroid
126 hormones[21,22]. Accordingly, we added these processing enzymes and modulators for the
127 corresponding hormones. Finally, we curated the hormone receptor genes that are responsible for
128 signaling in the target cells. Most hormones have characterized ligands and receptors, except for
129 endomorphins (tetrapeptides), the ligand gene of which remains unknown. In total, we collected
130 information for 84 groups of hormones and 350 genes, including 102 ligand genes, 41 synthases,
131 33 processing enzymes/modulators, and 174 receptor genes.

132 When a hormone included multiple ligand, receptor, synthase, or processing enzyme genes, we
133 incorporated AND/OR logic gates among the genes to determine if a cell type produces or is
134 targeted by a hormone (**Table 1**). When two or more of the genes were required for signaling,
135 genes were connected by AND (&) gates. For example, amylin receptors are heterodimeric
136 complexes of CALCR and RAMP proteins, and both subunits are required for function; thus,
137 CALCR and RAMP were connected by an AND symbol. Similarly, AND gates were applied

among hormone synthases that catalyze different steps, and between hormone ligands and the corresponding processing enzymes. On the other hand, OR (|) gates were applied when only one of the genes is required for function. For example, there are nine adrenergic receptor genes, all of which function independently and therefore were linked by OR gates.

We next looked up the mouse lemur orthologs of the human hormonal genes in the most up-to-date mouse lemur genome assembly (Mmur_3.0) with both NCBI and Ensembl ortholog databases (**Table 2**). Almost all (98.9%, 346/350) of the human hormone-related genes were annotated in the mouse lemur genome, and most (98.0%, 339/346) were one-to-one mappings; 7 were many-to-one. The four genes without lemur orthologs (LHB, GALP, INSL4, and DRD5) and 7 many-to-one mappings could have resulted from incomplete annotation of the mouse lemur genome. For one lemur-unannotated gene LHB (luteinizing hormone beta subunit), we identified by sequence homology[23] a candidate LHB gene region that has high sequence similarity and the conserved neighboring gene (RUVBL2) as human LHB[24] and was selectively expressed in the expected cells (pituitary gonadotrophs) (**Fig. S1**-luteinizing hormone). We concluded that the identified region is likely the mouse lemur LHB gene and included it in follow-up analyses. Thus, at least 347/350 (99.1%), and possibly all, of the human hormonal genes are present in the mouse lemur. For comparison, the mouse genome lacks orthologs for six genes (98.3% present, 344/350), five of which are known pseudogene or have been lost in the mouse genome (GNRH2, MCHR2, MLN, MLNR, NPBWR2 (Gm14489)) (**Table 2**). In addition, 14 human-mouse orthologs are one-to-many (6), many-to-one (4), or many-to-many (4) mappings, suggesting gene family expansions or contractions in mice or humans. The percentages of human hormonal orthologs present in lemur or mouse genomes were higher than the percentage of all protein-coding genes (PCGs) (>98.9% vs. 89.5% in the mouse lemur genome, and 98.3% vs. 89.8% in the mouse genome). Most (85.8%) human hormone-related proteins were more similar in sequence to their lemur orthologs than to their mouse homologs (**Fig. S2a**). These findings underscore the close similarity between human and lemur hormonal genes.

Organism-wide identification of hormone-producing and target cells

We systematically identified the source and target cells for each hormone by examining the expression of the hormone ligand, synthase, and receptor genes across 739 lemur cell types from 27 different tissues profiled by 10x scRNAseq[15]. Source cells were defined as cell types that expressed above-threshold levels of the ligand (for protein/peptide hormones) or synthase(s) (for small molecule hormones) plus any necessary modulator genes. Target cells were those that expressed hormone receptor genes. We generated a browsable set of figures and a web portal (https://tabula-microcebus.ds.czbiohub.org/hormone-atlas) that depict the global expression profiles of the hormonal genes (**Fig. S1**, **Fig. S3**, **Table 3**). **Fig. 1a-g** shows the expression of four representative examples of hormones (in red) and their receptor(s) (in blue) in the identified cell types across the seven, color-coded cell compartments (epithelial, endothelial, stromal, neural, germ, lymphoid and myeloid cells). This analysis identified many canonical sites of hormone secretion and targets, affirming the validity of the single-cell transcriptomic measurements and analysis approach. The analysis also revealed many less-recognized or unreported hormone source/target cells and interesting global patterns of hormone signaling.

181 Below, we highlight a few examples of well-known, lesser-known, and previously unknown
182 sources and target cells. We also showcase examples where hormonal expression is unique in the
183 mouse lemur versus mice or humans.

184 **Prolactin (PRL).** Prolactin is a classical endocrine hormone[25] secreted by pituitary lactotrophs.
185 In addition to its milk-promoting effect in females, PRL also plays pleiotropic roles in both
186 sexes[2]. These roles include regulation of water and electrolyte balance in the kidney, and control
187 of skin cell proliferation and hair/feather growth and shedding[26]. Prolactin also plays a major role
188 in energy homeostasis by regulating cell growth and metabolism in the liver, adipose tissues, and
189 pancreas in both sexes[27], and may be involved in the immune response[28]. These sex-non-specific
190 functions are conserved, not just among milk-producing mammals, but across all vertebrates.

191 As expected, prolactin transcripts were selectively expressed in the lactotrophs of the lemur
192 pituitary gland, and were not detected in other tissues (**Fig. 1a-g, Fig. S1**-prolactin). The
193 prolactin receptor (PRLR) was found in both male and female lemurs in the expected cell types,
194 including kidney nephron tubule cells, skin epithelial cells, pancreatic ductal and acinar cells,
195 hepatocytes, intestinal epithelial cells, adipocytes, reticular cells, plasma cells, choroid plexus
196 cells, and the neighboring TSH-secreting thyrotrophs and FSH/LH-secreting gonadotrophs in the
197 pituitary gland (**Fig. 1a-g, Fig. S1**-prolactin). Thus, scRNAseq data confirm that prolactin
198 signaling is similar in mouse lemurs and other animals.

199 **Adiponectin (ADIPOQ) and leptin (LEP).** Mouse lemurs undergo dramatic seasonal changes
200 in body weight and fat reserves[29–31] and therefore may experience seasonally-varying levels of
201 adipokines. Adiponectin and leptin are two important metabolic hormones secreted by
202 adipocytes[32,33]. Although adipocytes were originally regarded only as nutrient storage cells, it is
203 now clear that they also serve an endocrine role[34]. Surprisingly, leptin transcripts were almost
204 undetectable in the adipocytes captured in the atlas (see discussion in the accompanying
205 manuscript[16]) (**Fig. S1**-leptin).

206 However, adiponectin was abundantly and specifically expressed in mouse lemur adipocytes
207 captured from multiple tissues, including four adipose depots (subcutaneous, mesenteric,
208 interscapular brown, and perigonadal), as well as kidney, limb muscle, pancreas, and bone (**Fig.**
209 **1a-g**, **Fig. S1**-adiponectin). Both UCP1-low white-like and UCP1-high brown-like adipocytes
210 highly expressed ADIPOQ.

211 Previous research has characterized tissue-specific functions of adiponectin in the liver,
212 pancreas, skeletal muscle, endothelial cells, macrophages, and adipocytes[35]. While we indeed
213 observed expression of the adiponectin receptor ADIPOR1 in these tissues in the mouse lemur,
214 we also found ADIPOR1 to be abundantly expressed in almost all lemur cell types (**Fig. 1a-g**).
215 Similar ubiquitous expression of ADIPOR1 has been found in humans and mice (**Fig. S12**).
216 These results suggest that adiponectin exerts an organism-wide effect through ADIPOR1.

217 In comparison, ADIPOR2, the other adiponectin receptor, was expressed more selectively, most
218 notably in the male germ cells and adipocytes (**Fig. 1a-g**). Interestingly, the lemur expression
219 pattern of ADIPOR2 differed from that of the human and mouse in which ADIPOR2 was highly
220 expressed in the liver and only lowly expressed in the testis[36] (**Fig. S12**). Alveolar macrophages
221 from the mice, but not humans or lemurs, also showed high ADIPOR2 expression (**Fig. S12**),
222 suggesting differential ADIPOR2 effects across the three species.

223 **Motilin (MLN).** Motilin is canonically considered a gastrointestinal hormone that is secreted by
224 enteroendocrine cells and regulates gastrointestinal smooth muscle movement[18]. However,
225 rodents have lost both the motilin and the motilin receptor genes in evolution[37] (**Table 2**). The
226 lack of motilin signaling in rodent models has hampered progress on further characterizing
227 motilin function as well as the development of motilin agonists for the treatment of
228 gastroparesis[38]. Consistent with the canonical view, we observed motilin expression in lemur
229 enteroendocrine cells in the small intestine but not colon (**Fig. 1a-g**). However, we also observed
230 a broad range of other motilin-expressing cell types, including kidney nephron tubule cells,
231 chemosensory tuft cells from both the airway (lung and trachea) and small intestine, certain brain
232 neurons, adipocytes (higher in UCP1-high brown-like adipocytes than in white-like adipocytes),
233 mesothelial cells, and the majority of the CD4+CD8-CCL5- helper T cells (**Fig. 1a-g**, **Fig. S1**-
234 motilin). The receptor was found to be most highly expressed in pancreatic delta cells and
235 several epithelial cell types of the skin (e.g., sweat gland cells). Together, this expression pattern
236 suggests that motilin is involved in a diverse array of mouse lemur physiological functions in
237 addition to the regulation of gut motility.

238 Motilin had been detected in the human brain[18], as is the case in the lemur (**Fig. 1d**), but was not
239 previously known to be expressed in the kidney nephron tubule cells. Therefore, we performed
240 RNAscope, a single molecule mRNA fluorescent in situ hybridization (smFISH) assay to further
241 test whether motilin is expressed in the mouse lemur kidney. This revealed abundant motilin
242 transcripts in the epithelial cells of the proximal tubules but not in the glomerulus, which are
243 mainly composed of podocytes and glomerular capillary cells (**Fig. 1h-j**). This supports the
244 validity of the scRNAseq results (**Fig. 1a-g**). It will be interesting to examine, in future studies,
245 motilin expression in other uncanonical cell types outside the intestine, explore what functions
246 motilin plays in these cells, and whether their expression is conserved in humans.

247 **Resistin (RETN).** Resistin is a phylogenetically recent hormone, present only in mammals[2]. It is
248 expressed mainly by adipocytes in mice but by macrophages, monocytes, and neutrophils in
249 humans[39,40]. In the mouse lemur, we found that resistin is highly expressed in macrophages,
250 monocytes, and neutrophils, and nearly absent from adipocytes (**Fig. 1a-g, Fig. S1**-resistin), as it
251 is in humans (**Fig. S12**). Interestingly, resistin is also highly expressed in many of the vascular
252 endothelial cell types and in metastatic uterine tumor cells, suggesting additional sources for this
253 hormone in mouse lemurs (**Fig. S12**).

254 **Prohormone processing enzymes.** Prohormone processing enzymes are required for the
255 maturation of many peptide hormones, including insulin, adrenocorticotropic hormone (ACTH),
256 gastric inhibitory polypeptide (GIP), and somatostatin[18]. The required processing enzymes have
257 been identified for some but not all hormones[41,42]. In this study, we considered both the ligand
258 and the known or suggested processing enzymes when determining if a cell type produces a
259 hormone. Selective expression of the processing enzymes can help distinguish hormones that
260 share the same precursor gene. For example, proglucagon (GCG) is the precursor for both
261 glucagon and glucagon-like peptide-1 (GLP-1). GCG was expressed in both pancreatic α cells
262 and intestinal enteroendocrine cells, but the two cell types expressed different processing
263 enzymes: α cells expressed only PCSK2 which is required for glucagon synthesis, and
264 enteroendocrine cells expressed only PCSK1 which is required for GLP-1 synthesis (**Fig. S1**-
265 glucagon). Thus, as is the case in mice and humans[43], α cells are sources of glucagon and
266 enteroendocrine cells are sources of GLP-1 in the mouse lemur.

Interestingly, we noticed that some cell types in the mouse lemur transcribed prohormone genes without expressing the respective processing enzymes. For example, proopiomelanocortin (POMC), which is the precursor of ACTH, melanocyte-stimulating hormone (MSH), β-endorphin, and lipotropin, is first processed by PCSK1[44]. As expected, ACTH-secreting corticotrophs expressed both POMC and the necessary processing enzymes, but lemur male germ cells expressed abundant POMC without detectable PCSK1 transcripts (**Fig. S1**-proopiomelanocortin-derived hormones). Similarly, human and mouse male germ cells expressed POMC but no PCSK1 (**Fig. S12**). In addition, lemur male germ cells expressed GIP, which also requires PCSK1 processing; the intestinal and airway tuft cells expressed renin (REN) without the necessary PCSK1 (**Fig. S1**). These results suggest several possible hypotheses: different peptidases are involved, the prohormone transcripts are not translated, the prohormone proteins may function without proteolysis, or the processing enzymes may be expressed below detection levels in the sampled cells.

Plasma binding proteins. Plasma binding proteins are not only passive hormone transporters, but can affect hormone functions by modulating hormone half-life and levels of free, active hormones accessible to target cells. Other plasma binding proteins have been reported to potentiate the binding of hormones to their targets[45].

Steroid and thyroid hormones are transported in the blood by plasma binding proteins of the albumin family. While serum albumin (ALB) binds steroids with low specificity and affinity, four other albumins bind these hormones with high specificity and nanomolar affinity, including sex hormone binding globulin (SHBG) for androgens and estrogens, vitamin D binding protein (GC) for vitamin D, SERPINA6 for cortisol and progesterone, and SERPINA7 for thyroid hormones[21,22] (**Table 1**). Consistent with the notion that these hormone-binding albumins are produced in the liver[21,22], we identified specific expressions of SHBG, SERPINA6, and SERPINA7 in the lemur hepatocytes, and interestingly higher levels in the CPN2hi versus the CPN2lo hepatocyte subtypes (**Fig. 3f, Fig. S1**). GC was also expressed in the lemur hepatocytes with a higher level in the CPN2hi subtype; however, we also detected notable expression in pancreatic endocrine, ductal, enteroendocrine cells, and cholangiocytes. These novel sources may contribute to the circulating pool of GC or may have local or exocrine effects, such as regulating intestinal vitamin-D absorption[46].

In addition, peptide hormones IGF1 and activin are known to be bound by IGF binding proteins (IGFBPs) and FST respectively. In contrast to albumins, IGFBPs and FST were expressed by multiple distinct cell types and showed high cell type variability (**Fig. S1**).

In summary, we have depicted the organism-wide, single-cell expression patterns for hormones, synthases, hormone modulators, and receptors from 84 classes of hormones, and have systematically identified their sources and targets (**Fig. S1**). This global analysis detected canonical cell types underlying hormone secretion and target functions while also revealing previously unreported source and target cells. This organism-wide single-cell hormone atlas should facilitate the systematic study of hormone regulation in an unbiased, global manner, paving the way for the discovery of novel regulation and evolution of hormone signaling.

309 **Hormonal gene expression is highly cell type specific**

310 Next, we clustered mouse lemur cell types based on the transcriptional profiles of the hormonal
311 genes (**Fig. 2a-b**). We identified 74 clusters and summarized the hormones and hormone
312 receptors that were expressed by each cluster (**Table 4**). We noted that cells of the same type
313 almost always clustered closely irrespective of their tissue of origin, or of the sex or identity of
314 the sampled individual, whereas different cell types were well-separated (**Fig. 2b**, **Fig. S4**, **Table**
315 **4**). For example, all lymphatic endothelial cells clustered closely and showed characteristic IGF1
316 expression despite their coming from nine different tissues and four individuals (cluster 45, **Fig.**
317 **3b**, **Fig. S1**, **Table 4**). Mesothelial cells sampled from eight visceral organs formed a cluster
318 distant from other stromal cells and showed distinctive expression of NPR1, CFB, PTGIS,
319 ITGB3, and PNMT (cluster 35, **Fig. 2b**, **Fig. S1**, **Table 4**). Although there are only ~300
320 hormonal genes, ~1% of all detected genes, their expression pattern proved to be indicative of
321 cell type identity regardless of tissue source or location.

322 To further test this conclusion, we compared cell type clustering by either the hormonal genes
323 (~300 genes) or the full transcriptome (>30,000 genes). To visualize the results, we projected the
324 high-dimensional transcriptional data into two-dimensional cell type maps by uniform manifold
325 approximation and projection (UMAP), which illustrate cell type similarity based on the selected
326 genes. The cell type UMAPs by either the hormonal genes (~300 genes) (**Fig. 2b**) or the full
327 transcriptome (**Fig. S5a**) were remarkably similar (see **Fig. S7c** for comparison). The cell type
328 pairwise distances defined by hormonal genes versus the full transcriptome were also positively
329 correlated, with a Pearson correlation coefficient (*r*) of 0.70 (**Fig. S5b**). There were nevertheless
330 minor differences between the two UMAPs. For example, airway and intestinal tuft cells are both
331 chemosensory but are involved in different functions[47]. In the space of hormonal genes, tuft cells
332 from different tissues formed one cluster (cluster 58) with distinctive expression of renin (REN),
333 cyclooxygenase 1 (PTGS1), arachidonate 5-lipoxygenase-activating protein (ALOX5AP,
334 required for leukotriene production), and motilin (MLN) (**Fig. 2b**, **Fig. S1**, **Table 4**). However,
335 in the space of all genes, the lung, trachea, and intestinal tuft cells were separated from each
336 other (labeled as 58A*, 58B*, and 58C* in **Fig. S3**). Another notable exception was skin
337 melanocytes, which clustered with oligodendrocytes (cluster 31) by only the hormone-related
338 genes (**Fig. 2b**) but clustered more closely with skin epithelial cell types in the space of all genes
339 (**Fig. S5a**, oligodendrocytes and melanocytes labeled as 31A and 31B, respectively). Thus, cell
340 types were overall similarly clustered by the hormonal genes or the full transcriptomes, the
341 exceptions showcase rare examples of converged hormonal signaling in distant cell types.

342 We then assessed how well hormonal gene expression discriminates among different cell types
343 compared to all genes or random sets of PCGs (**Fig. 2c-e, Fig. S5b-e**). As a gold standard, we
344 used the cell annotations described in the accompanying manuscript[15], which are based on
345 expression of canonical cell markers and iterative clustering with highly variable genes. We then
346 scored how well the cell type pairwise transcriptional distances for these different sets of genes
347 correlated with a cell annotation-based distance (**Fig. S6c**). This annotation-based distance is
348 defined as an integer between 0 and 3: 0 when cell types were annotated with identical names but
349 from different tissues, 1 when the cell annotation names were different but classical histological
350 assignments (Cell Ontology[48]) were identical (i.e., different molecular subtypes), 2 when
351 classical Cell Ontologies were different but cell types were from the same compartment (e.g.,
352 both were epithelial), and 3 if cells were different cell types and from different compartments

353 (e.g., endothelial vs. stromal). The pairwise transcriptional distances based on the hormonal
354 genes alone correlated with this annotation-based distance better than that based on the full
355 transcriptome ($r = 0.51$ vs. $r = 0.30$) (**Fig. 2c-e**). Likewise, the hormonal-based distances
356 correlated better than distances from random sets of PCGs ($r = 0.51$ vs. $r = 0.29 \pm 0.03$, mean ±
357 S.D., $n = 100$) (**Fig. 2e**). This appeared to be because hormonal genes were more variably
358 expressed across different cell types than average PCGs (**Fig. 2f**); although the full transcriptome
359 contains more information, the discriminative power is diluted by the large number of low-
360 specificity genes. In support of this idea, when sets of randomly selected PCGs with similar
361 expression variability (dispersion) as hormonal genes were used, the correlation coefficients
362 were similar to that of the hormonal genes (**Fig. 2e**).

363 As a further test, we used a continuous Cell Ontology[48]-based metric as the benchmark (**Fig.
364 S5e**). This metric was calculated as the mean of the Cell Ontology embedding-based distances
365 from the Cell Ontology graph and the text-based distances from the text descriptions of the Cell
366 Ontology terms[49]. The hormonal-based cell type pairwise distances correlated better with this
367 Cell Ontology-based distance than those based on all genes or random sets of PCGs ($r = 0.45$ vs.
368 $r = 0.23$, 0.22 ± 0.04) (**Fig. S5e**), as was the case with the discrete annotation-based distance.
369 Thus, by both measures, hormonal genes do an unusually good job of predicting cell identity.

370 Finally, we examined if the expression of hormone ligands or receptors alone could distinguish
371 cell types. Interestingly, for most cell type clusters, hormone ligands or receptors alone classified
372 cell types similarly (**Fig. S7a-c**). This suggests that most cell types have stereotypical expression
373 of genes involved in both incoming and outgoing hormonal signaling. A small fraction of
374 clusters were mainly defined by only the ligands or receptors. For example, clusters of pituitary
375 neuroendocrine cells (cluster 7) and tuft cells (cluster 21) were distinguished mainly by hormone
376 ligands, whereas clusters of the skeletal muscle stem cells (cluster 17) and lung endothelial cells
377 (cluster 51) were mostly based on differences in hormone receptor expression (**Fig. S7c**).

378 In summary, we found that cells generally show stereotypical and cell-type-specific expression
379 of hormone ligands and receptors. Thus, hormone secretion and sensing essentially labels the
380 identity of the cells.

381

382 **Specific hormonal gene expression in cell subtypes**

383 Hormonal expression could sometimes distinguish cell subtypes that are at different
384 developmental stages, from different locations within an organ, from different organs, or from
385 normal vs. pathological tissue. Below we highlight several such examples (**Fig. 3**).

386 **Spermatogenesis.** Spermatogenesis occurs continuously and asynchronously in the male testis[50].
387 Thus, sampling the testis at one fixed time point can capture snapshots of the entire process. The
388 atlas includes seven sperm and sperm progenitor cell types that are at different spermatogenesis
389 stages as indicated by the expression of known stage markers[15]. The seven cell types fall into
390 three major stages: the undifferentiated spermatogonia, the spermatocytes (which undergo
391 meiosis), and the haploid spermatids that elongate and form mature sperms. Interestingly, these
392 cells exhibited stage-dependent hormone signaling, with over 50 differentially expressed
393 hormone ligands, enzymes, and receptors (**Fig. 3a**). Previous studies on spermatogenesis have

394 mainly focused on testosterone and on the supporting cells rather than sperms and sperm
395 progenitors[51,52]. The present data suggest that sperms and sperm progenitor cells are not only
396 differentially regulated by a variety of hormones but may also secrete a changing array of
397 signaling molecules as they mature. The data also clarify some incompletely understood aspects
398 of sperm regulation. For example, progesterone was known to activate a sperm-specific calcium
399 channel prior fertilization to induce Ca^{2+} influx, but the receptor(s) responsible for this effect
400 were unidentified[53]. The present data show that two non-classical progesterone membrane
401 receptors (PAQR5/9) are highly expressed in the lemur spermatids and therefore may mediate
402 the process (**Fig. 3a**). Interestingly, two additional membrane progesterone receptors (PAQR8,
403 PGRMC1) were specifically expressed in the undifferentiated spermatogonia (**Fig. 3a**),
404 suggesting that progesterone may also regulate early spermatogenesis[54]. In addition, insulin-like
405 factor 6 (INSL6), a member of the secretory relaxin family, was selectively expressed in the
406 lemur spermatocytes (**Fig. 3a**). Supporting a function in these cells, knockout of INSL6 arrests
407 spermatogenesis at late meiotic prophase in mice[55]. This analysis suggests that sperms and sperm
408 progenitor cells may directly communicate with other cells via hormones that regulate
409 spermatogenesis and sperm functions. Cross-species comparison among human, lemur, and
410 mouse germ cells identified many of the spermatogonia hormonal genes that exhibited conserved
411 dynamics among all three species, and others showing primate/species-specific expression
412 dynamics (**Fig. 7e-g**, **Fig. S13a-b**, and more discussion below).

413 **Kidney nephron and vasa recta.** Although discrete cell types were common in the mouse lemur
414 cell atlas, we noted several cell types that displayed a continuum of gene expression, including
415 the epithelial cells of the nephron and the endothelium of the vasa recta, the blood vessels that
416 supply the renal medulla[15] (**Fig. 3d**). Interestingly, these cells also displayed gradients of
417 hormone signaling along their spatial axes (**Fig. 3b-e**).

418 Nephrons are single-cell layered, one-directional tubules that serve as the structural and
419 functional units of the kidney. We identified a large number of hormonal genes specific to
420 different sections of the nephron epithelium (**Fig. 3b-c**). Some of these were receptors for
421 hormones known to target specific nephron sections to regulate urine formation. For example,
422 the antidiuretic vasopressin specifically promotes water reabsorption in the collecting duct
423 principal cells[2], and indeed, the vasopressin receptor AVPR2 was expressed exclusively in the
424 lemur collecting duct principal cells. Interestingly, the collecting duct intercalated cells
425 expressed another vasopressin receptor, AVPR1A (**Fig. 3b**), which has been recently reported to
426 mediate the regulation of acid homeostasis by vasopressin[56]. Although the kidney epithelium is
427 not commonly considered to be an endocrine tissue, many hormone ligands/synthases were
428 expressed in different nephron sections, including angiotensin (AGT), adrenomedullin 2
429 (ADM2), motilin (MLN), and neuropeptide Y (NPY). Consistent with the scRNAseq results,
430 smFISH by RNAscope confirmed expression of MLN and AGT in the nephron proximal tubule
431 cells but not in the podocytes and capillary cells of the glomerulus (**Fig. 1h-j**). Taken together,
432 these data suggest that nephron epithelium may play important roles in hormone production in
433 addition to urine formation.

434 The vasa recta aligns parallel to the nephron tubules in the kidney medulla (**Fig. 3c**) and
435 functions collaboratively with the nephrons in urine formation[57]. The vasa recta cells also
436 exhibited a gradual shift in hormonal signaling along its arteriole-to-venule spatial gradient. (**Fig.
437 3d**). **Fig. 3e** shows the hormonal genes that are significantly differentially expressed along the

438 vasa recta axis. Notably, several genes involved in IGF signaling were differentially expressed:
439 IGF1, which was highly expressed in the lemur lymphatic endothelial cells but almost absent
440 from other vascular endothelial types (**Fig. S1**, **Fig. 3h**), was highly expressed at the lymphatic-
441 like[58] venule end of the vasa recta (**Fig. 3e**); in contrast, IGF2 and IGF1R were more highly
442 expressed in the arteriole end; and four IGFBPs (IGFBP3-6), which modulate IGF signaling, also
443 exhibited different spatial patterns (**Fig. 3e**). This spatial organization of IGF signaling may be
444 evolutionarily conserved, as a recent study on mouse kidney vasculature development shows a
445 similar pattern of IGF1 expression in the mouse vasa recta[59].

446 **Hepatocyte subtypes.** The mouse lemur cell atlas identified multiple novel molecular subtypes
447 of known cell types. For example, the liver hepatocytes of the mouse lemur clustered into two
448 discrete subtypes, the CPN2 high and CPN2 low hepatocytes. They differed significantly by total
449 transcript count, and may correspond to the small diploid and large polyploid hepatocytes[15].
450 These subtypes were found in both females and males (**Fig. S6**), and seems to be independent of
451 the known zonal heterogeneity[15]. Interestingly, a number of hormone-related genes were
452 differentially expressed (**Fig. 3f**). Hormones including glucagon, androgens, and prolactin appear
453 to selectively target the CPN2hi hepatocytes as indicated by differential expression of the
454 corresponding receptors (GCGR, AR, PRLR). In addition, angiotensin (AGT), a canonical
455 hepatic hormone, was expressed at a much higher level in the CPN2hi hepatocytes, whereas no
456 subtype difference was detected in the expression of hepcidin (HAMP) or IGF1, two other
457 hormones abundantly produced by the liver.

458 We also identified similar hepatocytes in humans and mice and many of the subtype-specific
459 hormonal expressions were conserved (**Fig. S13c-d**). The hepatocyte subtypes and the subtype
460 specific hormonal expression were found in both male and female lemurs studied (**Fig. S8**), so
461 are not attributable to sex-specific differences in hormone regulation. However, there may exist
462 other sex-dependent differences in hormone regulation of hepatocytes as observed in other
463 species.

464 The liver is a central organ of metabolism and plays important roles in hormonal regulation. The
465 detected heterogeneity in hormone signaling suggests potentially important functional
466 divergence between the two subtypes. A deeper understanding of the mechanisms and regulation
467 of hepatocyte hormone heterogeneity would be particularly relevant to the study of mouse lemur-
468 specific physiology, like hibernation/torpor and seasonal body weight changes[30].

469 **Metastatic vs. primary tumor cells.** The atlas also contains diseased cells, including potential
470 primary endometrial tumor cells in the uterus (MUC16+ non-ciliated uterus epithelial cells) and
471 lung metastatic cells of endometrial cancer origin, as assessed by tumor gene signatures and
472 histology (see accompanying manuscripts[15,16]). Both tumor cell types clustered with the non-
473 tumor epithelial cells of the uterus[16] and shared characteristic expression of the oxytocin receptor
474 (OXTR) and the inhibin beta B subunit (INHBB) (**Fig. 3g**, **Fig. S1**, **Table 4**), suggesting that the
475 lung metastatic tumor originated from cells resembling the primary MUC16+ uterine tumor cells.
476 Certain aspects of hormone signaling seem to have been altered in the metastatic tumor (**Fig. 3g**).
477 Notably, the tumor cells showed a loss of estrogen receptors (ESR1), a change associated with
478 high grade and advanced stage endometrial cancers in humans[60] and more often reported in high
479 mortality type 2 human endometrial cancers[61].

480 Interestingly, the metastatic tumor cells also acquired new abilities in hormone production. For
481 example, elevated expression of prostaglandin E2 synthase (PTGES2) was present in metastatic
482 cells (**Fig. 3g**). PGE2 has been suggested to be a tumorigenic factor in many cancers[62]. A recent
483 study identified that the PGE2 synthase PTGES2 was elevated in human endometrial cancer
484 tissues and found that PGE2 promotes cell proliferation and invasion in *in vitro* cell assays[63].
485 Resistin was also found to be highly expressed in the metastatic cells (**Fig. 3g**). Resistin has been
486 reported to promote invasiveness of breast cancer cells *in vitro*[64]. Thus, endometrial tumors may
487 utilize autocrine resistin signaling to promote metastasis. The shift in hormone signaling
488 identified in the lemur metastatic endometrial tumor is similar overall to that reported in the
489 human. This suggests that the shifts in hormone signaling may be an important step in tumor
490 development and metastasis. Mouse lemurs may serve as a useful animal model to study human
491 cancers that are not well modeled in mice such as endometrial cancers[16].

492 **Vascular endothelium.** While hormonal gene expression is generally determined more by cell
493 type than by organ of origin, lung and brain vascular endothelial cells from arteries, veins, and
494 capillaries all exhibited unique organ-specific hormonal signatures (**Fig. 3h**).

495 Lung endothelial cells expressed higher levels of the hormone receptors VIPR1, CALCRL, and
496 RAMP1 (**Fig. 3h**) than did endothelial cells from other organs. VIPR1 is a receptor for
497 vasoactive intestinal peptide (VIP), a strong bronchodilator and one of the most abundant
498 signaling peptides in the lung[65]. Lung -specific VIPR1 expression was also observed in human
499 but not mouse endothelial cells (**Fig. S13e**, see more discussion below). RAMP1 forms
500 heterodimeric receptors with CALCR or CALCRL that are regulated by several hormone ligands
501 including CGRP, adrenomedullin, amylin, and calcitonin, all of which have been reported to
502 have vasodilatory effects[2]. Interestingly, RAMP1 is expressed in the lung endothelium of the
503 mouse lemur but not in mice or humans, whereas RAMP2 is expressed in all three species and
504 RAMP3 is only highly expressed in humans (**Fig. S13e**, see more discussion below). These
505 results suggest that lung vascular endothelium is a unique hormonal target in comparison to
506 vasculature elsewhere, possibly because of the distinctive nature of the pulmonary circulation
507 (e.g., high volume, low pressure) compared to the systemic circulation.

508 In contrast, brain vascular endothelium was found to express higher levels of a few hormone
509 ligands/synthases. Endothelin-3 (ET-3), a member of the vasoconstricting endothelin family, was
510 selectively expressed in the brain vascular endothelium (**Fig. 3h**). ET-3 peptide has been
511 detected at various brain locations in rodents, but it remained unsettled what cells secreted the
512 peptide and what physiological role it played[66]. Our results suggest that ET-3 is synthesized by
513 the endothelial cells in the brain, which could target the nearby EDNRB-expressing SLC7A10+
514 astrocytes and the EDNRA-expressing brain vascular smooth muscle cells and pericytes (**Fig.
515 S1**-endothelin). Additionally, the brain endothelium also expressed high levels of PTGES and
516 PTGS2/COX-2 (**Fig. 3h**), which are the synthases of prostaglandin E2 (PGE2). PGE2 has been
517 suggested to regulate inflammation-induced fever in mice[67,68]. Interestingly, brain endothelial
518 cells also selectively lacked expression of IGFBP4, which was abundantly expressed in the
519 endothelium of all other tissues in lemurs (**Fig. 3h**), as in humans and mice (**Fig. S12**).

520 These organ-specific hormone signatures were expressed at higher levels in endothelial cells than
521 other cell types from the same organ (**Fig. S1**). Thus, it is unlikely that they resulted from cross-
522 contamination (signal spreading). Altogether, lung and brain endothelial cells showcase rare

523 examples of organ-specific (and cell type-independent) hormonal signaling, which may underlie
524 organ-specific control of the blood flow.

525 In summary, we have highlighted five examples where closely related cells show detailed
526 specification in their hormone signaling. These examples demonstrate the precise and specialized
527 control of hormonal regulation across different cell types and/or organs.

528

529 **The hormonal cell communication network is densely connected**

530 Long-range hormonal signaling connects both nearby and distant cells through the bloodstream
531 and enables cross-organ communication. By linking the source cells that produce a hormone
532 ligand to the target cells that express the corresponding receptor, we constructed a global cell
533 communication network for mouse lemur hormone signaling (**Fig. 4a**). Nodes of the network are
534 cell types and edges are directed from hormone source to target cells.

535 The hormone network was remarkably densely connected; 54% of all possible directed edges
536 were found to be present. In fact, in the graphical depiction of the network (**Fig. 4a**), individual
537 edges are hardly distinguishable because the edges are so dense. The density of the hormone
538 network is comparable to that of the cytokine network[69], and much higher than the densities of
539 other characterized biological networks (**Fig. 4b**). For example, the network densities of the
540 yeast, fly, and human protein-protein interaction networks are all estimated to be less than 1%[70–
541 72], and the yeast genetic interaction network density is ~3%[73]. The average degree of a node in
542 the hormonal network was also exceptionally high (**Fig. 4c**), emphasizing that the average cell
543 communicates with a large number of different cell types. The dense connections between cell
544 types by hormonal regulation are also highly robust: 72% of all existing edges are connected by
545 more than one ligand-receptor pair, and the network maintains high density connection when
546 randomly removing 10% of the ligand-receptor pairs (**Fig. S9a**).

547 The hormone network has a high density because most cell types express multiple hormone
548 ligands and receptors (**Fig. 4d**). On average, cell types expressed 18.3 ± 8.2 (mean ± S.D.)
549 receptors or receptor complexes. In comparison, fewer hormone ligands were expressed (2.8 ±
550 2.6). Only a few cell types expressed 10 or more hormone ligands, and 37.6% of cell types
551 expressed a single ligand or no ligand. This indicates that cells in general respond to more
552 hormones than they produce.

553 Classical endocrine hormone-producing cells such as enteroendocrine cells, pancreatic endocrine
554 cells, hepatocytes, and neurons were among cells secreting the largest numbers of hormone
555 ligands (**Fig. S10**). Unexpectedly, many stromal cells such as fibroblasts also secreted a large
556 number of ligands, including IGF1, adrenomedullin, angiotensin, and asprosin (**Fig. S10**, **Fig.
557 S1**). Stromal cells were also particularly rich in the expression of hormone receptors, making
558 them among the most connected cell types in the hormone network (as indicated by their high
559 "hubs" and "betweenness" scores, **Fig. S10**). Given the abundance of stromal cells across various
560 tissues, these results suggest stromal cells must play vital roles in endocrine regulation.

561 Canonically, hormones are believed to be regulated in a hierarchical fashion. Among the most
562 well-known examples are the neuroendocrine cell types of the anterior pituitary—corticotrophs,

563 thyrotrophs, gonadotrophs, lactotrophs, and somatotrophs. These cells are components of
564 regulatory cascades, receiving regulatory signals from one or a few hormones produced in the
565 hypothalamus and in turn producing one or a few hormones to regulate a peripheral endocrine
566 gland. Yet these cells were found to express numerous receptors, ranging from 18 (corticotrophs)
567 to 30 (somatotrophs) (**Table 5**). These cells appeared to be regulated by growth factors,
568 neuropeptides, neurotransmitters (e.g., dopamine), classical hypothalamic hormones. Likewise,
569 they were found to produce hormones in addition to the classical hormones (**Table 5**). For
570 example, corticotrophs expressed galanin (GAL), gastrin (GAS), and cortistatin (CORT), as well
571 as the ACTH precursor (POMC) and its processing enzymes PCSK1, PCSK2, and CPE.

572 Taken together, this analysis suggests that virtually all cell types across the body are extensively
573 engaged in cell communication via hormonal signaling and that the connections are likely
574 evolutionarily robust to random mutations that disturb hormone regulation. The dense connection
575 of the network results in a large number of highly connected nodes and no obvious network cores
576 (**Fig. 4a**, **Fig. S10**). This differs from the commonly studied scale-free networks, which are
577 dominated by a small number of highly-connected hub nodes[74]. Studies on hormone regulation
578 usually focus on one specific site of secretion and/or target; our analysis emphasizes the
579 importance of a systems view in understanding hormone regulation.

580

581 **A small number of hormones are global regulators**

582 We next examined properties of the hormone network edges. In contrast to the protein-protein
583 interaction network and the genetic interaction network, the edges of the hormone
584 communication network are directional and can be distinguished into different types according to
585 the specific ligand-receptor pairing. The hormone network included 350 different edge types that
586 are selected pairings of 129 ligands and 175 receptors.

587 Some ligands and receptors were expressed in highly specific cell types while others were more
588 broadly expressed. We therefore quantified for each ligand or receptor a generality score to
589 evaluate the range of its expression across different cell types in the atlas (**Fig. 4f-g, Fig. S11a,**
590 **Table 6**). Strikingly, a small number of hormone receptors were globally expressed. As
591 mentioned above, adiponectin receptor 1 (ADIPOR1), was expressed in 95.7% of the cell types.
592 Other broadly expressed hormone receptors included the renin receptor ATP6AP2 (92.3%), the
593 membrane-associated progesterone receptor PGRMC1 (85.3%), the cortisol receptor NR3C1
594 (76.8%), a putative resistin receptor CAP1 (77.3%), the IGF1 receptor IGF1R (67.1%), the
595 opioid growth factor receptor OGFR (66.0%), and the thyroid hormone receptor THRA in
596 complex with RXRB (53.1%). While it has been recognized that some of these hormones exert
597 organism-wide effects, our results suggest that they target not only a broad range of tissues but
598 likely regulate a large portion or perhaps majority of the cells of the body.

599 However, the majority of hormone ligands and receptors were expressed in specific cell types;
600 ~85% of the hormone ligands and ~56% of the hormone receptors were detected in less than 5%
601 of the cell types. Certain hormones like follicle stimulating hormone (FSHB and CGA) were
602 only expressed by a single cell type. Only a few hormone ligands were relatively broadly
603 expressed, including adrenomedullin (ADM, 19.1%), acylation stimulating protein (C3, 19.4%),

604 IGF2 (18.0%), and resistin (RETN, 18.9%). The generality score followed a power-law
605 distribution toward the tail where a small number of globally expressed receptors dominated the
606 distribution (**Fig. S11b-c**). This resulted in a bimodal distribution of the network node outdegree
607 (abundance of outgoing edges/downstream regulation) (**Fig. 4a, e**, **Fig. S10**). Cells expressing
608 hormone ligand(s) to the high-generality receptors (e.g., adipocytes which secrete adiponectin)
609 sent globally connected outgoing edges, and other cells that only expressed ligand(s) to specific
610 receptors sent a much smaller number of outgoing edges. In contrast, the nodes' indegree
611 (abundance of incoming edges/upstream regulation) was more homogeneously distributed
612 because of the higher specificity of hormone ligand expression and large number of hormone
613 receptors expressed per cell type (**Fig. 4d-e**, **Fig. S10**).

614

615 **Alternative receptors for the same hormone tend to be expressed in mutually exclusive cell**
616 **types**

617 Many hormones can bind to multiple receptors, which may mediate different functions (**Table**
618 **1**). We therefore examined if receptors for the same ligand tend to be co-expressed or if their
619 expression is mutually exclusive. To quantitatively compare the target cell type profiles, we
620 calculated a Jaccard index (JI, intersection over union) for each qualifying receptor pair, namely
621 the ratio of cell types that co-expressed both receptors to the cell types that expressed either of
622 the receptors. This analysis revealed that the majority of receptor pairs had extremely low JIs:
623 24% (41/168) of the receptor pairs had a JI equaling zero, meaning no overlap in their target cell
624 types, and 56% (94/161) had a JI of less than 5% (**Fig. 4h**). A telling case is the adrenoceptors;
625 although epinephrine (adrenaline) targets many cell types, different adrenoceptor subtypes were
626 selectively employed in different cell types (**Fig. 4h, Fig. S1**-epinephrine/norepinephrine). For
627 example, adrenoceptors ADRA1D and ADRB3 shared no target cell types; ADRA1D was
628 expressed broadly in vascular smooth muscle cells and pericytes of multiple organs, certain glial
629 cells, and leptomeningeal cells, whereas ADRB3 mainly targeted adipocytes. Vasopressin
630 receptors AVPR1A and AVPR2 also had less than 3% overlap in their target cell types; AVPR2
631 was predominantly expressed in the kidney collecting duct principal cells, while AVPR1A was
632 highly expressed in the kidney collecting duct intercalated cells and broadly expressed in many
633 stromal cells (**Fig. S1**-vasopressin).

634 A few receptor pairs showed a tendency toward co-expression, suggesting possible interactions
635 in cell signaling. Supporting this possibility, a top ranked pair was the IGF receptors IGF1R and
636 IGF2R (JI=0.40), which are known to interact in IGF2 signaling. IGF2R internalizes after IGF2
637 binding and clears IGF2 from the cell surface, and therefore functions as a competitive inhibitor
638 of IGF2-IGF1R signaling[75,76]. Two other top ranked pairs were NPY1R/NPY5R (JI=0.49),
639 receptors for neuropeptide Y, peptide YY and pancreatic polypeptide[77], and
640 ADIPOR1/ADIPOR2 (0.39), receptors for adiponectin. Coexpression of NPY1R and NPY5R
641 has been identified in the rodent brain, and recent studies indicate that the two GPCRs may form
642 heterodimers, resulting in modulated agonist binding properties[78,79]. Similarly, biochemical
643 studies on ADIPOR1 and ADIPOR2 in cell culture systems suggest that the two receptors can
644 form heterodimers promoting membrane expression of ADIPOR2[80,81].

645 Taken together, this analysis showed that the expression of distinct receptors for the same
646 hormone tends to be mutually exclusive, reflecting functional divergence and specification
647 among hormone receptor subtypes. The rare cases of co-expressed receptors appear to involve
648 functional interaction or cross-regulation between the receptor pairs.

649

650 **Feedback circuits are widespread in the hormonal cell communication network**

651 Hormone regulation often involves feedback control. We therefore searched the mouse lemur
652 hormonal cell-cell communication network to systematically identify potential feedback
653 regulation. For simplicity, we focused on two-node feedback circuits, namely cell type pairs that
654 are connected by edges in both directions (**Fig. 5a**). This systematic search revealed a vast
655 number of feedback circuits; 32% of all node pairs formed feedback circuits, showing that
656 feedback control is widespread in the hormone network (**Table 7**). We then tested if feedback
657 circuits are enriched in the hormone network, i.e. more prevalent than would be expected by
658 chance. We applied degree-preserving random rewiring[82] to randomly permute edge connections
659 without changing node degree (i.e., network edge number and distribution). **Fig. 5b** shows the
660 distribution of the feedback circuit counts from such randomly permuted networks (n = 1000).
661 Results suggest that feedback circuits are enriched in the hormone network compared to random
662 permutations (p=0.047). However, the difference was small (<1% on average). Additionally, we
663 randomly removed 10% of ligand-receptor pairs to test how perturbations to ligand-receptor
664 binding affect feedback distribution of the network. This analysis found that the network
665 feedback circuits remained abundant despite edge removal (**Fig. S9b**) as cell-cell connections
666 usually involved multiple ligand-receptor pairs (**Fig. 4d-e**). Taken together, this analysis suggests
667 that feedback circuits are abundantly and robustly distributed as a result of the dense connection
668 of the hormone network. Evolution may have further enriched hormonal feedback circuits as
669 suggested by the random rewiring analysis.

670 We next reviewed selected feedback circuits between endocrine cell types (**Fig. 5c-l**). The
671 analysis successfully detected well-known feedback regulation. **Fig. 5c** shows the detected
672 feedback loop between pituitary gonadotrophs and the estrogen-producing granulosa cells of the
673 ovary (fortuitously obtained from female perigonadal fat), a classical example of hormonal
674 feedback control that is evolutionarily conserved across vertebrates[83]. Consistent with humans,
675 lemur gonadotrophs expressed two highly-conserved gonadotropins, follicle stimulating
676 hormone (FSH, a dimer of FSHB and CGA) and luteinizing hormone (LH, LHB/CGA dimer),
677 which target granulosa cells through the corresponding receptors FSHR and LHCGR. Granulosa
678 cells, in turn, expressed key synthases required for the production of sex hormones, which feed
679 back to gonadotrophs through androgen and estrogen receptors (AR, ESR1). Additional feedback
680 regulation from granulosa cells to gonadotrophs was also mediated through anti-Müllerian
681 hormone (AMH) and inhibin/activin signaling. We also detected the well-established feedback
682 loop between pituitary somatotrophs and hepatocytes in the liver, which was mediated through
683 growth hormone (GH), IGF1[2,84], and potentially FGF21[85] and hepcidin signaling (**Fig. 5d**).
684 Additionally, feedback circuits were detected between pancreatic α and β cells through glucagon
685 and insulin signaling and between α and δ cells through glucagon and somatostatin signaling[86]
686 (**Fig. 5e-f**).

687 The analysis also revealed a long list of potential endocrine feedback circuits that have not been
688 reported, or only sparsely reported (**Fig. 5g-l**). For example, we detected a feedback loop
689 between pancreatic α cells and hepatocytes mediated by glucagon, IGF1 and FGF21 (**Fig. 5g**).
690 Regulation of hepatocyte glycogenolysis and gluconeogenesis by glucagon is well-established[87].
691 Less is known about how glucagon affects hepatocyte hormone secretion, and whether the two
692 cell types were involved in feedback regulation. Interestingly, two previous studies have
693 separately shown that injection of glucagon increases plasma FGF21 in humans[88] and injection
694 of FGF21 reduces glucagon in mice[89]. A recent study also observed that plasma IGF1 and
695 glucagon levels are negatively correlated in non-diabetic humans and found that IGF1 negatively
696 modulates glucagon secretion in an α cell culture model[90]. Considering that the liver is a major
697 source of circulating IGF1 and FGF21, these data suggest that α cells likely form a negative
698 feedback loop with hepatocytes in maintaining metabolic homeostasis.

699 Additionally, adipocytes, through adiponectin, formed possible feedback loops with pituitary
700 neuroendocrine cells, including the growth hormone secreting somatotrophs, the prolactin
701 secreting lactotrophs, and the ACTH secreting corticotrophs (**Fig. 5h-j**). It has been reported that
702 growth hormone, prolactin, and ACTH reduce adiponectin secretion in adipocytes[91–93], but much
703 less is known about the effect of adiponectin on pituitary neuroendocrine cells. Interestingly, a
704 recent study using cultured primary pituitary cells from two non-human primate species found
705 that adiponectin decreases growth hormone and ACTH release and increases prolactin release[94].
706 Altogether, it suggests that adipocytes form a negative feedback loop with lactotrophs which
707 possibly stabilizes prolactin and adiponectin levels, and form double-negative feedback loops
708 with somatotrophs and corticotrophs, possibly functioning as bistable switches[95]. It remains to be
709 characterized how adiponectin affects pituitary hormone secretion, what are the physiological
710 functions of the pituitary-adipocyte feedback control, and whether this regulation is specific to
711 primates.

712 Some of the individual legs of the feedback loops shown in **Fig. 5** may not be biologically
713 significant. For example, oxytocin and vasopressin are part of the feedback circuits among
714 pancreatic endocrine cells (**Fig. 5e-f**), between pancreatic α cells and hepatocytes (**Fig. 5g**), and
715 between enteroendocrine cells and pancreatic β cells (**Fig. 5k**). The intra-pancreatic feedback
716 regulation (**Fig. 5e-f**) may be plausible local circuits, but the vasopressin and oxytocin mediated
717 cross-organ communications (**Fig. 5g, k**) seem less plausible, because most of the oxytocin and
718 vasopressin in the bulk circulation is derived from specific hypothalamic neurons and secreted in
719 the posterior pituitary[2]. The lemur pancreatic endocrine and enteroendocrine cells expressed
720 lower levels of oxytocin and vasopressin than many of the neuronal cell types (**Fig. S1**-oxytocin,
721 vasopressin), thus are unlikely major sources of these hormones in circulation despite their
722 potential role in local communications.

723 Several others of the regulatory circuits identified here may not fit well with the conventional
724 view, but could actually be biologically significant, such as IGF1 and FGF21 mediated
725 communication from adipocytes to somatotrophs, corticotrophs, and enteroendocrine cells (**Fig.**
726 **5h, j, l**). Canonically, circulating IGF1 and FGF21 are believed to be predominantly produced by
727 hepatocytes[20,96,97]. However, we identified high IGF1 expression in the mouse lemur stromal
728 compartment, in particular adipocytes and fibroblasts (**Fig. S1**-IGF1). FGF21 expression levels
729 were also comparable between adipocytes and hepatocytes (**Fig. S1**-FGF21). Given that
730 adipocytes are abundant in the mouse lemur and their weight varies by season, it is plausible that

731 adipocytes contribute significantly to the production and temporal variations of the circulating
732 IGF1 and FGF21.

733 Taken together, this analysis identified an extensive list of potential feedback circuits in the
734 global hormonal cell communication network (**Table 7**), providing a rich resource for generating
735 hypotheses on endocrine regulations and to compare their regulatory mechanisms in different
736 species.

737

738 **Exploring hormonal regulation of the circannual rhythms that control organismal biology**

739 The mouse lemur hormone atlas may bring new insights to the study of mouse lemur-specific
740 physiology, such as their circannual rhythms[31,98], social interactions[99], and aging[12–14,100]. As an
741 adaptation to seasonal environmental changes, mouse lemurs have evolved striking seasonal
742 rhythms in metabolism, behavior, and reproduction that persist throughout their 5–10-year
743 lifespan. Mouse lemurs build fat reserves in preparation for the winter and enter daily torpor, a
744 hypometabolic state, to preserve energy, while in the summer the animals maintain a lean body
745 and regrow their reproductive organs for mating. The global nature of these phenotypic changes
746 suggests that they may be hormonally mediated. To date, only 12 circulating hormones have
747 been measured in mouse lemurs, but all showed dramatic seasonal changes (**Fig. 6a**, **Table 8**).
748 This suggests that hormones are likely the key messengers coordinating and driving various
749 seasonal changes among different organs. The hormone atlas suggests that these seasonally
750 changing hormones target a broad array of cells and tissues; 95% of the cell types possessed
751 receptors for at least one of these 12 hormones (**Fig. 6b-l**). Several of the seasonal hormones,
752 such as cortisol, thyroxine, and IGF1 are global regulators, targeting over 50% of the cell types
753 (**Fig. 6e-g**). Others, such as GLP and GIP, are highly specific, targeting 0.2% and 5% of the cell
754 types, respectively (**Fig. 6h, k**). Estrogen, androgen, insulin, PYY/PPY target many cell types,
755 but their receptor expression was restricted to only certain cell type compartments (e.g., stromal,
756 epithelial) (**Fig. 6c-d, i-j**). For melatonin, receptor expression was not detected (**Fig. 6l**), possibly
757 due to incomplete sampling of melatonin-expressing brain regions. Comparing across cell types,
758 stromal and epithelial cell types tend to be targeted by most seasonal hormones (**Fig. 6c-l**). These
759 data suggest that seasonal rhythms engage not only tissues that demonstrate obvious
760 morphological changes (e.g., adipose tissues and gonads), but involve global shifts in cellular
761 metabolism and physiology. While it is now clear that ligands of at least 12 hormones are
762 produced in a seasonal manner in the mouse lemur, it remains to be explored if more hormones
763 are seasonal and if hormone receptors are seasonally expressed to control mouse lemur seasonal
764 rhythms.

765

766 **Evolution of hormonal gene expression in the human, lemur, and mouse**

767 Lastly, to study evolution of hormone signaling, we compiled comparable scRNAseq datasets of
768 human and mouse and performed cross-species comparison of hormonal gene expression across
769 human, mouse lemur, and mouse. Six tissues were studied, including lung, skeletal muscle, liver
770 (epithelium only), testis (germ cells only), and two immune tissues, bone marrow and spleen

771 (immune cells only). For consistency, cells from the human and mouse datasets were reannotated
772 through the same pipeline and with the same cell type markers as for the mouse lemur cell atlas.
773 Data from different species were further integrated and cell annotations unified to ensure that cell
774 types are comparable across species[15]. This resulted in 62 orthologous cell types with enough
775 cells for comparisons in all three species. We next identified the hormonal genes with one-to-
776 one-to-one orthology mapping across the three species and examined if the gene exists in all the
777 analyzed scRNAseq datasets (**Table 2**). A total of 295 genes were identified and their cross-
778 species expression patterns plotted in **Fig. S12**. By comparing the correlation of the overall
779 hormonal gene expression, we found that human and lemur showed a higher (p-value = 0.006)
780 correlation coefficient (r = 0.50) compared to that between human and mouse (r = 0.48) (**Fig.
781 7a**), suggesting that overall hormonal gene expression is more similar between humans and
782 lemurs compared to mice. For comparison, the mean sequence identity between these 295 human
783 and lemur one-to-one orthologs was 0.86, and for human and mouse orthologs 0.82 (**Fig. S2b**).
784 Thus, humans are more similar to lemurs in both gene sequences and expression patterns,
785 compared to mice.

786 Next, we examined individual hormonal genes and compared the conservation of their
787 expression patterns between the orthologous cell types of human and lemur vs. that between
788 human and mouse. For each gene, we calculated the correlation coefficient for expression in the
789 62 orthologous cell types for human vs. lemur (i.e., r(human, lemur)), human vs. mouse
790 (r(human, mouse)) , and lemur vs. mouse (r(lemur, mouse)), and we used the correlation
791 coefficients as a gauge of expression pattern similarity (**Fig. 7b-c**). Many of the genes showed a
792 conserved expression among all three species, such as endothelium-specific RAMP2, liver-
793 specific GC, and fibroblast- and pericyte-specific EDNRA (**Fig. 7b-d**, **Fig. S12**).

794 Interestingly, four genes (RETN, VIPR1, PROK2, and PTGDR) were highly correlated between
795 human and lemur but poorly correlated between human and mouse (**Fig. 7b-c**), suggesting that
796 their expression patterns are conserved in primates and/or diverged in mice. As discussed above,
797 VIPR1 (vasoactive intestinal peptide receptor 1) was selectively expressed in the lung
798 endothelial cells of humans and lemurs but not mice (**Fig. 7d**, **Fig. 13a**). RETN (resistin) was
799 most highly expressed in the neutrophils, monocytes, and macrophages in humans and lemurs
800 but not mice (**Fig. 7d**). Similarly, PTGDR (prostaglandin D2 receptor) was expressed in the
801 natural killer (NK) and NK T cells in humans and lemurs but not mice (**Fig. 7d**). PROK2
802 (prokineticin 2) was selectively expressed in neutrophils and at lower levels in other myeloid
803 cells in humans and lemurs, but was not expressed in these cell types in mice; instead it was
804 expressed in spermatocytes (**Fig. 7d**).

805 In contrast, only one gene, neurotensin (NTS) was found to be more similar between human and
806 mouse vs. that of human and lemur, when applying the same threshold (**Fig. 7b-c**). Among the
807 cell types examined in all three species, NTS was selectively expressed in the lymphatic cells in
808 human and mouse but not lemur (**Fig. 7d**). Across all mouse lemur atlas cell types, NTS was
809 most highly expressed in the small intestine enteroendocrine cells (**Fig. S1**-
810 neurotensin/neuromedin N), which is also the canonical site of NTS secretion in humans[18].
811 However, we currently lack cross-species scRNAseq data of the enteroendocrine cells for
812 comparison. Presumably, the major site of NTS secretion is conserved across the three species
813 (in enteroendocrine cells), whereas the uncanonical lymphatic NTS expression is specific in
814 humans and mice but not lemurs. It will be interesting to compare, in human and mouse, levels

815 of NTS expression in the lymphatic cells to that of enteroendocrine cells and explore the function
816 of this uncanonical source of NTS.

817 We also identified one gene (PAQR5, a membrane progesterone receptor) whose expression
818 pattern is more similar between lemur and mouse than between either of the species and human
819 (**Fig. 7c**). Both lemur and mouse spermatids show the highest PAQR5 expression, whereas
820 human cholangiocytes show the highest expression among the cell types examined (**Fig. 7d**).

821 In addition, a number of genes showed low conservation in their expression patterns among all
822 three species, such as RAMP1, RAMP3, PTGDS, PNMT, PAQR6 (**Fig. 7b-d**). For example,
823 RAMP1, as previously discussed, was most highly expressed in the lung vascular endothelial
824 cells in the lemur. However, mouse myeloid cells, such as monocytes, macrophages, and
825 dendritic cells show the highest RAMP1 expression. In humans, RAMP1 was moderately
826 expressed in the lung ciliated epithelium, hepatocytes (CPN2hi subtype), and skeletal muscle
827 cells, two of which also displayed moderate RAMP1 expression in the lemur and mouse.

828 Lastly, the cross-species dataset included male germ cells which form a continuous gradient of
829 expression patterns (**Fig. 7e-f**). Spermatogenesis is known to have undergone extensive
830 molecular evolution[101]. Thus, we analyzed the expression dynamics of the stage-specific
831 hormonal genes identified in **Fig. 3a** and examined their conservation across the three species
832 (**Fig. 7g-h**, **Fig. S13a-b**). Although many spermatogonia-specific hormonal genes showed a
833 conserved expression across the three species, some genes displayed species differences. Some
834 involve small shifts or modifications in the expression dynamics. For example, consistent across
835 all three species, PTGES expressed in spermatogonia and spermatocytes and not in spermatids
836 (**Fig. 7g-h**). However, in humans and lemurs, PTGES expression was gradually reduced in the
837 course of sperm differentiation, whereas in mice expression was maintained at a high level
838 through mid to late spermatocytes (**Fig. 7g-h**). Other species-specific expression involved lack of
839 expression, or substantially reduced expression. Examples include the previously discussed
840 PAQR5, which was highly expressed in spermatids in lemurs and mice, but only slightly
841 expressed in human spermatids. In addition, PGRMC1 was expressed only in spermatogonia in
842 humans and lemurs, and was highly expressed during the spermatocyte-spermatid transition in
843 mice (**Fig, 7g-h**).

844 Taken together, cross-species comparison revealed an overall more similar pattern of hormonal
845 gene expression between human and lemur vs. human and mouse. Analysis of individual
846 hormonal genes identified interesting examples that are highly conserved or display
847 primate/species specific expression. This analysis revealed interesting candidates for future
848 studies to understand the evolution of hormone signaling.

849 Discussion

850 Hormonal signaling is vital to multicellular life, allowing cells to communicate with both
851 surrounding cells and remote cells in other tissues. In this study, we systematically mapped
852 hormone-producing and -target cells across the 739 cell types from 27 different tissues from the
853 mouse lemur molecular cell atlas. We generated a browsable atlas that depicts gene expression of
854 ligands, modulators, and receptors for 84 hormone classes (**Fig. S1**, https://tabula-
855 microcebus.ds.czbiohub.org/hormone-atlas). This dataset complements the scale and resolution

856 of classical endocrine studies and brings a cellular and molecular foundation for studying
857 primate hormone regulation.

858 The hormone atlas also provides an opportunity to extract global principles of hormone
859 signaling. The hormone-related genes exhibited cell-type-dependent, stereotypical expression
860 patterns, and their transcriptional profiles faithfully define cell type identities, despite their
861 constituting less than 1% of the transcriptome (**Fig. 2**). Ligands or receptors alone also classified
862 cell types well, with certain clusters mostly defined by their ligands and others by their receptors
863 (**Fig. S7**). Cell type clusters defined by the hormonal genes often show further cell type, subtype,
864 or stage-dependent specification within clusters, such as the extensive shifts in hormonal
865 signaling during spermatogenesis, across the spatial gradient of the kidney nephron epithelium
866 and vasa recta endothelial, between subtypes of hepatocytes, and during tumor metastasis (**Fig.
867 3a-g**). There is also an interesting organ-dependent clustering of the lung and brain vascular
868 endothelial cells, showcasing a rare example of organ-specific rather than cell type-specific
869 hormone signatures (**Fig. 3h**). Altogether, it is remarkable how well a cell's intercellular
870 communication repertoire encapsulates the cell's identity, indicating precise and highly
871 specialized hormonal control in different cells across the body.

872 To study the properties of global hormonal regulation, we constructed an organism-wide cell
873 communication network for mouse lemur hormone signaling, by connecting the hormone-
874 producing cells to the corresponding target cells (**Fig. 4**). This hormone network was
875 exceptionally dense (**Fig. 4a-b**), which mainly resulted from two network features. First, most
876 cells in the network expressed multiple hormone receptors and/or ligands (**Fig. 4d**). Second,
877 although most hormone ligands and receptors were expressed in specific cell types, a small
878 fraction of hormone receptors were nearly ubiquitously expressed, resulting in almost global
879 connection of the relevant hormone-producing cells (**Fig. 4e-g**). Thanks to its dense connection,
880 the hormone network is highly robust to random perturbations that delete individual edges (**Fig.
881 S9**). Although the regulatory circuits of individual hormones may be hierarchical, as classically
882 viewed, overall the network is decentralized, which de-emphasizes the contribution of any one
883 hormone-receptor pair. Many of the hormone-secreting cells are diffusely distributed throughout
884 the organism, in line with the concept of a diffuse neuroendocrine system espoused by Feyrter[102].
885 It is worth noting that, although changes to a single hormone-receptor pair may only minimally
886 affect the overall hormone network structure, the impact to animal physiology and metabolism
887 could be significant. Information flow in the hormone network depends not only on whether an
888 edge exists but also the identity of the connecting edge(s), i.e., the hormone-receptor pair(s).
889 Interestingly, despite the density of the hormone signaling network, subtypes of hormone
890 receptors that bind to the same ligand were generally expressed in a mutually exclusive fashion,
891 supporting the notion that different hormone receptor subtypes usually mediate different
892 physiological functions through separate target cells (**Fig. 4h**).

893 Feedback regulation was widespread in hormonal signaling, and it was robust to network
894 perturbations (**Fig. 5b**, **Fig. S9B**). The analysis identified well-known feedback circuits among
895 several endocrine cell pairs and detected additional, previously unreported, hormones involved in
896 feedback control (**Fig. 5c-f**). We also identified many novel feedback circuits (**Fig. 5g-l**, **Table
897 7**) which may be involved in adaptation or homeostasis (negative feedback circuits) or in
898 generating switch-like responses (positive and double-negative feedback circuits). It is worth
899 emphasizing that not all detected feedback circuits will necessarily be biologically significant. In

900 particular, for hormones that travel and mix in the bulk circulation for long-distance cell
901 communication, signals from a particular hormone-producing cell type could be overwhelmed by
902 other cell types that produce larger amounts of the same hormone. Future analysis may include
903 information on cell numbers of individual cell types and genes responsible for rate-limiting steps
904 to more systematically compare total hormone production in each cell type and discriminate
905 major and minor hormone sources. Nevertheless, this analysis represents a first step to
906 systematically identify endocrine feedback circuits for future functional validation and
907 characterization. Our findings may also inform studies of the systems biology and network
908 topology of hormone signaling (see for example Karin et al.[103]).

909 Mouse lemurs display dramatic seasonal changes in body weight, hibernation propensity, and
910 reproductive activities[31,98,104]. Such seasonal rhythms are likely regulated, at least in part, by
911 seasonally-varying long-range hormones that coordinate the changes across different organs of
912 the body (**Fig. 6a**). The hormone atlas shows that almost all (95%) of the mouse lemur cell types
913 are regulated by seasonally varying hormones (**Fig. 6b**). This suggests that most, if not all,
914 mouse lemur cells across all organs of the body experience seasonal changes in metabolism,
915 growth, and function. By systematic mapping of hormone secreting and target cells, the atlas also
916 points to candidate cell types and signaling to explore the upstream and downstream regulation
917 for each of the seasonally varying hormones. Given that all 12 hormones measured in the mouse
918 lemur showed significant seasonal changes, we suspect that more hormones will prove to be
919 seasonal. Future work should systematically characterize seasonal patterns of hormones with
920 higher temporal resolution, and to sample animals in different seasons to detect seasonal
921 expression changes in hormone receptors, ligands, and synthases, which could indicate seasonal
922 restructuring of the hormone network. Circannual rhythms are widespread in nature[105,106] and
923 humans display seasonally varying hormone levels and cellular transcriptomes[107–109]. The
924 findings of the present study may apply to species beyond the mouse lemur, and may bring new
925 insights for season-associated human diseases[110–112].

926 Mouse lemurs are genetically closer to humans than mice are. Likewise, the lemur better models
927 human hormonal signaling than does the mouse. At the genomic level, there were fewer
928 hormonal genes that were lost (or became pseudogenes) in lemurs (3) than mice (6). More
929 human genes had one-to-one mapping in lemur (338, if counting LHB) than mouse (330).
930 Further, more human genes (85.8%) had a higher sequence identity with their lemur ortholog
931 than their mouse ortholog (**Fig. S2**). Given that mouse lemur genome and gene annotations
932 remain lower in quality than those of humans and mice, some of the lemur genes may be
933 unannotated or incorrectly annotated, like LHB. Thus, the above comparisons may underestimate
934 human-lemur similarity. Lastly, by comparing the expression patterns of the one-to-one
935 orthologs across the three species, we also found mouse lemurs had an overall higher similarity
936 with humans compared to mice (**Fig. 7a**). For hormonal genes that show a highly species-
937 specific expression pattern, more (4) were conserved between humans and lemurs and unique in
938 mice compared to the opposite (only 1) (**Fig. 7b**).

939 Single-cell RNA sequencing is a powerful tool for assaying cellular function and activity, but
940 there are limitations. Although the technique has improved rapidly in sensitivity, accuracy, and
941 efficiency, scRNAseq still faces low capture efficiency and high transcript dropout[113]. With the
942 large number of cells assayed in the mouse lemur molecular cell atlas, we averaged gene
943 expression across cells of the same cell type to smooth the noise in individual cells from dropout.

In the analysis of hormone regulation, genes involved in hormone production, such as ligands and modulators, tended to be abundantly expressed; but certain hormone receptor proteins may be low in copy number and slow in turnover, and therefore may result in false-negative errors. In addition, there can be false-positive errors caused by contamination from other cells in the same sample (i.e., signal spreading). This is most notable for abundantly expressed ligand genes and tissues affected by endogenous digestive enzymes (e.g., pancreas). In this study, we scored positive expression of a hormone ligand only when both the ligand gene and the necessary modulators (such as prohormone processing enzymes) were present. This approach mitigated false-positive detection of highly abundant ligands. Lastly, scRNAseq has low capture efficiency for certain cells such as neurons and large sized adipocytes. Particularly relevant for the study, hypothalamic neurons were not captured in the current lemur dataset. Nevertheless, the mouse lemur cell atlas included several neuronal subtypes from the brain cortex, brainstem, and retina, as well as both UCP1-high and UCP1-low adipocytes from multiple tissues[15]. Although not yet a complete nor ideal sampling, the mouse lemur cell atlas is one of the most comprehensive and accurately-annotated organism-wide scRNAseq datasets reported to date. Other organism-wide scRNAseq atlases have been created or are being created for other species, including mouse[114–116], ascidian[117], macaques[118,119], and human[120], bringing exciting resources to the study of the evolution of hormone signaling.

Finally, it is worth emphasizing that the mouse lemur scRNAseq atlas used in the study was constructed with four aged and diseased donors. For example, both females had uterine tumors with metastasis, and all four lemurs exhibited chronic kidney disease which may have affected the transcriptional profiles of the kidney cells. Nonetheless, in the cross-species analysis, we have shown that hormone profiles of individual cell types are overall conserved across human, lemur, and mouse. Human and lemur actually correlated better in their overall transcriptional and hormonal profiles than between human and mouse, despite the fact that mouse data were derived from younger, healthier animals[114] and that human data was possibly affected by different pathologies[120]. While previous studies reported that concentrations of hormones may change over age[121], we suspect that the global principles of hormone signaling—e.g. a densely connected, decentralized network with abundant feedback regulation —learned through the mouse lemur atlas may also be pertain to younger lemurs and likely apply to other species. In addition, we have taken advantage of the disease conditions of the mouse lemurs, such as the two females with primary and metastatic uterine adenocarcinoma, which revealed interesting metastasis associated changes in hormone profiles.

Traditionally, biologists focus on one particular cell type and/or organ system. However, hormone signaling by its very nature connects different cell types and organs. The emerging organism-wide atlases open a new door in understanding the cross-organ communication systems that allow organisms to function as a reliable robust whole.

Methods

985 **Animals husbandry, tissue procurement and processing**: Details on animal husbandry and
986 sample collection and processing have been described in accompanying manuscripts[15,17]. In
987 brief, mouse lemurs were maintained for noninvasive phenotyping and genetic research as
988 approved by the Stanford University Administrative Panel on Laboratory Animal Care (APLAC
989 #27439) and in accordance with the *Guide for the Care and Use of Laboratory Animals*[122].
990 Animals were housed indoors in an AAALAC-accredited facility in a temperature (24°) and
991 light-controlled environment (daily 14:10 h and 10:14 h light:dark alternating every 6 months to
992 stimulate seasonal breeding behavior and metabolic changes). Animals in declining health that
993 did not respond to standard therapy were euthanized by pentobarbital overdose under isoflurane
994 and tissue samples were collected for scRNAseq and histopathology analysis. Details of animal
995 histopathology can be found in Casey et al.[17] and animal age and tissue sampling/processing
996 pipelines has been described in the accompanying manuscript[15]. Pathologies common to all four
997 animals were fibrous osteodystrophy, chronic renal disease, uterine tumors (females only),
998 cataracts, and osteoarthritis. Tissues not described in Casey et al.[17] were histologically normal.

999

1000 **Mapping and counting transcript reads**: The single-cell gene expression matrix of the mouse
1001 lemur cell atlas was obtained from the accompanying manuscript[15] where methods and
1002 parameters to extract the transcript counts can be found. In this study, we used only the 10x
1003 droplet-based sequencing derived data for all analysis. In brief, the *Microcebus murinus* genome
1004 assembly (Mmur 3.0, NCBI) was used to create a genome FASTA file. Sequencing reads were
1005 processed with Cell Ranger (version 2.2, 10x Genomics) to generate cell barcodes and the gene
1006 expression matrix. We additionally counted reads for three genes (MC1R, SCT, LHB) that are
1007 unannotated in Mmur 3.0, NCBI. For MC1R and SCT, we used their annotation in the Ensembl
1008 *Microcebus murinus* genome. For LHB, we used the uTAR-scRNA-seq pipeline described by
1009 Wang et al.[23] to first predict its chromosome location in the mouse lemur genome. In brief, the
1010 pipeline employs the approach of groHMM[123] to detect transcriptionally active regions (TARs)
1011 from aligned sequencing data and annotates these TARs as unannotated (uTARs) or annotated
1012 (aTARs) based on their overlap with the existing annotation. For the LHB_uTAR counts, we
1013 uncovered uTARs from the mouse lemur pituitary and hypothalamus dataset and used
1014 BLASTn[124,125] to find nucleotide sequence homology of all uTARs against human LHB. We
1015 found one uTAR at position NC_033681.1:19143249-19145949 with high sequence homology
1016 to human and macaque LHB. The LHB_uTAR is highly differentially expressed in the expected
1017 cell type (gonadotroph). The LHB_uTAR is located next to gene RUVBL2, in conservation with
1018 the co-location pattern of the genes in humans and mice[24]. We therefore conclude that the
1019 identified LHB_uTAR is the likely coding region of the mouse lemur LHB gene. We then used
1020 Drop-seq tools[126] to extract transcript counts for the three genes (MC1R, SCT, LHB_uTAR).

1021

1022 **Orthology and protein sequence analysis**: Gene orthology mapping across human, mouse
1023 lemur, and mouse was based on the combination of both the NCBI and Ensembl ortholog
1024 databases. Details to combine the two databases were described in the accompanying
1025 manuscript[15]. To compare sequence similarity between orthologs of human and mouse or lemur,
1026 protein sequences were retrieved from NCBI according to protein RefSeq using the Matlab built-
1027 in function getgenpept. Conversion between gene ID and protein Refseq identifier was
1028 performed using bioDBnet (https://biodbnet.abcc.ncifcrf.gov/db/db2db.php). We aligned

1029 ortholog protein sequences and used the maximal scores in the cases of multiple transcript
1030 sequences and non one-to-one ortholog mapping. Global alignment was carried out using the
1031 Needleman-Wunsch algorithm and default parameters of the function nwalign.

1032

1033 **Identification of hormone-producing and target cells**: The functional concentration is
1034 different for different proteins, so we applied adaptive thresholding to determine if a gene is
1035 positively expressed in a cell type, where cell type is defined as a unique combination of the
1036 cells' annotation and tissue of origin, as described in the accompanying Tabula Microcebus
1037 manuscript[15]. For example, vein cells of the lung and brain were considered two different cell
1038 types. Cell types that were of low quality (low gene count or transcript count) or annotated as
1039 technical doublets were removed from the analysis. For each gene, two cell type parameters were
1040 used, mean expression level and percentage of nonzero (positive) cells. Single-cell expression
1041 levels were first normalized by total transcript counts, multiplied by 10,000, averaged across all
1042 cells in the cell type, then natural log transformed (i.e.,
1043 log(1+Average_UMI_count_Per_10K_Transcripts); note that 1 is added to the average so that
1044 genes with zero transcripts will yield zero rather than negative infinity). To determine positive
1045 expression at the cell type level, we applied adaptive thresholding that compares the expression
1046 to the maximally expressing cell types. The algorithm involves 4 parameters which were selected
1047 to capture a list of well-studied cell types and hormonal genes. We first applied a low-level
1048 absolute threshold on average expression level (0.037) and percent of nonzero cells (5%) below
1049 either of which we considered the expression to be negative. Second, we calculated a "maximal"
1050 expression level of the gene by searching the high-expression levels across the atlas.
1051 Specifically, we considered the 99th percentile of the cells that passed the first thresholding to be
1052 the maximum to increase the robustness of the analysis. Lastly, we applied relative thresholding
1053 of the "maximal" level (for circulating proteins such as ligand genes at 20% and other gene types
1054 at 5%). Cell types that passed all thresholding criteria were considered to have functional
1055 expression of the gene. We used a higher relative threshold for the ligand genes because 1)
1056 ligands are secreted into the circulation so a highly expressing source outshadows a low
1057 expressing source, whereas non-ligand products of other genes (e.g., receptors, synthases,
1058 processing enzymes) function inside individual cells; 2) we noted that ligand genes were usually
1059 expressed at higher levels and were more easily affected by cross-contamination (signal
1060 spreading) inside a tissue. For hormone ligands and receptors that included multiple genes, we
1061 applied AND or OR logic gates as indicated in **Table 1** to determine if a cell type expressed the
1062 ligand or receptor. For an AND logic gate, a functional cell type should express all its
1063 components above the functional level; while for an OR logic gate, expression of any of its
1064 components would suffice.

1065

1066 **Cell type distances, clustering, and visualization**: We performed hierarchical clustering of the
1067 cell types included in the mouse lemur atlas based on the transcriptional profiles of hormone
1068 ligand, synthase, modulator, and receptor genes. Analysis was carried out at the cell type level
1069 and relative average gene expression levels were used to calculate cell-type pairwise distances.
1070 To test consistency of hormone-related gene expression among mouse lemur individuals, we
1071 separated cells from different lemurs. Because circulating immune cells sampled from different
1072 tissues were already kept as different cell types, immune cell types were not separated for

1073 different lemurs to avoid overcrowding of the data. We found that this simplification only
1074 slightly influenced the clustering results of individual cell types and did not affect the overall
1075 clustering pattern (**Fig. S4**). Next, cell types were filtered to remove potentially low quality cell
1076 types that were: 1) low in cell number, 2) technical doublets, or 3) low in transcript and/or gene
1077 count. We also manually corrected for notable cross-contamination in certain cell types. For
1078 example, almost all non-endocrine cell types of the pancreas showed high expression of insulin
1079 (INS) and proglucagon (GCG), probably caused by cross-contamination due to autolysis in the
1080 pancreas during tissue processing. We therefore removed INS and GCG expression from all non-
1081 endocrine pancreatic cell types. Additionally, we corrected contamination of GUCA2A,
1082 GUCA2B, GIP, NTS, and SST from stromal, endothelial, and immune cells of the intestine
1083 (small intestine and colon). Matlab built-in functions were used in the hierarchical clustering
1084 analysis. We used cosine distances to calculate cell type pairwise distances and then applied
1085 average-linkage to construct the dendrogram (cophenetic correlation coefficient = 0.81). Cell
1086 type clusters were then divided at a threshold of 0.49 with minor manual inputs to further divide
1087 certain large clusters or merge an apparently close neighboring leaf. We obtained 74 total
1088 clusters and numbered them according to their sequence in the dendrogram shown in **Fig. 2a**. We
1089 also named the clusters according to the shared characteristics of its cell types. Cell types
1090 included in each cluster are listed in **Table 4** with the list of hormones, hormone receptors, and
1091 hormone-related genes that were expressed in the majority (≥ 50%) of the cell types for each
1092 cluster.

1093 In addition to visualizing the cell type clustering via dendrogram, we also applied uniform
1094 manifold approximation and projection (UMAP)[127] to embed the high dimensional expression
1095 data to 2D using a Matlab UMAP package[128]. Cell type pairwise cosine distances were used as
1096 input when generating the UMAPs.

1097 For comparative analysis, we additionally calculated cell type pairwise distances by the
1098 transcriptomes of all genes, the non-hormonal transcriptome, 100 random sets of PCGs (same
1099 number of genes as the hormonal genes), 100 random sets of PCGs controlling for expression
1100 variability (dispersion). These transcriptional distances were calculated similarly as the hormone-
1101 based distances were, with relative expression levels of genes used to calculate pairwise cosine
1102 distances. To select for gene sets with similar distribution of expression specificity, we first
1103 binned genes based on their cell type expression dispersion (i.e., variance-to-mean ratio) to 21
1104 uniform bins and then randomly selected the same number of genes in each bin as the hormonal
1105 genes.

1106 These transcriptional distances were compared to a benchmark cell annotation-based distance by
1107 Pearson correlation. Cell annotations, as defined in the accompanying manuscript[15], was based
1108 on expression of canonical cell markers and iterative clustering with highly variable genes. This
1109 annotation-based distance was defined as an integer between 0 and 3 based on the following
1110 criteria: distance is 0 when cell types were annotated with identical names but from different
1111 tissues, 1 when our cell annotation names were different but classical histological assignments
1112 (Cell Ontology[48]) were identical (i.e., different molecular subtypes), 2 when classical Cell
1113 Ontologies were different but cell types were from the same compartment (e.g., both were
1114 epithelial), and 3 if cells were different cell types and from different compartments (e.g.,
1115 endothelial vs. stromal).

1116 We additionally calculated a Cell Ontology-based distance. Each cell type was assigned a Cell
1117 Ontology term (i.e., its classical histological cell type category) during cell type annotation[15].
1118 Cell Ontology distances were calculated as the mean of Cell Ontology embedding-based
1119 distances and text-based distances[49]. Cell Ontology embedding-based distances represent
1120 distances between cell types in the Cell Ontology graph. Text-based distances were calculated
1121 using an adapted version of Sentence-BERT[49,129].

1122 To estimate the quality of the clustering results, we calculated silhouette values and compared
1123 cluster average silhouette values based on only the hormone ligand genes, hormone receptor
1124 genes, or the full transcriptome. Silhouette values for a cell type i is from the equation $s(i) =$
1125 $\frac{b(i)-a(i)}{max\{b(i),a(i)\}}$, for cell types belonging to a cluster with more than one member. $a(i)$ is the mean
1126 in-cluster distance, namely the mean distance between cell type i and all other cell types in the
1127 same cluster. $b(i)$ is the minimal out-cluster distance, namely the minimal mean distance between
1128 cell type i and members of other clusters.

1129

1130 **Trajectory analysis**: Analysis was performed independently for kidney samples from three
1131 mouse lemur individuals and for the cross-species spermatogenesis dataset using an in-house
1132 program written in Matlab. To detect the vasa recta arteriole-to-venule trajectory, data were first
1133 pre-processed following the standard procedure as in Seurat[130]. In brief, single cell transcript
1134 counts for all sequenced genes were normalized to total transcript counts, log transformed, and
1135 linearly scaled so that each gene has a mean expression of 0 and standard deviation of 1. Then
1136 genes with high dispersion (variance-to-mean ratio) compared to other genes with the same mean
1137 expression were selected as highly variable genes for principal component analysis (PCA).
1138 Following PCA, the top 20 principal components that were not driven by extreme outlier data
1139 points or immediate early genes were used to generate a 2D UMAP using cell-cell Euclidean
1140 distances as input[127]. For the cross-species spermatogenesis, we used species-integrated UMAP
1141 of the testis germ cells[15]. To quantify the trajectories, we detected the probability density ridge of
1142 the data points in the UMAP using automated image processing. The direction of the trajectory
1143 was manually assigned according to marker gene expression. Individual cells were aligned to the
1144 trajectory by finding the shortest connecting point to the trajectory. Data points that were too
1145 distant from the trajectory were deemed outliers and removed from the following analysis. To
1146 detect the vasa recta hormone-related genes that follow a trajectory dependent expression
1147 pattern, we calculated the Spearman correlation coefficient between the gene expression level
1148 and 20 unimodal patterns. These preassigned patterns have their data smoothly changing along
1149 the trajectory and have a single peak. We let the 20 patterns have their peaks uniformly
1150 distributed from 0 to 1. This analysis tested, for each gene, whether its distribution along the
1151 trajectory follows one or more of the 20 unimodal patterns. All p values were then multi-testing
1152 corrected to detect significant genes and their associated patterns. Lastly, we compared results
1153 from the three kidney samples and kept the genes that showed consistent patterns in all three
1154 samples.

1155

1156 **Identification of differentially expressed genes**: We used the Wilcoxon rank-sum test to detect
1157 differentially expressed hormone genes among cell populations. Genes that were expressed

above functional level in any of the analyzed cell populations were included in the analysis. For hormone-related genes differentially expressed during spermatogenesis, we tested whether each gene is differentially expressed in one of the three sperm cell clusters compared to the other two clusters. For the analysis of endothelial cells, we tested whether each gene is differentially expressed in the lung or brain endothelial cells compared to all other endothelial cells. For the kidney nephron analysis, we tested whether each gene is differentially expressed in one of the nephron clusters compared to the rest of the nephron epithelial cells. For the hepatocyte analysis, we tested whether each gene is differentially expressed in one subtype compared to the other in both the mouse lemur and the mouse. The mouse hepatocyte data was obtained from the Tabula Muris Senis[114] smartseq2 plate-based sequencing of mouse hepatocytes. For the tumor cell analysis, we tested whether each gene is differentially expressed in the metastatic cells versus the MUC16+ non-ciliated uterus epithelial cells. All *p* values were multi-testing corrected, and then all genes with corrected *p* values less than 0.05 were examined to confirm consistent expression of the gene in all relevant cell types and mouse lemur individuals.

Constructing and analyzing the hormonal cell communication network: Cells with the same cell type annotation and tissue of origin were grouped as a cell type/node. Data from different lemur individuals were merged in the analysis. Cell types that were likely low quality were removed. Edge connections were determined independently for all possible cell type pairs. For example, if cell type A expressed a hormone ligand and cell type B expressed the corresponding hormone receptor(s), a directed edge from A to B was drawn. Note that this allows self-loops on any cell type that expresses both the ligand and corresponding receptor. When multiple directed edges connected two cell types, they were merged for the purpose of edge counting.

Network density is defined as the number of edges divided by the number of possible edges in the network. Because the hormone and cytokine networks are directed, its network density is calculated as $\frac{N_{edges}}{N_{nodes}^2}$. For comparison, the density of an undirected network is calculated as $\frac{2*N_{edges}}{N_{nodes}\cdot(N_{nodes}+1)}$ if it allows self-loops (e.g., protein interaction network) , or $\frac{2*N_{edges}}{N_{nodes}\cdot(N_{nodes}-1)}$ if it does not allow self-loops (e.g., genetic-interaction network).

Outdegree and indegree are node features and defined as the relative number of outgoing edges (node expressing a ligand) and incoming edges (node expressing a receptor). Edge counts were normalized by cell type abundance so that node degrees range from 0-100% and represent the fraction of the cell types that the node connects with by outgoing or incoming edges. To normalize the node degrees, we used a weighted cell type abundance determined by the clustering so that each cluster contributes the same weight. This is because certain cell types like circulating immune cells are likely over-represented in the network as they appear in multiple tissues and would be categorized as different cell types by our definition. We did not merge circulating cell types from different tissues because it is challenging for some cell types like T cells to determine whether they are circulating or potentially tissue specific or tissue-resident. We also tried simply normalizing the node degree by the total number of nodes; similar conclusions were reached using either method.

1199 **Calculating generality scores for hormone ligands and receptors**: To calculate generality
1200 scores for the hormone ligands and receptors, we counted the cell types that express the ligand or
1201 receptor. Cell types that were likely low quality were removed from the analysis. Cell type
1202 counts were normalized by cell type abundances similarly as was the node degree, so that the
1203 generality score was not dominated by over-represented cell types. In comparison, we also
1204 counted the cell type clusters that express the hormone ligands and receptors. Here we defined
1205 that a gene was expressed in a cell type cluster if more than 50% of the cell types in the cluster
1206 positively expressed the gene.

1207 To analyze the distribution of generality scores, we tested if the distribution followed normal,
1208 exponential, lognormal, or gamma distributions. We first performed parametric distribution
1209 fitting and then performed Kolmogorov–Smirnov tests comparing the fitted versus data
1210 cumulative distribution functions. This analysis used Matlab built-in functions fitdist and kstest.
1211 Additionally, we tested if the data followed a power law distribution using plfit and plpva
1212 functions[131].

1213

1214 **Calculating target cell Jaccard indices for different receptors that bind to the same ligand**:
1215 We calculated Jaccard indices for pairs of receptors that 1) can bind to the same ligand as
1216 described in **Table 1, and 2**) were both expressed in at least one atlas cell type. Jaccard index
1217 here is calculated as the number of cell types that express both receptors divided by the number
1218 of cell types that express either of the receptors.

1219

1220 **Network perturbation analysis**: We performed two types of network perturbations: degree-
1221 preserving random rewiring and random edge removal. For degree-preserving random rewiring,
1222 we applied the algorithm developed by Maslov and Sneppen[82]. The algorithm starts with the
1223 original network and performs repeated rewiring steps. For each rewiring, it randomly identifies
1224 two edges (e.g., A→B and C→D) and swaps the connections (i.e., A→D and C→B). This allows
1225 constructing a random network while preserving the node indegree and outdegree of the original
1226 network. For the perturbation by edge removal, we randomly selected 10% of the edge types
1227 (ligand-receptor pairs) and removed these edges from the original network. Note for this
1228 analysis, multiple directed edges connecting the same cell type pairs were not merged. Therefore,
1229 the connection between two cell types would be removed only if all of its redundant edges (of
1230 different ligand-receptor pairs) were selected to be removed.

1231

1232 **Hormone concentration measurements (related to Fig. 6)**: Cortisol concentrations (ng/ml)
1233 were measured in duplicates from urine samples by Cortisol Urine ELISA (LDN®, catalog no.
1234 MS E-5100). Urine creatinine (mg/ml) was measured using MicrovueTM Creatinine Elisa kit
1235 (Quidel R Corporation, catalog no. 8009). Creatinine concentration was used to normalize urine
1236 measurements as an indicator of renal filtration activity. Cortisol measurements are thus
1237 expressed in ng/mg creatine. Thyroxine (T4, nmol/L) was assayed in plasma samples using T4
1238 ELISA kit (LDN®, catalog no. TF E-2400) and the 6-point standard curve was adapted from 0 to
1239 100 nmol/L.

1240

1241 **RNAscope experiments**: Mouse lemur specific RNAscope® probes for MLN, AGT, and CUBN
1242 were designed and produced by Advanced Cell Diagnostics, Inc. (ACD) (cat #. 1260231,
1243 1263051, 1263061). The kidney samples analyzed were collected from the same lemurs profiled
1244 by scRNAseq[15] and analyzed in this study. Samples were procured, fixed, dehydrated, OCT-
1245 embedded, and biobanked at -80°. Cryosections (15 µm thick coronal sections) of the kidney
1246 were prepared using a Leica Cm3050s cryostat, stored overnight at -80°, and subsequently
1247 processed using the standard RNAscope multiplex fluorescent v2 protocol for fixed-frozen
1248 samples (UM 323100 Rev B), with the RNAscope® Multiplex Fluorescent Reagent Kit v2 (cat#.
1249 323270). In brief, sections were first pre-treated during which tissue slides were PBS washed,
1250 baked, post-fixed, dehydrated by ethanol, treated with hydrogen peroxide, submerged in
1251 RNAscope 1X Target Retrieval Reagent (99°) for 5 min, and finally treated with RNAscope
1252 Protease III. Next, sections were hybridized with all three probes for 2h at 40°. To visualize the
1253 probes, sections were incubated with each of the three RNAscope Multiplex FL v2 AMP for 30
1254 min at 40°, and then with RNAscope Multiplex FL v2 HRP for 15 min at 40°, and the respective
1255 TSA Vivid Dye for 30 min at 40°, and finally the RNAscope Multiplex FL v2 HRP blocker for
1256 15 min at 40°. Lastly, tissue slides were mounted with Prolong Gold Antifade Mounting
1257 containing DPAI and stored in 4° before imaging. Images were taken using a Zeiss LSM 880
1258 Confocal Laser Scanning Microscope under the Airyscan mode. The MLN, AGT, and CUBN
1259 channels were stained with TSA Vivid Fluorophore 570, 650, and 520, and imaged using the
1260 Cy3, Cy5, and FITC filters, respectively.

1261

1262 **Cross-species comparisons of hormonal gene expression**: We compared cells of the lung,
1263 skeletal muscle, liver, testis, bone marrow, and spleen. All lemur data was from the 10x data of
1264 the accompanying Tabula Microcebus manuscript[15]. Human data were from the 10x data of the
1265 Tabula Sapiens[120], except for the lung which we used the 10x data from the Human Lung Cell
1266 Atlas[132] and the testis which we used drop-seq data from Shami et al.[133]. Mouse data were from
1267 10x data of the Tabula Muris Senis[114] except for the testis which we used 10x data from Ernst et
1268 al.[134]. For lung and muscle, all cell types were included in the analysis, whereas we only
1269 analyzed the epithelial cells for the liver, immune cells for the bone marrow and spleen, and
1270 germ cells for the testis. We used one-to-one orthologs across all three species. This resulted in
1271 ~15,000 genes (324 hormonal genes), ~13,000 of which were included in all scRNAseq datasets
1272 (295 hormonal genes).

1273 To unify cell type annotations, human and mouse datasets were first separately re-annotated
1274 according to the same pipeline and marker genes as for the lemur data. Next, to ensure cell types
1275 are comparable across species, we applied Portal[135] to integrate data (one-to-one orthologs only)
1276 from different species. Portal projects data into a space that minimizes species differences, from
1277 which an integrated UMAP is generated to visualize cell clustering from different species.
1278 Integration was performed separately for each tissue, except for bone marrow and spleen which
1279 were integrated jointly. We manually inspected each integration UMAP and ensured that cells of
1280 the same type showed reasonable cross-species co-clustering and separation from other cell
1281 types. We also made small modifications to the cell annotations/clustering during this process to
1282 unify annotations across species. For example, proliferating cells might co-cluster with the main
1283 non-proliferating population in the original dataset if the number of cells are too few, but cluster

separately with the proliferating populations of the other species in the integrated UMAP. In such a scenario, we would separately annotate these cells as a proliferating subtype. Additional details to compile the cross-species scRNAseq datasets were described in the accompanying manuscript[15].

Cell types with more than 15 cells in all three species were then used for the cross-species comparisons, resulting in a total of 62 orthologous cell types (62*3=186 cell type entries in all three species). Cell type average expressions were calculated separately for each species. Note that cellular expression levels in the species-integrated dataset were normalized by the sum of only the one-to-one orthologs, rather than all the genes, thus at high levels compared to the non-integrated data. Cross-species similarity was calculated separately for individual genes. We first identified genes that are at least moderately expressed in the analyzed cell types (≥3 cell type entries with mean expression >1), which resulted in a total of 90 genes for follow-up analysis. Expression levels were then normalized by the maximally expressed cell type in each species and cross-species correlation coefficients between human and lemur (r(human, lemur)) and between human and mouse (r(human, mouse)) were calculated. $\Delta r = r$(human, lemur)-r(human, mouse) was calculated. Lastly, we identified genes that are more conserved between humans and lemurs compared to mice ($\Delta r>0.5$), and in contrast genes that are more conserved between humans and mice compared to lemurs ($\Delta r<-0.5$). To compare overall similarity of transcriptional profiles of the hormonal genes or all genes, we concatenated cell type expression profiles for individual genes and calculated correlation coefficients between human and lemur and between human and mouse. p-values of the difference in correlation coefficients were calculated using Fisher's Z-transformation[136].

Acknowledgments

We are grateful to Sandra Schmid, Uri Alon, Chaitan Khosla, Mathieu Lemaire, the Krasnow lab, and the Ferrell lab for helpful discussions and comments on the manuscript. This work is supported by NIH grant R35 GM131792 to J. E. Ferrell, funding from Wall Center to M. A. Krasnow, and a fellowship from the Wu Tsai Neurosciences Institute to S. Liu. M. A. Krasnow is an investigator of the Howard Hughes Medical Institute.

Author Contributions

S. Liu, M.A. Krasnow, and J.E. Ferrell conceived the project. S. Liu designed and performed all the analyses with input from C. Ezran, Z. Li, C. Kuo, J. Epelbaum, J. Terrien, M.A. Krasnow, and J.E. Ferrell. S. Liu, C. Kuo, and J. Long assembled the hormone list. M.F.Z. Wang and I.D. Vlaminck performed uTAR analysis on the candidate lemur LHB gene. S. Wang calculated the cell ontology distances. S. Liu, J. Epelbaum, and J. Terrien analyzed the seasonally oscillating hormones. S. Liu and C. Kuo performed the RNAscope experiments. K. Awayan constructed the

interactive web portal. The Tabula Microcebus Consortium constructed the mouse lemur molecular cell atlas. S. Liu and J.E. Ferrell wrote the manuscript with input from all authors.

Figure legends

Fig. 1. **Expression of selected hormone ligands and receptors across mouse lemur cell types. a-g**. Dot plot showing expression of four exemplary sets of hormone ligands and receptors across the ~700 cell types from the mouse lemur cell atlas, including: prolactin (ligand: PRL, receptor: PRLR), adiponectin (ligand: ADIPOQ, receptors: ADIPOR1, ADIPOR2), motilin (ligand: MLN, receptor: MLNR), and resistin (ligand: RETN, receptors: CAP1, DCN, ROR1, TLR4). Cell types are arranged by compartment: epithelial cells (**a**), stromal cells (**b**), endothelial cells (**c**), neural cells (**d**), germ cells (**e**), lymphoid cells (**f**), and myeloid cells (**g**). Within each panel, rows are cell types ordered by tissue of origin. Cell type names are labeled on the right, organs and tissues on the left, and gene symbols on the top (red for ligand genes, blue for receptor genes). Dots represent average gene expression (circle color) and percent of cells positive for the gene (circle size). The red/blue circle edges indicate expression was above threshold (see **Methods**) for the ligand or receptor. Cell types that are potentially low quality (e.g., low cell count) are excluded from this plot. Note that granulosa cells and acinar cells, which presumably are derived from the ovary and pancreas, respectively, were also found in perigonadal and mesenteric fat samples. This was likely caused by accidentally including small pieces of adjacent tissues during tissue procurement. A complete set of figures that display ligand and receptor gene expression for all 84 hormone classes can be found in **Fig. S1** and cross-species expression patterns in **Fig. S12**. **h-j**. Single plane confocal images of mouse lemur kidney assayed by RNAscope for two hormones, motilin (MLN) and angiotensin (AGT), and the proximal tubule marker cubilin (CUBN). Cells were also stained with DAPI to visualize nuclei. Note the MLN and AGT expression in the CUBN+ proximal tubule cells and not in the glomerulus, which is mainly composed of podocytes and glomerular capillary cells. Panel **h** shows a global view (merged 20× tile scans) with a single glomerulus in the view and many proximal tubules. The glomerulus and a representative proximal tubule are outlined by dashed curves. Panels **i** and **j** are magnified views of the boxed areas in **h** showing a proximal tubule and glomerulus respectively. See also **Fig. 3b** for scRNAseq data on MLN and AGT expression across kidney nephron epithelium.

Fig. 2. Hormonal gene expression is cell type specific. a. Clustering of mouse lemur cell types by hormonal gene expression. At the top is a dendrogram of the hierarchical clustering. Clusters of cell types are color-coded, and cluster numbers are labeled as space allows. The cell types included in each cluster are listed in **Table 4**. The lower part of the panel shows a heatmap of relative gene expression levels. Cluster-specific genes are ordered based on the cluster with the highest expression level, with the genes preferentially expressed in the left-hand cell type clusters on the top. Broadly expressed genes (expressed in more than 35% of cell types) are placed in the bottom and ordered from least to most broadly expressed. **b**. UMAP visualization of mouse lemur cell types based on the expression of hormonal genes. Circles are cell types (unique combination of annotation name and tissue of origin) and color-coded by cell type compartment types (epithelial, neural, germ, stromal, endothelial, lymphoid, and myeloid).

1365 Dashed lines circumscribe the cell type clusters as in panel **a**, and cluster IDs and names were
1366 labeled nearby. One extremely distant cluster (# 35. mesothelial cells) was shifted up in UMAP-2
1367 towards the center of the figure for display purposes. **c**. Hormonal (**c**) or full transcriptome (**d**) -
1368 based cell type pairwise distances compared to the benchmark cell annotation-based distance. *r*
1369 represents Pearson's correlation coefficient. Red lines show linear fitting of the data. **e**.
1370 Correlation coefficients of cell type transcriptional distances based on different sets of genes
1371 with the benchmark cell annotation-based distance. **f**. Distributions of expression variability
1372 (dispersion) of the hormonal genes or all protein-coding genes (PCGs).

1373

1374 **Fig. 3. Specific hormonal regulation in related cell types.** Expression of hormone ligand,
1375 synthase, modulator, and receptor genes that are differentially expressed in (**a**) male germ cells
1376 across different stages of spermatogenesis, (**b**) epithelial cells along the spatial axis of the kidney
1377 nephron tubule, (**e**) endothelial cells along the arteriole-to-venule spatial axis of the kidney vasa
1378 recta, (**f**) the CPN2hi vs CPN2lo subtypes of hepatocytes, (**g**) between metastatic tumor cells in
1379 the lung of lemur L2 and the putative cell type of metastatic origin (MUC16+ non-ciliated uterus
1380 epithelial cells) sampled from L3, and (**h**) endothelial cells of the lung and brain compared to
1381 other organs. Panel **c** shows a diagram of the nephron and vasa recta that illustrates the spatial
1382 distribution of the respective cell types, related to panels **b**, **d** and **e**. Panel **d** shows a UMAP
1383 visualization of the vasa recta cells based on expression of all genes. The black line shows the
1384 detected arteriole-to-venule trajectory with the arrow pointing in the direction of blood flow.
1385 Cells are color-coded according to the cell type annotation names in the atlas. Grey lines show
1386 the alignment of the individual cells to the trajectory. Panels **a-b, f-h** are dot plots showing
1387 average gene expression and percent of positive cells of the indicated genes and cell types,
1388 merging data from different lemur individuals. In **a**, cell types are arranged along the course of
1389 the spermatogenesis. In **b**, cell types are arranged according to their spatial distribution along the
1390 kidney nephron tubule. Solid arrowheads point to AGT and MLN; their kidney expression was
1391 confirmed by RNAscope (**Fig. 1h-j**). In **h**, endothelial cells are arranged by tissue of origin. In **e**,
1392 scatter plots show gene expression levels along the arteriole-to-venule trajectory for the
1393 endothelial markers and hormonal genes that are differentially expressed. Shown here is vasa
1394 recta data from one animal. Similar results were obtained from two other lemurs. **PCT**: proximal
1395 convoluted tubule. **PT**: proximal tubule. **PST**: proximal straight tubule (also called loop of Henle
1396 thick descending limb). **LHd**: loop of Henle thin descending limb. **LHa thin**: loop of Henle thin
1397 ascending limb. **LHa thick**: loop of Henle thick ascending limb. **DCT**: distal convoluted tubule.
1398 **MD**: macula densa. **CDp**: collecting duct principal cell. **CDiα**: collecting duct α intercalated cell.
1399 **CDiβ**: collecting duct β intercalated cell. **D** shows the fitted arteriole-to-venule trajectory of the
1400 kidney vasa recta capillary network (upper panel) and single-cell gene expression levels along
1401 the trajectory for the endothelial markers and differentially expressed hormone-related genes.
1402 Shown here are representative results from one of three lemur vasa recta samples. **VRD**: vasa
1403 recta descending section. **VRA**: vasa recta ascending section.

1404

1405 **Fig. 4. The hormonal cell-cell communication network**. **a.** A representation of the network as
1406 constructed by force-directed graph drawing. Nodes (cell types) are color-coded according to the
1407 node outdegree (% of cell types connected to the current node by outgoing edges) and the node

circle size shows the node indegree (% of cell types connected to the current node by incoming edges). Network edges are directed and connect nodes expressing a hormone ligand to all nodes expressing the corresponding hormone receptor. **b-c**. Bar plot of network density (**b**) and average node degree (i.e., the number of connected nodes per node) (**c**) for different biological networks. **d.** Number of ligand and receptor types expressed by the network nodes (cell types), ranked from most to fewest. **e.** Indegrees and outdegrees of the network nodes (cell types), ranked from high to low values. Node degree is normalized to the total number of nodes and cluster size and measures the percentage of cell types connected from or to a network node. **f.** Generality score of all hormone ligands and receptors ranked from the most generally expressed to most selectively expressed. Generality is defined as the percentage of nodes (cluster size normalized) positively expressing the gene(s) involved in ligand synthesis or receptor binding. Also see **Fig. S11a** for generality score defined as the number of cell type clusters positively expressing the gene(s). **g.** Scatter plot showing generality scores of the hormone ligands and corresponding receptors. Each circle is a unique ligand-receptor pair. **h.** Ranking (left) and distribution (right) of Jaccard indices of receptor pairs binding to the same ligand across all hormone receptors.

Fig. 5. Feedback circuits in the hormonal cell-cell communication network. a. Definition of two-node feedback circuits. **b**. Comparison of the number of 2-node feedback circuits identified in the hormonal cell-cell communication network (red dashed line) and that of permuted networks (n = 1000). Permutation preserved node outdegree and indegree. **c-h**. Examples of two-node feedback circuits identified in the network, focusing on the endocrine cell types. Solid black arrows indicate known regulation, dashed orange arrows indicate predicted regulation with partial literature support, and dotted arrows indicate predicted regulation without earlier knowledge that are potentially biologically relevant (red) or insignificant (grey). A leg is considered biologically insignificant if the connected hormone-producing cell type is unlikely to be the major source of the hormone (cells had lower expression levels than the canonical major source cells) and if the signaling is not local. Parentheses are used to group multiple genes that are expressed in the relevant cell type that function either together (&) or independently (/).

Fig. 6. Seasonality of hormone concentrations in the mouse lemur affects almost all cells and tissues. a. Concentrations of twelve hormones measured under long-photoperiod (daily 14:10 h light:dark , summer-like) and short-photoperiod (10:14 h light:dark, winter-like) conditions in captive mouse lemurs. Animals were kept indoors under constant temperature (24°) and with photoperiods alternated between long and short photoperiods every 6 months. Bars represent fold changes in hormone concentration compared to average summer levels. Error bars represent 95% confidence intervals. p-values were calculated by 2-sample t-tests. Data are listed in **Table 8**, collected from literature as follows and supplemented with additional new measurements: estradiol[137,138], testosterone[139–141], thyroxine[137,142] (and additional data in **Table 8**), DHEA[138], cortisol[143] (and additional data in **Table 8**), IGF1[144], melatonin[145], and gut hormones (GIP, PPY, insulin, PYY, and GLP-1)[146,147]. **b.** Mouse lemur cell types targeted by any of these 12 seasonal hormones. Cell types are displayed in the same UMAP plot as in **Fig. 2b**. Circles are cell types and are color coded according to whether they express receptors for any of the 12 hormones. Dashed lines circumscribe the cell type clusters and are colored according to

1451 cell type compartments. **c-l**. Mouse lemur cell types targeted by each of these 12 seasonal
1452 hormones displayed in the same UMAP format as in **b**.

1453

1454 **Fig. 7. Cross-species comparisons of hormonal gene expression across humans, mouse**
1455 **lemurs, and mice. a**. Correlation coefficients of overall expression patterns for all the hormonal
1456 one-to-one orthologs (left) or all one-to-one orthologs (right) between human and lemur vs.
1457 between human and mouse. *p*-value indicates the significance of a higher correlation between
1458 human and lemur vs. between human and mouse, calculated by comparing the two correlation
1459 coefficients using Fisher's Z-transformation. **b**. Comparison of correlation coefficients between
1460 the expression patterns of human and lemur (*x*-axis) versus that between human and mouse (*y*-
1461 axis) for individual hormonal genes. **c**. Comparison of correlation coefficients between the
1462 expression patterns of human and lemur (*x*-axis) versus between lemur and mouse (*y*-axis) for
1463 individual hormonal genes. Black lines in **b** and **c** indicate 1-1 relationship between the two
1464 coefficients. **d**. Dot plot showing expression patterns of highly species-conserved and species-
1465 variable example genes in the 62 orthologous cell types across all three species. Rows are
1466 orthologous genes, indicated with the respective human gene symbols. Columns are cell types,
1467 displayed as triplets of the respective expression in humans, lemurs, and mice. Vertical grey lines
1468 segment different cell type triplets. Cell types are ordered first by compartments, then by tissue,
1469 and finally by species. **e-f**. Species-integrated UMAPs of the male germ cells with cells color
1470 coded by species (**e**) or spermatogenesis stage (**f**). Black lines indicate the identified
1471 spermatogenesis trajectory with arrows pointing to the direction of maturation. **g**. Dot plot
1472 showing cross-species expression patterns of spermatogenesis stage-specific hormonal genes in
1473 germ cells grouped and ordered by the integrated spermatogenesis trajectory. Cell grouping in
1474 the UMAP format is shown in **Fig. S13a**. **e**. Scatter plots showing the species-conserved or
1475 species-variable expression patterns of example genes in **g**. Points are single cells color coded by
1476 species. Solid curves show a moving average of the expression level along the spermatogenesis
1477 trajectory. In panels **d**, **g**, and **h**, colored bars next to the genes indicate the species conservation
1478 patterns as in panels **b**-**c**.

1479

1480

1481 **Fig. S1. Dot plot of hormone ligand, receptor, and modulator gene expression for 84 classes**
1482 **of hormones across the mouse lemur cell atlas.** Each dot plot shows one of the 84 hormone
1483 groups and one of the five cell compartment groups (1. epithelial/neural/germ cells (combined
1484 for space saving); 2. endothelial cells; 3. stromal cells; 4. lymphoid cells; and 5. myeloid cells).
1485 The hormone group name and cell compartment type is indicated on the top right of the figure.
1486 The dot plots are arranged in a polar coordinate style. Radial lines represent individual cell types,
1487 with cell type names labeled inside the inner circle and the tissue source labeled outside the outer
1488 circle. Cell types are arranged, by either their tissue of origin or by their cell type name. Circular
1489 arcs represent the related genes for this hormone group (red for ligands, light red for synthases
1490 and processing enzymes, green for modulators, and blue for receptor genes). The dark colored
1491 dots on the intersections of the radial lines and circular arcs depict mean gene expression levels
1492 (by dot shade) and percent of positive cells (by dot size) for the respective gene and cell type.

1493 The outermost red or blue dots indicate positive expression of one of the hormone(s) (red) or
1494 hormone receptor(s) (blue), or both (purple) for the hormone group by the respective cell type
1495 (see **Methods**). The outermost grey dots indicate potentially low-quality cell types (e.g., low cell
1496 number (<10) and pancreatic cells that show notable signal contamination) with outlines
1497 indicating whether or not the cell type expresses one the hormone ligand(s) (red outline),
1498 receptor(s) (blue outline), both (purple outline), or neither (no outline). These figures can be
1499 assessed interactively at https://tabula-microcebus.ds.czbiohub.org/hormone-atlas.

1500

1501 **Fig. S2. Protein sequences of hormonal genes are generally more similar between human**
1502 **and mouse lemur than human and mouse. a**. Scatter plot comparing pairwise gene sequence
1503 identity between human and lemur vs. human and mouse. Each circle is a hormone-related
1504 protein. Sequences were aligned by the Needleman-Wunsch algorithm and sequence identity was
1505 calculated as the percentage of identical amino acids. Points below the red line are proteins more
1506 similar between human and mouse lemur than between human and mouse. **b**. Bar plot showing
1507 mean and 95% confidence interval of the average sequence identity between human and lemur
1508 vs. human and mouse. Grey dots show individual genes.

1509

1510 **Fig. S3. Number of positive cell types for each hormone ligand and receptor when changing**
1511 **the parameters for adaptive thresholding.** Parameters include cell type mean expression (**a**),
1512 percent of mean expression relative to the maximally expressing cell types separately for
1513 circulating peptide hormones (ligand genes) (**b**) or small molecule hormones (synthase genes)
1514 and hormone receptors (**c**), and the percent of positive cells in a cell type (**d**). Red vertical lines
1515 represent the parameters used in the follow-up analysis. Each row represents one hormone or
1516 receptor, ordered by the number of positive cell types at the selected parameter.

1517

1518 **Fig. S4. Cell types clustered similarly in both sexes and across sampled mouse lemurs.**
1519 Shown here are cell type clustering dendrograms with cluster IDs labeled nearby and two color
1520 bars indicating the lemur individual and sex the cell type sampled from. The two dendrograms
1521 compare cell type clustering patterns when separating (right) or not separating (left) immune
1522 populations from different lemur individuals.

1523

1524 **Fig. S5. Comparison of cell type clustering by the hormonal genes with that by the full**
1525 **transcriptome. a.** UMAP visualization of mouse lemur cell types based on the full
1526 transcriptome. Circles (cell types) are color-coded by cell compartment types (epithelial, neural,
1527 germ, stromal, endothelial, lymphoid, and myeloid). Dashed lines circumscribe cell type clusters
1528 as in **Fig. 2a-b** and cluster IDs and names are labeled next to the cell type clusters. Cell types
1529 that were clustered by the hormonal genes but not the full transcriptome are labeled separately
1530 (i.e., 31B and 31A; 58A, 58B and 58C). Note some cell types that formed discrete clusters based
1531 on hormonal gene expression intermingled with other clusters when mapped based on the non-
1532 hormonal transcriptome (e.g., cluster 46-52), and therefore were annotated together. **b-d**. Scatter

1533 plots and correlation of cell type pairwise distances based on hormonal genes vs. that of all genes
1534 (**b**), hormonal genes vs. Cell Ontology (**c**), and all genes vs. Cell Ontology (**d**). **e**. Bar plot of
1535 correlation coefficients comparing cell type pairwise distances of different metrics compared to a
1536 benchmark Cell Ontology-based distance. Also see **Fig. 2e** for comparisons with the benchmark
1537 of cell annotation-based distances.

1538

1539 **Fig. S6. Heatmap representation of cell type pairwise distances based on the hormonal**
1540 **genes (a), the full transcriptome (b), the cell type annotations (c), and Cell Ontology (d).**
1541 Cell types were ordered by cluster as in **Fig. 2a**, and cluster IDs were labeled along the diagonal
1542 for large clusters.

1543

1544 **Fig. S7. Classification of mouse lemur cell types using only the hormone ligand or the**
1545 **receptor genes. a-b**, UMAP visualization of cell types based on the transcriptional distances of
1546 only the hormone ligands/modulators (**a**) or the hormone receptors (**b**). Circles (cell types) are
1547 color-coded by the cell compartment types (epithelial, neural, germ, stromal, endothelial,
1548 lymphoid, and myeloid). Dashed lines circumscribe cell type clusters as in **Fig. 2a-b** and cluster
1549 IDs are annotated nearby. As UMAPs qualitatively display relationships among data points, the
1550 extremely distant clusters in panel **a** (i.e., cluster 35. mesothelial cells by hormone ligand genes)
1551 were shifted towards the center of the figure for display purposes. **c.** Cluster averaged silhouette
1552 values of the 74 cell type clusters by both hormone ligand and receptor genes (black), only the
1553 hormone ligand genes (red), only the hormone receptor genes (blue), or the non-hormonal
1554 transcriptome (blank). The silhouette values are a measure of how well each cell type cluster was
1555 classified (see **Methods**). Asterisks (*****) indicate clusters with only a single cell type, thus
1556 silhouette values cannot be calculated.

1557

1558 **Fig. S8. Hormonal gene expression in two hepatocyte subtypes plotted separately for male**
1559 **and female animals** (in comparison to **Fig. 3f).**

1560

1561 **Fig. S9. The hormonal cell-cell communication network is robust to edge removal.**
1562 Distribution of network density (**a**) and number of 2-node feedback circuits (**b**) in networks
1563 where 10% of ligand-receptor connections were randomly removed.

1564

1565 **Fig. S10. Node properties of the hormonal cell-cell communication network.** Heatmap of
1566 indegree, outdegree, number of hormone ligands and receptors expressed, and six node centrality
1567 measurements (hubs, authorities, incloseness, outcloseness, pagerank, and betweenness) for all
1568 nodes (cell types) of the hormonal cell-cell communication network. Because the scales of the
1569 node properties are different, shown here are normalized values linearly scaled by median and
1570 median-absolute-deviation. Cell types (columns) are ordered by the clustering of the hormonal

genes (as in **Fig. 2a**) and cluster numbers are labeled as space allowed. Node properties (rows) are ordered by hierarchical clustering of the normalized values.

Fig. S11. Generality scores for the hormone ligands and receptors. a. Generality score, defined as the number of clusters with positive expression of the ligand or receptor (see **Fig. 4f** for comparison), ranked from most generally expressed to most selectively expressed. **b-c**. Fitting the distribution of the ligand and receptor generality scores. Normal, exponential, log-normal, and gamma distributions failed to fit the distribution (**b**). The tail of the distribution can be approximated by a power law distribution $prob(x) \propto x^{-\alpha}$ for $x \geq x_{min}$ (**c**).

Fig. S12. Expression of the hormonal genes across human, lemur, and mouse cell types. Expression is visualized by a dot plot with dot color indicating the cell type average expression and dot size indicating the percent of positive cells in the cell type. Rows are 295 one-to-one-to-one orthologs of the hormonal genes, labeled with the respective human symbols, and ordered alphabetically. Columns are arranged as triplets showing respective expressions in humans, lemurs, and mice. Triplets of different cell types are segregated by vertical gray lines. The orthologous cell type triplets are ordered first by compartments (e.g., epithelial, stromal), then by tissue, and lastly by the cell type annotation.

Fig. S13. Cross-species comparison of hormonal gene expression related to examples in Fig. 3. **a**. Group of male germ cells by the species-integrated trajectory, related to **Fig. 7g**. **b**. Expression of the spermatogenesis stage-specific hormonal genes identified in **Fig. 3a** across human, lemur, and mouse. Shown here are examples with variable expression patterns across the three species. Also see **Fig. 7g-h** for additional examples with either conserved or variable expression patterns across the three species. **c-d**. Expression of the hepatocyte subtype related hormonal genes in the two hepatocyte subtypes across human, lemur, and mouse. The two panels separately show the genes with conserved (**c**) or variable (**d**) expression patterns across the three species. **a**. Expression of the lung-specific hormone signatures in the lung and muscle endothelial cells across human, lemur, and mouse.

Supplemental Tables

Table 1. Genes involved in the biosynthesis and sensing of 84 classes of hormones. Rows show hormones and columns show the hormone class name, hormone name(s), type of hormones, symbol of the human genes for the respective hormone ligands, synthases and other enzymes, receptors, and plasma binding proteins, whether the hormone synthesis or maturation requires coordination of multiple tissues, years discovered, classical sites of secretion and targets, approximate plasma concentrations in humans, and references.

1608

1609 **Table 2. Lemur and mouse orthologs of the human hormonal genes in Table 1.** Rows show
1610 genes and columns show gene type, NCBI and Ensembl gene IDs, NCBI and Ensembl gene
1611 symbols of human, lemur, and mouse genes respectively, as well as the ortholog type for the
1612 human-lemur and human-mouse ortholog mapping. Each row shows a unique human gene.
1613 Entries in columns "Symbol_Lemur" and "Symbol_Lemur" may include multiple genes
1614 (separated by commas) for one-to-many mappings. The "all orthology" tab includes the
1615 orthology mapping for all hormonal genes. The "non one-to-one orthology" tab shows only the
1616 genes with non one-to-one mapping in either lemur or mouse. The "cross-species missing" tabs
1617 show the genes with one-to-one orthology mapping but were not included in the cross-species
1618 analysis because they were missing from one or more of the analyzed datasets.

1619

1620 **Table 3. Cell types with positive expression of each of the hormones and receptors.** Rows
1621 are hormone ligands or receptors and columns show the respective hormone class, hormone
1622 name(s), hormone type, entry type (ligand or receptor), related genes, and list of positive cell
1623 types.

1624

1625 **Table 4. Clusters of mouse lemur cell types according to the expression of hormonal genes.**
1626 Rows show clusters and columns show cluster ID, name, cell types included in the cluster, and
1627 the hormones, receptors, and hormone-related genes that were positively expressed in the
1628 majority (≥50%) of the cluster cell types.

1629

1630 **Table 5. Hormones that regulate or are produced by the anterior pituitary neuroendocrine**
1631 **cells.** Rows show the hormones and hormone receptors expressed in individual pituitary
1632 neuroendocrine cell types. Columns show the corresponding genes, hormone names, and
1633 upstream/downstream cell types.

1634

1635 **Table 6. Generality scores of the hormone ligands, modulators and receptors.** Rows show
1636 hormone ligands, modulators, or receptors, ordered by descending generality. Columns show
1637 entry types, symbols of human and mouse lemur genes, whether the entry includes a single or
1638 multiple genes, and generality scores calculated as the percentage of positive cell types and the
1639 number of positive clusters.

1640

1641 **Table 7. Two node feedback circuits detected from the mouse lemur hormone cell-cell**
1642 **communication network.** Rows show the detected circuits and columns show the two cell types
1643 and hormone signaling that connects the cell types.

Table 8. Measurements of concentrations of mouse lemur seasonally-changing hormones. Rows show individual measurements and columns show the season of measurements, concentration, hormone names and concentration unit, as well as the samples used in the measurements.

References

1. W. M. Bayliss, E. H. S. The mechanism of pancreatic secretion. *J. Physiol.* **28**, 325 (1902).
2. Takei, Y., Ando, H. & Tsutsui, K. *Handbook of Hormones: Comparative Endocrinology for Basic and Clinical Research*. (Academic Press, 2015).
3. Tata, J. R. One hundred years of hormones. *EMBO Rep.* **6**, 490 (2005).
4. Lewis, G. F. & Brubaker, P. L. The discovery of insulin revisited: lessons for the modern era. *J. Clin. Invest.* **131**, (2021).
5. Horby, P. *et al.* Dexamethasone in Hospitalized Patients with Covid-19. *N. Engl. J. Med.* **384**, (2021).
6. Sterne, J. A. C. *et al.* Association Between Administration of Systemic Corticosteroids and Mortality Among Critically Ill Patients With COVID-19: A Meta-analysis. *JAMA* **324**, (2020).
7. Scheja, L. & Heeren, J. The endocrine function of adipose tissues in health and cardiometabolic disease. *Nat. Rev. Endocrinol.* **15**, 507–524 (2019).
8. Jabbour, H. N., Kelly, R. W., Fraser, H. M. & Critchley, H. O. D. Endocrine regulation of menstruation. *Endocr. Rev.* **27**, 17–46 (2006).
9. Deb, A., Deshmukh, B., Ramteke, P., Bhati, F. K. & Bhat, M. K. Resistin: A journey from metabolism to cancer. *Transl. Oncol.* **14**, 101178 (2021).
10. Ezran, C. *et al.* The Mouse Lemur, a Genetic Model Organism for Primate Biology, Behavior, and Health. *Genetics* **206**, 651–664 (2017).
11. Bons, N., Rieger, F., Prudhomme, D., Fisher, A. & Krause, K. H. Microcebus murinus: a useful primate model for human cerebral aging and Alzheimer's disease? *Genes Brain Behav.* **5**, (2006).
12. Languille, S. *et al.* The grey mouse lemur: a non-human primate model for ageing studies. *Ageing Res. Rev.* **11**, (2012).
13. Kraska, A. *et al.* Age-associated cerebral atrophy in mouse lemur primates. *Neurobiol. Aging* **32**, 894–906 (2011).
14. Pifferi, F. *et al.* Promoting healthspan and lifespan with caloric restriction in primates. *Commun Biol* **2**, 107 (2019).
15. The Tabula Microcebus Consortium. Tabula Microcebus: A transcriptomic cell atlas of mouse lemur, an emerging primate model organism. *bioRxiv* 2021.12.12.469460 (2021) doi:10.1101/2021.12.12.469460.
16. The Tabula Microcebus Consortium *et al.* Mouse lemur transcriptomic atlas elucidates primate genes, physiology, disease, and evolution. *bioRxiv* 2022.08.06.503035 (2022) doi:10.1101/2022.08.06.503035.
17. Casey, K. M., Karanewsky, C. J., Pendleton, J. L., Krasnow, M. R. & Albertelli, M. A. Fibrous Osteodystrophy, Chronic Renal Disease, and Uterine Adenocarcinoma in Aged Gray Mouse Lemurs (*Microcebus murinus*). *Comparative Medicine* vol. 71 256–266 Preprint at https://doi.org/10.30802/aalas-cm-20-000078 (2021).
18. Kastin, A. *Handbook of Biologically Active Peptides*. (Academic Press, 2013).
19. Romere, C. *et al.* Asprosin, a Fasting-Induced Glucogenic Protein Hormone. *Cell* **165**, 566–579

(2016).
20. Itoh, N., Ohta, H. & Konishi, M. Endocrine FGFs: Evolution, Physiology, Pathophysiology, and Pharmacotherapy. *Front. Endocrinol.* **6**, 154 (2015).
21. Hammond, G. L. Plasma steroid-binding proteins: primary gatekeepers of steroid hormone action. *J. Endocrinol.* **230**, R13–25 (2016).
22. Geoffrey L. Hammond, Lesley A. Hill, Phillip W. Round. Roles of Plasma Binding Proteins in Modulation of Hormone Action and Metabolism. in *Encyclopedia of Endocrine Diseases (Second Edition)* (ed. Ilpo Huhtaniemi, L. M.) 51–60 (Academic Press, 2019).
23. Wang, M. F. Z. *et al.* Uncovering transcriptional dark matter via gene annotation independent single-cell RNA sequencing analysis. *Nat. Commun.* **12**, 1–10 (2021).
24. Parfait, B. *et al.* Human TIP49b/RUVBL2 gene: genomic structure, expression pattern, physical link to the human CGB/LHB gene cluster on chromosome 19q13.3. *Ann. Genet.* **43**, 69–74 (2000).
25. Riddle, O., Bates, R. W. & Dykshorn, S. W. THE PREPARATION, IDENTIFICATION AND ASSAY OF PROLACTIN—A HORMONE OF THE ANTERIOR PITUITARY. *American Journal of Physiology-Legacy Content* vol. 105 191–216 Preprint at https://doi.org/10.1152/ajplegacy.1933.105.1.191 (1933).
26. Bole-Feysot, C., Goffin, V., Edery, M., Binart, N. & Kelly, P. A. Prolactin (PRL) and its receptor: actions, signal transduction pathways and phenotypes observed in PRL receptor knockout mice. *Endocr. Rev.* **19**, 225–268 (1998).
27. Tovar, S. & Diéguez, C. Prolactin and energy homeostasis: pathophysiological mechanisms and therapeutic considerations. *Endocrinology* vol. 155 659–662 (2014).
28. Paré, P. *et al.* Molecular evolutionary insights from PRLR in mammals. *Gen. Comp. Endocrinol.* **309**, 113791 (2021).
29. Giroud, S. *et al.* The Grey Mouse Lemur Uses Season-Dependent Fat or Protein Sparing Strategies to Face Chronic Food Restriction. *PLoS ONE* vol. 5 e8823 Preprint at https://doi.org/10.1371/journal.pone.0008823 (2010).
30. Terrien, J. *et al.* Metabolic and genomic adaptations to winter fattening in a primate species, the grey mouse lemur (Microcebus murinus). *International Journal of Obesity* vol. 42 221–230 Preprint at https://doi.org/10.1038/ijo.2017.195 (2018).
31. Perret, M. & Aujard, F. Regulation by Photoperiod of Seasonal Changes in Body Mass and Reproductive Function in Gray Mouse Lemurs (Microcebus murinus): Differential Responses by Sex. *Int. J. Primatol.* **22**, 5–24 (2001).
32. Maeda, K. *et al.* cDNA cloning and expression of a novel adipose specific collagen-like factor, apM1 (AdiPose Most abundant Gene transcript 1). *Biochem. Biophys. Res. Commun.* **221**, 286–289 (1996).
33. Zhang, Y. *et al.* Positional cloning of the mouse obese gene and its human homologue. *Nature* **372**, (1994).
34. Galic, S., Oakhill, J. S. & Steinberg, G. R. Adipose tissue as an endocrine organ. *Molecular and Cellular Endocrinology* vol. 316 129–139 Preprint at https://doi.org/10.1016/j.mce.2009.08.018 (2010).
35. Ruan, H. & Dong, L. Q. Adiponectin signaling and function in insulin target tissues. *Journal of Molecular Cell Biology* vol. 8 101–109 Preprint at https://doi.org/10.1093/jmcb/mjw014 (2016).
36. Yamauchi, T. *et al.* Cloning of adiponectin receptors that mediate antidiabetic metabolic effects. *Nature* **423**, 762–769 (2003).
37. He, J., Irwin, D. M., Chen, R. & Zhang, Y.-P. Stepwise loss of motilin and its specific receptor genes in rodents. *J. Mol. Endocrinol.* **44**, 37–44 (2010).
38. Sanger, G. J., Wang, Y., Hobson, A. & Broad, J. Motilin: towards a new understanding of the gastrointestinal neuropharmacology and therapeutic use of motilin receptor agonists. *Br. J. Pharmacol.* **170**, 1323–1332 (2013).
39. Hu, Q., Tan, H. & Irwin, D. M. Evolution of the Vertebrate Resistin Gene Family. *PLoS One* **10**, e0130188 (2015).

40. Schwartz, D. R. & Lazar, M. A. Human Resistin: Found in Translation From Mouse to Man. *Trends Endocrinol. Metab.* **22**, 259 (2011).
41. Zhang, X. *et al.* Neuropeptidomic Analysis Establishes a Major Role for Prohormone Convertase-2 in Neuropeptide Biosynthesis. *J. Neurochem.* **112**, 1168 (2010).
42. Seidah, N. G. The proprotein convertases, 20 years later. *Methods Mol. Biol.* **768**, 23–57 (2011).
43. Sandoval, D. A. & D'Alessio, D. A. Physiology of proglucagon peptides: role of glucagon and GLP-1 in health and disease. *Physiol. Rev.* **95**, 513–548 (2015).
44. Wardlaw, S. L. Hypothalamic proopiomelanocortin processing and the regulation of energy balance. *Eur. J. Pharmacol.* **660**, 213 (2011).
45. Allard, J. B. & Duan, C. IGF-Binding Proteins: Why Do They Exist and Why Are There So Many? *Front. Endocrinol.* **9**, 117 (2018).
46. Bouillon, R., Schuit, F., Antonio, L. & Rastinejad, F. Vitamin D Binding Protein: A Historic Overview. *Front. Endocrinol.* **10**, 484325 (2020).
47. Schneider, C., O'Leary, C. E. & Locksley, R. M. Regulation of immune responses by tuft cells. *Nat. Rev. Immunol.* **19**, 584–593 (2019).
48. Smith, B. *et al.* The OBO Foundry: coordinated evolution of ontologies to support biomedical data integration. *Nat. Biotechnol.* **25**, 1251–1255 (2007).
49. Wang, S. *et al.* Leveraging the Cell Ontology to classify unseen cell types. *Nat. Commun.* **12**, 5556 (2021).
50. Griswold, M. D. Spermatogenesis: The Commitment to Meiosis. *Physiol. Rev.* **96**, 1–17 (2016).
51. Smith, L. B. & Walker, W. H. The regulation of spermatogenesis by androgens. *Seminars in Cell & Developmental Biology* vol. 30 2–13 Preprint at https://doi.org/10.1016/j.semcdb.2014.02.012 (2014).
52. Ruwanpura, S. M., McLachlan, R. I. & Meachem, S. J. Hormonal regulation of male germ cell development. *Journal of Endocrinology* vol. 205 117–131 Preprint at https://doi.org/10.1677/joe-10-0025 (2010).
53. Lishko, P. V., Botchkina, I. L. & Kirichok, Y. Progesterone activates the principal Ca2+ channel of human sperm. *Nature* **471**, 387–391 (2011).
54. Lue, Y. *et al.* Functional role of progestin and the progesterone receptor in the suppression of spermatogenesis in rodents. *Andrology* **1**, 308–317 (2013).
55. Burnicka-Turek, O. *et al.* Inactivation of insulin-like factor 6 disrupts the progression of spermatogenesis at late meiotic prophase. *Endocrinology* **150**, 4348–4357 (2009).
56. Giesecke, T. *et al.* Vasopressin Increases Urinary Acidification via V1a Receptors in Collecting Duct Intercalated Cells. *Journal of the American Society of Nephrology* vol. 30 946–961 Preprint at https://doi.org/10.1681/asn.2018080816 (2019).
57. Pannabecker, T. L. & Dantzler, W. H. Three-dimensional architecture of inner medullary vasa recta. *Am. J. Physiol. Renal Physiol.* **290**, F1355–66 (2006).
58. Kenig-Kozlovsky, Y. *et al.* Ascending Vasa Recta Are Angiopoietin/Tie2-Dependent Lymphatic-Like Vessels. *J. Am. Soc. Nephrol.* **29**, 1097–1107 (2018).
59. Barry, D. M. *et al.* Molecular determinants of nephron vascular specialization in the kidney. *Nat. Commun.* **10**, 5705 (2019).
60. Backes, F. J. *et al.* Estrogen receptor-alpha as a predictive biomarker in endometrioid endometrial cancer. *Gynecol. Oncol.* **141**, 312–317 (2016).
61. Shen, F., Gao, Y., Ding, J. & Chen, Q. Is the positivity of estrogen receptor or progesterone receptor different between type 1 and type 2 endometrial cancer? *Oncotarget* vol. 8 506–511 Preprint at https://doi.org/10.18632/oncotarget.13471 (2017).
62. Nakanishi, M. & Rosenberg, D. W. Multifaceted roles of PGE2 in inflammation and cancer. *Semin. Immunopathol.* **35**, 123–137 (2013).
63. Ke, J. *et al.* Prostaglandin E2 (PGE2) promotes proliferation and invasion by enhancing SUMO-1 activity via EP4 receptor in endometrial cancer. *Tumour Biol.* **37**, 12203–12211 (2016).
64. Lee, J. O. *et al.* Resistin, a fat-derived secretory factor, promotes metastasis of MDA-MB-231

1791 human breast cancer cells through ERM activation. *Sci. Rep.* **6**, 18923 (2016).
1792 65. Groneberg, D. A., Springer, J. & Fischer, A. Vasoactive intestinal polypeptide as mediator of
1793 asthma. *Pulm. Pharmacol. Ther.* **14**, 391–401 (2001).
1794 66. Barnes, K. & Turner, A. J. The endothelin system and endothelin-converting enzyme in the brain:
1795 molecular and cellular studies. *Neurochem. Res.* **22**, 1033–1040 (1997).
1796 67. Wilhelms, D. B. *et al.* Deletion of prostaglandin E2 synthesizing enzymes in brain endothelial cells
1797 attenuates inflammatory fever. *J. Neurosci.* **34**, 11684–11690 (2014).
1798 68. Engström, L. *et al.* Lipopolysaccharide-induced fever depends on prostaglandin E2 production
1799 specifically in brain endothelial cells. *Endocrinology* **153**, 4849–4861 (2012).
1800 69. Frankenstein, Z., Alon, U. & Cohen, I. R. The immune-body cytokine network defines a social
1801 architecture of cell interactions. *Biol. Direct* **1**, (2006).
1802 70. Giot, L. *et al.* A protein interaction map of Drosophila melanogaster. *Science* **302**, 1727–1736
1803 (2003).
1804 71. Yook, S. H., Oltvai, Z. N. & Barabási, A. L. Functional and topological characterization of protein
1805 interaction networks. *Proteomics* **4**, (2004).
1806 72. Rolland, T. *et al.* A proteome-scale map of the human interactome network. *Cell* **159**, 1212–1226
1807 (2014).
1808 73. Costanzo, M. *et al.* The Genetic Landscape of a Cell. *Science* **327**, 425–431 (2010).
1809 74. Barabási, A.-L. Scale-Free and Hierarchical Structures in Complex Networks. *AIP Conference*
1810 *Proceedings* Preprint at https://doi.org/10.1063/1.1571285 (2003).
1811 75. Iams, W. T. & Lovly, C. M. Molecular Pathways: Clinical Applications and Future Direction of
1812 Insulin-like Growth Factor-1 Receptor Pathway Blockade. *Clin. Cancer Res.* **21**, 4270–4277 (2015).
1813 76. Ghosh, P., Dahms, N. M. & Kornfeld, S. Mannose 6-phosphate receptors: new twists in the tale. *Nat.*
1814 *Rev. Mol. Cell Biol.* **4**, 202–212 (2003).
1815 77. Larhammar, D. & Salaneck, E. Molecular evolution of NPY receptor subtypes. *Neuropeptides* **38**,
1816 141–151 (2004).
1817 78. Kilpatrick, L. E., Humphrys, L. J. & Holliday, N. D. A G protein-coupled receptor dimer imaging
1818 assay reveals selectively modified pharmacology of neuropeptide Y Y1/Y5 receptor heterodimers.
1819 *Mol. Pharmacol.* **87**, (2015).
1820 79. Gehlert, D. R., Schober, D. A., Morin, M. & Berglund, M. M. Co-expression of neuropeptide Y Y1
1821 and Y5 receptors results in heterodimerization and altered functional properties. *Biochem.*
1822 *Pharmacol.* **74**, 1652–1664 (2007).
1823 80. Almabouada, F. *et al.* Adiponectin Receptors Form Homomers and Heteromers Exhibiting Distinct
1824 Ligand Binding and Intracellular Signaling Properties. *J. Biol. Chem.* **288**, 3112–3125 (2013).
1825 81. Keshvari, S. *et al.* Characterisation of the adiponectin receptors: the non-conserved N-terminal
1826 region of AdipoR2 prevents its expression at the cell-surface. *Biochem. Biophys. Res. Commun.* **432**,
1827 28–33 (2013).
1828 82. Maslov, S. & Sneppen, K. Specificity and stability in topology of protein networks. *Science* **296**,
1829 910–913 (2002).
1830 83. Dwyer, A. A. & Quinton, R. Anatomy and Physiology of the Hypothalamic-Pituitary-Gonadal
1831 (HPG) Axis. *Advanced Practice in Endocrinology Nursing* 839–852 Preprint at
1832 https://doi.org/10.1007/978-3-319-99817-6_43 (2019).
1833 84. Martín-Estal, I., de la Garza, R. G. & Castilla-Cortázar, I. Intrauterine Growth Retardation (IUGR)
1834 as a Novel Condition of Insulin-Like Growth Factor-1 (IGF-1) Deficiency. *Rev. Physiol. Biochem.*
1835 *Pharmacol.* **170**, 1–35 (2016).
1836 85. Inagaki, T. *et al.* Inhibition of growth hormone signaling by the fasting-induced hormone FGF21.
1837 *Cell Metab.* **8**, 77–83 (2008).
1838 86. Hartig, S. M. & Cox, A. R. Paracrine signaling in islet function and survival. *J. Mol. Med.* **98**, 451–
1839 467 (2020).
1840 87. Habegger, K. M. *et al.* The metabolic actions of glucagon revisited. *Nat. Rev. Endocrinol.* **6**, 689–
1841 697 (2010).

88. Habegger, K. M. *et al.* Fibroblast growth factor 21 mediates specific glucagon actions. *Diabetes* **62**, 1453–1463 (2013).
89. Mu, J. *et al.* FGF21 analogs of sustained action enabled by orthogonal biosynthesis demonstrate enhanced antidiabetic pharmacology in rodents. *Diabetes* **61**, 505–512 (2012).
90. Mancuso, E. *et al.* Insulin-like growth factor-1 is a negative modulator of glucagon secretion. *Oncotarget* **8**, 51719–51732 (2017).
91. Kopchick, J. J., Berryman, D. E., Puri, V., Lee, K. Y. & Jorgensen, J. O. L. The effects of growth hormone on adipose tissue: old observations, new mechanisms. *Nat. Rev. Endocrinol.* **16**, 135–146 (2020).
92. Carré, N. & Binart, N. Prolactin and adipose tissue. *Biochimie* vol. 97 16–21 Preprint at https://doi.org/10.1016/j.biochi.2013.09.023 (2014).
93. Iwen, K. A. *et al.* Melanocortin crosstalk with adipose functions: ACTH directly induces insulin resistance, promotes a pro-inflammatory adipokine profile and stimulates UCP-1 in adipocytes. *J. Endocrinol.* **196**, (2008).
94. Sarmento-Cabral, A. *et al.* Adipokines (Leptin, Adiponectin, Resistin) Differentially Regulate All Hormonal Cell Types in Primary Anterior Pituitary Cell Cultures from Two Primate Species. *Sci. Rep.* **7**, 43537 (2017).
95. Ferrell, J. E., Jr. Self-perpetuating states in signal transduction: positive feedback, double-negative feedback and bistability. *Curr. Opin. Cell Biol.* **14**, 140–148 (2002).
96. Tezze, C., Romanello, V. & Sandri, M. FGF21 as Modulator of Metabolism in Health and Disease. *Front. Physiol.* **10**, 419 (2019).
97. Kineman, R. D., Del Rio-Moreno, M. & Sarmento-Cabral, A. 40 YEARS of IGF1: Understanding the tissue-specific roles of IGF1/IGF1R in regulating metabolism using the Cre/loxP system. *J. Mol. Endocrinol.* **61**, T187–T198 (2018).
98. Petter-Rousseaux, A. Age of Microcebus murinus at the onset of testicular development : Preliminary observations on photoperiodic effect. *Ann. Biol. anim. Bioch. Biophys.* **19**, 1801–1806 (1979).
99. Perret, M. Environmental and social determinants of sexual function in the male lesser mouse lemur (Microcebus murinus). *Folia Primatol.* **59**, 1–25 (1992).
100. Epelbaum, J. & Terrien, J. Mini-review: Aging of the neuroendocrine system: Insights from nonhuman primate models. *Prog. Neuropsychopharmacol. Biol. Psychiatry* **100**, (2020).
101. Murat, F. *et al.* The molecular evolution of spermatogenesis across mammals. *Nature* **613**, 308–316 (2023).
102. Champaneria, M. C., Modlin, I. M., Kidd, M. & Eick, G. N. Friedrich Feyrter: a precise intellect in a diffuse system. *Neuroendocrinology* **83**, (2006).
103. Karin, O. *et al.* A new model for the HPA axis explains dysregulation of stress hormones on the timescale of weeks. *Mol. Syst. Biol.* **16**, e9510 (2020).
104. Perret, M. & Aujard, F. Daily hypothermia and torpor in a tropical primate: synchronization by 24-h light-dark cycle. *American Journal of Physiology-Regulatory, Integrative and Comparative Physiology* vol. 281 R1925–R1933 Preprint at https://doi.org/10.1152/ajpregu.2001.281.6.r1925 (2001).
105. Gwinner, E. *Circannual Rhythms: Endogenous Annual Clocks in the Organization of Seasonal Processes*. (Springer, 2011).
106. Lincoln, G. A brief history of circannual time. *J. Neuroendocrinol.* **31**, (2019).
107. Tendler, A. *et al.* Hormone seasonality in medical records suggests circannual endocrine circuits. *Proc. Natl. Acad. Sci. U. S. A.* **118**, (2021).
108. Sailani, M. R. *et al.* Deep longitudinal multiomics profiling reveals two biological seasonal patterns in California. *Nat. Commun.* **11**, 4933 (2020).
109. Dopico, X. C. *et al.* Widespread seasonal gene expression reveals annual differences in human immunity and physiology. *Nat. Commun.* **6**, 7000 (2015).
110. Moriyama, M., Hugentobler, W. J. & Iwasaki, A. Seasonality of Respiratory Viral Infections.

1893 *Annual review of virology* **7**, (2020).
1894 111. Marti-Soler, H. *et al.* Seasonal Variation of Overall and Cardiovascular Mortality: A Study in 19
1895 Countries from Different Geographic Locations. *PLoS One* **9**, e113500 (2014).
1896 112. Kurlansik, S. L. & Ibay, A. D. Seasonal affective disorder. *Am. Fam. Physician* **86**, (2012).
1897 113. Chen, G., Ning, B. & Shi, T. Single-Cell RNA-Seq Technologies and Related Computational Data
1898 Analysis. *Front. Genet.* **10**, 317 (2019).
1899 114. Tabula Muris Consortium. A single-cell transcriptomic atlas characterizes ageing tissues in the
1900 mouse. *Nature* **583**, 590–595 (2020).
1901 115. The Tabula Muris Consortium. Single-cell transcriptomics of 20 mouse organs creates a Tabula
1902 Muris. *Nature* **562**, 367–372 (2018).
1903 116. Han, X. *et al.* Mapping the Mouse Cell Atlas by Microwell-Seq. *Cell* **172**, (2018).
1904 117. Cao, C. *et al.* Comprehensive single cell transcriptome lineages of a proto-vertebrate. *Nature* **571**,
1905 349 (2019).
1906 118. Han, L. *et al.* Single-cell atlas of a non-human primate reveals new pathogenic mechanisms of
1907 COVID-19. *Cold Spring Harbor Laboratory* 2020.04.10.022103 (2020)
1908 doi:10.1101/2020.04.10.022103.
1909 119. Qu, J. *et al.* A reference single-cell regulomic and transcriptomic map of cynomolgus monkeys. *Nat.*
1910 *Commun.* **13**, 4069 (2022).
1911 120. Tabula Sapiens Consortium* *et al.* The Tabula Sapiens: A multiple-organ, single-cell transcriptomic
1912 atlas of humans. *Science* **376**, eabl4896 (2022).
1913 121. van den Beld, A. W. *et al.* The physiology of endocrine systems with ageing. *The Lancet Diabetes &*
1914 *Endocrinology* **6**, 647–658 (2018).
1915 122. National Research Council. *Guide for the Care and Use of Laboratory Animals: Eighth Edition*.
1916 (2010).
1917 123. Chae, M., Danko, C. G. & Lee Kraus, W. groHMM: a computational tool for identifying
1918 unannotated and cell type-specific transcription units from global run-on sequencing data. *BMC*
1919 *Bioinformatics* **16**, 1–16 (2015).
1920 124. Johnson, M. *et al.* NCBI BLAST: a better web interface. *Nucleic Acids Res.* **36**, (2008).
1921 125. Altschul, S. F., Gish, W., Miller, W., Myers, E. W. & Lipman, D. J. Basic local alignment search
1922 tool. *J. Mol. Biol.* **215**, 403–410 (1990).
1923 126. Macosko, E. Z. *et al.* Highly Parallel Genome-wide Expression Profiling of Individual Cells Using
1924 Nanoliter Droplets. *Cell* **161**, 1202–1214 (2015).
1925 127. McInnes, L., Healy, J. & Melville, J. UMAP: Uniform Manifold Approximation and Projection for
1926 Dimension Reduction. (2018).
1927 128. Meehan, C., Ebrahimian, J., Moore, W. & Meehan, S. *Uniform Manifold Approximation and*
1928 *Projection (UMAP). MATLAB Central File Exchange.*
1929 *https://www.mathworks.com/matlabcentral/fileexchange/71902*. (2021).
1930 129. Reimers, N. & Gurevych, I. Sentence-BERT: Sentence Embeddings using Siamese BERT-Networks.
1931 (2019).
1932 130. Butler, A., Hoffman, P., Smibert, P., Papalexi, E. & Satija, R. Integrating single-cell transcriptomic
1933 data across different conditions, technologies, and species. *Nat. Biotechnol.* **36**, 411–420 (2018).
1934 131. Clauset, A., Shalizi, C. R. & Newman, M. E. J. Power-law distributions in empirical data. *SIAM Rev.*
1935 *Soc. Ind. Appl. Math.* **51**, 661–703 (2009).
1936 132. Travaglini, K. J. *et al.* A molecular cell atlas of the human lung from single-cell RNA sequencing.
1937 *Nature* **587**, 619–625 (2020).
1938 133. Shami, A. N. *et al.* Single-Cell RNA Sequencing of Human, Macaque, and Mouse Testes Uncovers
1939 Conserved and Divergent Features of Mammalian Spermatogenesis. *Dev. Cell* **54**, 529–547.e12
1940 (2020).
1941 134. Ernst, C., Eling, N., Martinez-Jimenez, C. P., Marioni, J. C. & Odom, D. T. Staged developmental
1942 mapping and X chromosome transcriptional dynamics during mouse spermatogenesis. *Nat.*
1943 *Commun.* **10**, 1251 (2019).

135. Zhao, J. *et al.* Adversarial domain translation networks for integrating large-scale atlas-level single-cell datasets. *Nature Computational Science* **2**, 317–330 (2022).
136. Fisher, R. A. Frequency Distribution of the Values of the Correlation Coefficient in Samples from an Indefinitely Large Population. *Biometrika* **10**, 507–521 (1915).
137. Noiret, A. *et al.* Sex-Specific Response to Caloric Restriction After Reproductive Investment in Microcebus murinus: An Integrative Approach. *Front. Physiol.* **11**, (2020).
138. Perret, M. & Aujard, F. Aging and season affect plasma dehydroepiandrosterone sulfate (DHEA-S) levels in a primate. *Exp. Gerontol.* **40**, 582–587 (2005).
139. Dal-Pan, A. *et al.* Caloric restriction or resveratrol supplementation and ageing in a non-human primate: first-year outcome of the RESTRIKAL study in Microcebus murinus. *Age* **33**, (2011).
140. Petter-Rousseaux, A. & Picon, R. Annual variation in the plasma testosterone in Microcebus murinus. *Folia Primatol.* **36**, (1981).
141. Schilling, A. & Perret, M. Removal of the olfactory bulbs modifies the gonadal responses to photoperiod in the lesser mouse lemur (Microcebus murinus). *Biol. Reprod.* **49**, 58–65 (1993).
142. Petter-Rousseaux, A. Annual variations in the plasma thyroxine level in Microcebus murinus. *Gen. Comp. Endocrinol.* **55**, 405–409 (1984).
143. Perret, M. & Predine, J. Effects of long-term grouping on serum cortisol levels in Microcebus murinus (Prosimii). *Horm. Behav.* **18**, 346–358 (1984).
144. Aujard, F., Bluet-Pajot, M. T., Zizzari, P., Perret, M. & Epelbaum, J. IGF-1: a marker of individual life-span in a primate. *Ageing Research* **1**, (2010).
145. Aujard, F. *et al.* Artificially accelerated aging by shortened photoperiod alters early gene expression (Fos) in the suprachiasmatic nucleus and sulfatoxymelatonin excretion in a small primate, Microcebus murinus. *Neuroscience* vol. 105 403–412 Preprint at https://doi.org/10.1016/s0306-4522(01)00202-0 (2001).
146. Giroud, S. *et al.* Gut hormones in relation to body mass and torpor pattern changes during food restriction and re-feeding in the gray mouse lemur. *J. Comp. Physiol. B* **179**, 99–111 (2009).
147. Dal-Pan, A., Blanc, S. & Aujard, F. Resveratrol suppresses body mass gain in a seasonal non-human primate model of obesity. *BMC Physiol.* **10**, (2010).

The Tabula Microcebus Consortium

Name	Email	Lab	Affiliations
Snigdha Agarwal	snigdha.agarwal@czbiohub.org	CZ Biohub	Chan Zuckerberg Biohub, San Francisco, CA, USA.
Aditi Agrawal	aditi.agrawal@czbiohub.org	CZ Biohub	Chan Zuckerberg Biohub, San Francisco, CA, USA.
Ahmad Al-Moujahed	ahmadm@stanford.edu	Albert Wu	Department of Ophthalmology, Stanford University School of Medicine, Stanford, CA, USA.
Alina Alam	alina.ara.alam@gmail.com	Charles Chan	Institute for Stem Cell Biology and Regenerative Medicine, Stanford University School of Medicine, Stanford, CA, USA.
Megan A. Albertelli	albertel@stanford.edu	Megan Albertelli	Department of Comparative Medicine, Stanford University School of Medicine, Stanford, CA, USA.
Paul Allegakoen	paul.allegakoen@ucsf.edu	Franklin Huang	Division of Hematology/Oncology, Department of Medicine, University of California San Francisco, San Francisco, CA, USA.
Thomas Ambrosi	ambrosi@stanford.edu	Charles Chan	Institute for Stem Cell Biology and Regenerative Medicine, Stanford University School of Medicine, Stanford, CA, USA.
Jane Antony	janetony@stanford.edu	Michael Clarke	Institute for Stem Cell Biology and Regenerative Medicine, Stanford University School of Medicine, Stanford, CA, USA.
Steven Artandi	sartandi@stanford.edu	Steven Artandi	Stanford Cancer Institute, Stanford University School of Medicine, Stanford, CA, USA.; Department of Medicine, Stanford University School of Medicine, Stanford, CA, USA.; Department of Biochemistry, Stanford University School of Medicine, Stanford, CA, USA.
Fabienne Aujard	fabienne.aujard@mnhn.fr	Fabienne Aujard	Adaptive Mechanisms and Evolution (MECADEV), UMR 7179, National Center for Scientific Research, National Museum of Natural History, Brunoy, France.
Kyle Awayan	kyle.awayan@czbiohub.org	CZ Biohub	Chan Zuckerberg Biohub, San Francisco, CA, USA.
Ankit Baghel	abaghel@stanford.edu	Philip Beachy	Department of Biology, Stanford University, Stanford, CA, USA.
Isaac Bakerman	isaacbakerman@email.arizona.edu	Patricia Nguyen	Department of Medicine, Division of Cardiovascular Medicine, Stanford University, Stanford, CA, USA.
Trygve E. Bakken	trygveb@alleninstitute.org	Allen Institute for Brain Science	Human Cell Types Department, Allen Institute for Brain Science, Seattle, WA, USA.
Jalal Baruni	baruni@stanford.edu	Mark Krasnow; Liqun Luo	Department of Anesthesiology, Perioperative and Pain Medicine, Stanford University School of Medicine, Stanford, CA, USA.; Department of Biochemistry, Stanford University School of Medicine, Stanford, CA, USA.; Department of Biology, Stanford University, Stanford, CA, USA.; Howard Hughes Medical Institute, USA.
Philip Beachy	pbeachy@stanford.edu	Philip Beachy	Institute for Stem Cell Biology and Regenerative Medicine, Stanford University School of Medicine, Stanford, CA, USA.; Department of Developmental Biology, Stanford University School of Medicine, Stanford, CA, USA.; Department of Urology, Stanford University School of Medicine, Stanford, CA, USA.; Department of Chemical and Systems Biology, Stanford University School of Medicine, Stanford, CA, USA.
Biter Bilen	biterbilen@gmail.com	Thomas Rando	Department of Neurology and Neurological Sciences, Stanford University School of Medicine, Stanford, CA, USA.
Olga Botvinnik	olga.botvinnik@gmail.com	CZ Biohub	Chan Zuckerberg Biohub, San Francisco, CA, USA.
Scott D. Boyd	sboyd1@stanford.edu	Scott Boyd	Department of Pathology, Stanford University School of Medicine, Stanford, CA, USA.
Deviana Burhan	deviana.burhan@ucsf.edu	Bruce Wang	Department of Medicine and Liver Center, University of California San Francisco, San Francisco, CA, USA.
Kerriann M. Casey	kmcasey@stanford.edu	Kerriann Casey	Department of Comparative Medicine, Stanford University School of Medicine, Stanford, CA, USA.
Charles Chan	chazchan@stanford.edu	Charles Chan	Institute for Stem Cell Biology and Regenerative Medicine, Stanford University School of Medicine, Stanford, CA, USA.
Charles A. Chang	changca@stanford.edu	Seung Kim	Department of Developmental Biology, Stanford University School of Medicine, Stanford, CA, USA.; Stanford Diabetes Research Center, Stanford, CA, USA.
Stephen Chang	scthree@stanford.edu	Mark Krasnow	Department of Biochemistry, Stanford University School of Medicine, Stanford, CA, USA.; Department of Medicine, Division of Cardiovascular Medicine, Stanford University, Stanford, CA, USA.; Howard Hughes Medical Institute, USA.
Ming Chen	ming2017@stanford.edu	Douglas Vollrath	Department of Genetics, Stanford University School of Medicine, Stanford, CA, USA.
Michael F. Clarke	mfclarke@stanford.edu	Michael Clarke	Institute for Stem Cell Biology and Regenerative Medicine, Stanford University School of Medicine, Stanford, CA, USA.
Sheela Crasta	sheelat@stanford.edu	CZ Biohub	Chan Zuckerberg Biohub, San Francisco, CA, USA.
Rebecca Culver	becca.culver@gmail.com	Kerwyn Casey Huang	Department of Genetics, Stanford University School of Medicine, Stanford, CA, USA.

Jessica D'Addabbo	jcdaddab@stanford.edu	Patricia Nguyen	Division of Cardiovascular Medicine, Stanford University, Stanford, CA, USA.; Stanford Cardiovascular Institute, Stanford, CA, USA.
Spyros Darmanis	spyros.darmanis@czbiohub.org	CZ Biohub	Chan Zuckerberg Biohub, San Francisco, CA, USA.
Roozbeh Dehghannasiri	rdehghan@stanford.edu	Julia Salzman	Department of Biochemistry, Stanford University School of Medicine, Stanford, CA, USA.; Department of Biomedical Data Science, Stanford University, Stanford, CA, USA.
Song-Lin Ding	songd@alleninstitute.org	Allen Institute for Brain Science	Human Cell Types Department, Allen Institute for Brain Science, Seattle, WA, USA.
Connor V. Duffy	cvduffy@stanford.edu	Silvana Konermann	Department of Genetics, Stanford University School of Medicine, Stanford, CA, USA.; Howard Hughes Medical Institute, USA.
Jacques Epelbaum	jacques.epelbaum@inserm.fr	Jacques Epelbaum	Adaptive Mechanisms and Evolution (MECADEV), UMR 7179, National Center for Scientific Research, National Museum of Natural History, Brunoy, France.; Unité Mixte de Recherche en Santé 894 INSERM, Centre de Psychiatrie et Neurosciences, Université Paris Descartes, Sorbonne, Paris, France
F. Hernán Espinoza	hespinoz@stanford.edu	Mark Krasnow	Department of Biochemistry, Stanford University School of Medicine, Stanford, CA, USA.; Howard Hughes Medical Institute, USA.
Camille Ezran	camillee@stanford.edu	Mark Krasnow	Department of Biochemistry, Stanford University School of Medicine, Stanford, CA, USA.; Howard Hughes Medical Institute, USA.
Jean Farup	jean@biomed.au.dk	Thomas Rando	Department of Neurology and Neurological Sciences, Stanford University School of Medicine, Stanford, CA, USA.; Department of Biomedicine, Aarhus University, Aarhus, Denmark.
James E. Ferrell, Jr.	james.ferrell@stanford.edu	James Ferrell	Department of Chemical and Systems Biology, Stanford University School of Medicine, Stanford, CA, USA.; Department of Biochemistry, Stanford University School of Medicine, Stanford, CA, USA.
Hannah K. Frank	hkfrank@tulane.edu	Scott Boyd	Department of Pathology, Stanford University School of Medicine, Stanford, CA, USA.; Department of Ecology and Evolutionary Biology, Tulane University, New Orleans, LA, USA.
Margaret Fuller	mtfuller@stanford.edu	Margaret Fuller	Department of Developmental Biology, Stanford University School of Medicine, Stanford, CA, USA.; Department of Genetics, Stanford University School of Medicine, Stanford, CA, USA.
Astrid Gillich	agillich@stanford.edu	Mark Krasnow	Department of Biochemistry, Stanford University School of Medicine, Stanford, CA, USA.; Howard Hughes Medical Institute, USA.
Elias Godoy	eligodoy@stanford.edu	Stanford Veterinary Service Center	Department of Comparative Medicine, Stanford University School of Medicine, Stanford, CA, USA.
Dita Gratzinger	ditag@stanford.edu	Dita Gratzinger	Department of Pathology, Stanford University School of Medicine, Stanford, CA, USA.
Lisbeth A. Guethlein	libbyg@stanford.edu	Peter Parham	Department of Structural Biology, Stanford University School of Medicine, Stanford, CA, USA.; Department of Microbiology and Immunology, Stanford University School of Medicine, Stanford, CA, USA.
Yan Hang	yanh@stanford.edu	Seung Kim	Department of Developmental Biology, Stanford University School of Medicine, Stanford, CA, USA.; Stanford Diabetes Research Center, Stanford, CA, USA.
Kazuteru Hasegawa	kazuteru@stanford.edu	Steven Artandi	Stanford Cancer Institute, Stanford University School of Medicine, Stanford, CA, USA.; Department of Medicine, Stanford University School of Medicine, Stanford, CA, USA.; Department of Biochemistry, Stanford University School of Medicine, Stanford, CA, USA.
Rebecca D. Hodge	rebeccah@alleninstitute.org	Allen Institute for Brain Science	Human Cell Types Department, Allen Institute for Brain Science, Seattle, WA, USA.
Malachia Hoover	malachia@stanford.edu	Charles Chan	Institute for Stem Cell Biology and Regenerative Medicine, Stanford University School of Medicine, Stanford, CA, USA.
Franklin W. Huang	franklin.huang@ucsf.edu	Franklin Huang	Division of Hematology/Oncology, Department of Medicine, University of California San Francisco, San Francisco, CA, USA.
Kerwyn C. Huang	kchuang@stanford.edu	Kerwyn Casey Huang	Department of Bioengineering, Stanford University, Stanford, CA, USA.; Department of Microbiology and Immunology, Stanford University School of Medicine, Stanford, CA, USA.; Chan Zuckerberg Biohub, San Francisco, CA, USA.
Shelly Huynh	shelly.huynh@czbiohub.org	CZ Biohub	Chan Zuckerberg Biohub, San Francisco, CA, USA.
Taichi Isobe	tisobe.kyushu@gmail.com	Michael Clarke	Department of Oncology and Social Medicine, Kyushu University, Japan.

Carly Israel	carly.israel@yale.edu	CZ Biohub	Chan Zuckerberg Biohub, San Francisco, CA, USA.
SoRi Jang	sorijang@stanford.edu	Mark Krasnow	Department of Biochemistry, Stanford University School of Medicine, Stanford, CA, USA.; Howard Hughes Medical Institute, USA.
Qiuyu Jing	qjingab@connect.ust.hk	Angela Wu	Division of Life Science, Hong Kong University of Science and Technology, Hong Kong SAR, China.
Robert C. Jones	jonesbob@stanford.edu	Stephen Quake	Department of Bioengineering, Stanford University, Stanford, CA, USA.
Jengmin Kang	jminkang@stanford.edu	Thomas Rando	Department of Neurology and Neurological Sciences, Stanford University School of Medicine, Stanford, CA, USA.
Caitlin J. Karanewsky	ckaranew@stanford.edu	Mark Krasnow	Department of Biochemistry, Stanford University School of Medicine, Stanford, CA, USA.; Howard Hughes Medical Institute, USA.
Jim Karkanias	jim.karkanias@czbiohub.org	CZ Biohub	Chan Zuckerberg Biohub, San Francisco, CA, USA.
Justus Kebschull	justus@kebschull.me	Justus Kebschull	Department of Biomedical Engineering, Johns Hopkins School of Medicine, Baltimore, MD, USA.
Aaron Kershner	kershner@stanford.edu	Philip Beachy	Department of Biochemistry, Stanford University School of Medicine, Stanford, CA, USA.; Institute of Stem Cell Biology and Regenerative Medicine, Stanford University School of Medicine, Stanford, CA, USA.
Lily Kim	lilykim@stanford.edu	Douglas Vollrath	Department of Genetics, Stanford University School of Medicine, Stanford, CA, USA.
Seung K. Kim	seungkim@stanford.edu	Seung Kim	Department of Developmental Biology, Stanford University School of Medicine, Stanford, CA, USA.; Stanford Diabetes Research Center, Stanford, CA, USA.; JDRF Center of Excellence, Stanford, CA, USA.; Department of Medicine, Stanford University School of Medicine, Stanford, CA, USA.
E. Christopher Kirk	eckirk@austin.utexas.edu	E. Christopher Kirk	Department of Anthropology, University of Texas at Austin, Austin, TX, USA.
Winston Koh	Winston_koh@imcb.a-star.edu.sg	Molecular Engineering Lab	Institute of Bioengineering and Bioimaging, Agency of Science Technology and Research, Singapore; Bioinformatics Institute, Agency of Science Technology and Research, Singapore
Silvana Konermann	silvanak@stanford.edu	Silvana Konermann	Department of Biochemistry, Stanford University School of Medicine, Stanford, CA, USA.; Howard Hughes Medical Institute, USA.
William Kong	wwkong@stanford.edu	Philip Beachy	Institute for Stem Cell Biology and Regenerative Medicine, Stanford University School of Medicine, Stanford, CA, USA.
Mark A. Krasnow	krasnow@stanford.edu	Mark Krasnow	Department of Biochemistry, Stanford University School of Medicine, Stanford, CA, USA.; Howard Hughes Medical Institute, USA.
Christin Kuo	ckuo@stanford.edu	Christin Kuo	Department of Pediatrics, Stanford University School of Medicine, Stanford, CA, USA.
Corinne Lautier	corinne.lautier@umontpellier.fr	Corinne Lautier	MMDN, University of Montpellier, EPHE-PSL, INSERM, Montpellier, France.
Song Eun Lee	songlee@stanford.edu	Tony Wyss-Coray	Department of Neurology and Neurological Sciences, Stanford University School of Medicine, Stanford, CA, USA.; Wu Tsai Neurosciences Institute, Stanford, CA, USA.
Ed S. Lein	edl@alleninstitute.org	Allen Institute for Brain Science	Human Cell Types Department, Allen Institute for Brain Science, Seattle, WA, USA.
Rebecca Lewis	rjlewis@austin.utexas.edu	Rebecca Lewis	Department of Anthropology, University of Texas at Austin, Austin, TX, USA.
Peng Li	penglium@umich.edu	Mark Krasnow	Department of Biochemistry, Stanford University School of Medicine, Stanford, CA, USA.; Howard Hughes Medical Institute, USA.
Zhengda Li	lzd@stanford.edu	James Ferrell	Department of Chemical and Systems Biology, Stanford University School of Medicine, Stanford, CA, USA.
Shengda Lin	shengda_lin@zju.edu.cn	Steven Artandi; Shengda Lin	Zhejiang Provincial Key Laboratory for Cancer Molecular Cell Biology, Life Sciences Institute, Zhejiang University, Hangzhou, Zhejiang, China.
Shixuan Liu	shixuan@stanford.edu	Mark Krasnow; James Ferrell	Department of Chemical and Systems Biology, Stanford University School of Medicine, Stanford, CA, USA.; Department of Biochemistry, Stanford University School of Medicine, Stanford, CA, USA.; Howard Hughes Medical Institute, USA.
Yin Liu	yinl@stanford.edu	Mark Krasnow	Department of Biochemistry, Stanford University School of Medicine, Stanford, CA, USA.; Howard Hughes Medical Institute, USA.
Gabriel Loeb	gabriel.loeb@ucsf.edu	Gabriel Loeb	Division of Nephrology, Department of Medicine, University of California San Francisco, San Francisco, CA, USA.
Jonathan Z. Long	jzlong@stanford.edu	Jonathan Long	Department of Pathology, Stanford University School of Medicine, Stanford, CA, USA.; Stanford ChEM-H, Stanford, CA, USA.
Wan-Jin Lu	wjlu@stanford.edu	Philip Beachy	Institute for Stem Cell Biology and Regenerative Medicine, Stanford University School of Medicine, Stanford, CA, USA.

Katherine Lucot	kllucot@stanford.edu	Tom Montine	Department of Pathology, Stanford University School of Medicine, Stanford, CA, USA.
Liqun Luo	lluo@stanford.edu	Liqun Luo	Department of Biology, Stanford University, Stanford, CA, USA.; Howard Hughes Medical Institute, USA.
Aaron McGeever	aaron.mcgeever@czbiohub.org	CZ Biohub	Chan Zuckerberg Biohub, San Francisco, CA, USA.
Ross Metzger	rmetzger@stanford.edu	Ross Metzger	Department of Pediatrics, Stanford University School of Medicine, Stanford, CA, USA.; Division of Cardiology, Stanford University School of Medicine, Stanford, CA, USA.
Jingsi Ming	jsming@fem.ecnu.edu.cn	Can Yang; Jingsi Ming	Academy of Statistics and Interdisciplinary Sciences, KLATASDS-MOE, East China Normal University, Shanghai, China.; Department of Mathematics, Hong Kong University of Science and Technology, Hong Kong SAR, China.
Tom Montine	tmontine@stanford.edu	Tom Montine	Department of Pathology, Stanford University School of Medicine, Stanford, CA, USA.
Antoine de Morree	demorree@stanford.edu	Thomas Rando	Department of Neurology and Neurological Sciences, Stanford University School of Medicine, Stanford, CA, USA.; Department of Biomedicine, Aarhus University, Aarhus, Denmark.
Maurizio Morri	morri@stanford.edu	CZ Biohub	Chan Zuckerberg Biohub, San Francisco, CA, USA.
Karim Mrouj	karim.mrouj@stanford.edu	Philip Beachy	Institute for Stem Cell Biology and Regenerative Medicine, Stanford University School of Medicine, Stanford, CA, USA.
Shravani Mukherjee	smukherj@stanford.edu	Albert Wu	Department of Ophthalmology, Stanford University School of Medicine, Stanford, CA, USA.
Ahmad Nabhan	anabhan123@gmail.com	Mark Krasnow	Department of Biochemistry, Stanford University School of Medicine, Stanford, CA, USA.; Howard Hughes Medical Institute, USA.
Saba Nafees	saba.nafees@czbiohub.org	CZ Biohub	Chan Zuckerberg Biohub, San Francisco, CA, USA.
Norma Neff	norma.neff@czbiohub.org	CZ Biohub	Chan Zuckerberg Biohub, San Francisco, CA, USA.
Patrick Neuhöfer	pneuhoef@stanford.edu	Steve Artandi	Stanford Cancer Institute, Stanford University School of Medicine, Stanford, CA, USA.; Department of Medicine, Stanford University School of Medicine, Stanford, CA, USA.; Department of Biochemistry, Stanford University School of Medicine, Stanford, CA, USA.
Patricia Nguyen	pknguyen@stanford.edu	Patricia Nguyen	Department of Medicine, Stanford University School of Medicine, Stanford, CA, USA.; Stanford Cardiovascular Institute, Stanford, CA, USA.; Division of Cardiovascular Medicine, Stanford University, Stanford, CA, USA.
Jennifer Okamoto	jenokamoto@gmail.com	CZ Biohub	Chan Zuckerberg Biohub, San Francisco, CA, USA.
Julia Olivieri	jolivier@stanford.edu	Julia Salzman	Institute for Computational and Mathematical Engineering, Stanford University, Stanford, CA, USA.
Youcef Ouadah	yzouadah@caltech.edu	Mark Krasnow	Department of Biochemistry, Stanford University School of Medicine, Stanford, CA, USA.; Program in Cancer Biology, Stanford University School of Medicine, Stanford, CA, USA.
Honor Paine	honor.paine@ucsf.edu	Bruce Wang	Department of Medicine and Liver Center, University of California San Francisco, San Francisco, CA, USA.
Peter Parham	peropa@stanford.edu	Peter Parham	Department of Structural Biology, Stanford University School of Medicine, Stanford, CA, USA.; Department of Microbiology and Immunology, Stanford University School of Medicine, Stanford, CA, USA.
Jozeph L. Pendleton	zephpen@stanford.edu	Mark Krasnow	Department of Biochemistry, Stanford University School of Medicine, Stanford, CA, USA.; Howard Hughes Medical Institute, USA.
Lolita Penland	lpenland@calicolabs.com	CZ Biohub	Chan Zuckerberg Biohub, San Francisco, CA, USA.
Martine Perret	martine.perret@mnhn.fr	Martine Perret	Adaptive Mechanisms and Evolution (MECADEV), UMR 7179, National Center for Scientific Research, National Museum of Natural History, Brunoy, France.
Angela Oliveira Pisco	angela.pisco@czbiohub.org	CZ Biohub	Chan Zuckerberg Biohub, San Francisco, CA, USA.
Zhen Qi	zhenqi@stanford.edu	Michael Clarke	Institute for Stem Cell Biology and Regenerative Medicine, Stanford University School of Medicine, Stanford, CA, USA.
Stephen R. Quake	steve@czbiohub.org; steve@quake-lab.org	Stephen Quake; CZ Biohub	Department of Bioengineering, Stanford University, Stanford, CA, USA.; Chan Zuckerberg Biohub, San Francisco, CA, USA.; Department of Applied Physics, Stanford University, Stanford, CA, USA.
Ute Radespiel	ute.radespiel@tiho-hannover.de	Ute Radespiel	Institute of Zoology, University of Veterinary Medicine Hannover, Germany.
Thomas A. Rando	rando@stanford.edu	Thomas Rando	Department of Neurology and Neurological Sciences, Stanford University School of Medicine, Stanford, CA, USA.

Hajanirina Noëline Ravelonjanahary	hajanravel@gmail.com	Mark Krasnow	Department of Animal Biology, Faculty of Science, University of Antananarivo, Antananarivo 101, BP 566, Madagascar.
Andriamahery Razafindrakoto	amaherix@gmail.com	Mark Krasnow	Department of Animal Biology, Faculty of Science, University of Antananarivo, Antananarivo 101, BP 566, Madagascar.
Julia Salzman	horence@stanford.edu	Julia Salzman	Department of Biochemistry, Stanford University School of Medicine, Stanford, CA, USA.; Department of Biomedical Data Science, Stanford University, Stanford, CA, USA.
Nicholas Schaum	ndschaum@gmail.com	Tony Wyss-Coray	Department of Neurology and Neurological Sciences, Stanford University School of Medicine, Stanford, CA, USA.
Robert Schopler	bobby.schopler@duke.edu	Duke Lemur Center	Duke Lemur Center, Durham, NC, USA.
Bronwyn Scott	bronwyns@stanford.edu	Albert Wu	Department of Ophthalmology, Stanford University School of Medicine, Stanford, CA, USA.
Liza Shapiro	liza.shapiro@austin.utexas.edu	Liza Shapiro	Department of Anthropology, University of Texas at Austin, Austin, TX, USA.
Hosu Sin	hosu@stanford.edu	Margaret Fuller	Department of Developmental Biology, Stanford University School of Medicine, Stanford, CA, USA.
Rahul Sinha	sinhar@stanford.edu	Irving Weissman	Stanford Institute for Stem Cell Biology and Regenerative Medicine, Stanford, CA, USA.
Rene Sit	rene.sit@czbiohub.org	CZ Biohub	Chan Zuckerberg Biohub, San Francisco, CA, USA.
Geoff Stanley	gmstanle@stanford.edu	Stephen Quake	Department of Bioengineering, Stanford University, Stanford, CA, USA.
Lubert Stryer	stryer@stanford.edu	Lubert Stryer	Department of Neurobiology, Stanford University School of Medicine, Stanford, CA, USA.
Varun Ramanan Subramaniam	varunramanan608@gmail.com	Albert Wu	Department of Ophthalmology, Stanford University School of Medicine, Stanford, CA, USA.
Aditi Swarup	aswarup@stanford.edu	Albert Wu	Department of Ophthalmology, Stanford University School of Medicine, Stanford, CA, USA.
Weilun Tan	weilun.tan@czbiohub.org	CZ Biohub	Chan Zuckerberg Biohub, San Francisco, CA, USA.
Alexander Tarashansky	tarashanst@gmail.com; alexander@tarashansky.com	Bo Wang; CZ Biohub	Department of Bioengineering, Stanford University, Stanford, CA, USA.; Chan Zuckerberg Biohub, San Francisco, CA, USA.
Aris Taychameekiatchai	aris.taychameekiatchai@ucsf.edu	Bruce Wang	Department of Medicine and Liver Center, University of California San Francisco, San Francisco, CA, USA.
Jérémy Terrien	jeremy.terrien@mnhn.fr	Jérémy Terrien	Adaptive Mechanisms and Evolution (MECADEV), UMR 7179, National Center for Scientific Research, National Museum of Natural History, Brunoy, France.
Kyle J. Travaglini	ktrav@stanford.edu	Mark Krasnow	Department of Biochemistry, Stanford University School of Medicine, Stanford, CA, USA.; Howard Hughes Medical Institute, USA.
Andoni Urtasun	a.urtasun.arricaberri@gmail.com	Thomas Rando	Department of Neurology and Neurological Sciences, Stanford University School of Medicine, Stanford, CA, USA.
Sivakamasundari V	sivav@stanford.edu	Philip Beachy	Institute for Stem Cell Biology and Regenerative Medicine, Stanford University School of Medicine, Stanford, CA, USA.
Avin Veerakumar	avinv@stanford.edu	Mark Krasnow	Department of Biochemistry, Stanford University School of Medicine, Stanford, CA, USA.; Department of Bioengineering, Stanford University, Stanford, CA, USA.; Medical Scientist Training Program, Stanford University School of Medicine, Stanford, CA, USA.; Howard Hughes Medical Institute, USA.
Venkata N. P. Vemuri	pranathi.vemuri@czbiohub.org	CZ Biohub	Chan Zuckerberg Biohub, San Francisco, CA, USA.
Jean-Michel Verdier	jean-michel.verdier@ephe.psl.eu	Jean-Michel Verdier	MMDN, University of Montpellier, EPHE-PSL, INSERM, Montpellier, France.
Iwijn De Vlaminck	vlaminck@cornell.edu; idevlaminck@gmail.com	Iwijn De Vlaminck	Nancy E. and Peter C. Meinig School of Biomedical Engineering, Cornell University, Ithaca, NY, USA.
Douglas Vollrath	vollrath@stanford.edu	Douglas Vollrath	Department of Genetics, Stanford University School of Medicine, Stanford, CA, USA.
Bo Wang	wangbo@stanford.edu	Bo Wang	Department of Bioengineering, Stanford University, Stanford, CA, USA.
Bruce Wang	bruce.wang@ucsf.edu	Bruce Wang	Department of Medicine and Liver Center, University of California San Francisco, San Francisco, CA, USA.
Gefei Wang	gwangas@connect.ust.hk	Can Yang	Department of Mathematics, Hong Kong University of Science and Technology, Hong Kong SAR, China.
Michael F.Z. Wang	fw262@cornell.edu	Iwijn De Vlaminck	Nancy E. and Peter C. Meinig School of Biomedical Engineering, Cornell University, Ithaca, NY, USA.; Department of Computational Biology, Cornell University, Ithaca, NY, USA.
Sheng Wang	swang@cs.washington.edu	Sheng Wang	Paul G. Allen School of Computer Science & Engineering, University of Washington, Seattle, WA, USA.
James Webber	james.webber@czbiohub.org	CZ Biohub	Chan Zuckerberg Biohub, San Francisco, CA, USA.

Hannah Weinstein	hnw2105@cumc.columbia.edu	Franklin Huang	Division of Hematology/Oncology, Department of Medicine, University of California San Francisco, San Francisco, CA, USA.; Helen Diller Family Comprehensive Cancer Center, University of California San Francisco, San Francisco, CA, USA.; Bakar Computational Health Sciences Institute, University of California San Francisco, San Francisco, CA, USA.
Irving L. Weissman	irv@stanford.edu	Irving Weissman	Stanford Institute for Stem Cell Biology and Regenerative Medicine, Stanford, CA, USA.
Amanda L. Wiggenhorn	awiggen@stanford.edu	Jonathan Long	Department of Pathology, Stanford University School of Medicine, Stanford, CA, USA.; Department of Chemistry, Stanford University, Stanford, CA, USA.
Cathy V. Williams	cathy.williams@duke.edu	Duke Lemur Center	Duke Lemur Center, Durham, NC, USA.
Patricia Wright	Patricia.Wright@Stonybrook.edu; patchapplewright@gmail.com	Patricia Wright	Department of Anthropology, Stony Brook University, NY, USA.
Albert Y. Wu	awu1@stanford.edu	Albert Wu	Department of Ophthalmology, Stanford University School of Medicine, Stanford, CA, USA.
Angela Wu	angelawu@ust.hk	Angela Wu	Division of Life Science, Hong Kong University of Science and Technology, Hong Kong SAR, China.; Department of Chemical and Biological Engineering, Hong Kong University of Science and Technology, Hong Kong SAR, China.; Center for Aging Science, Hong Kong University of Science and Technology, Hong Kong SAR, China.
Tony Wyss-Coray	twc@stanford.edu	Tony Wyss-Coray	Department of Neurology and Neurological Sciences, Stanford University School of Medicine, Stanford, CA, USA.; Wu Tsai Neurosciences Institute, Stanford, CA, USA.
Bao Xiang	bxli@stanford.edu	Albert Wu	Department of Ophthalmology, Stanford University School of Medicine, Stanford, CA, USA.
Jia Yan	rose.yan@czbiohub.org	CZ Biohub	Chan Zuckerberg Biohub, San Francisco, CA, USA.
Can Yang	macyang@ust.hk	Can Yang	Department of Mathematics, Hong Kong University of Science and Technology, Hong Kong SAR, China.
Jinxurong Yang	jyang@diagnoa.com	Angela Wu	Division of Life Science, Hong Kong University of Science and Technology, Hong Kong SAR, China.
Anne D. Yoder	anne.yoder@duke.edu	Anne Yoder	Department of Biology, University Program in Genetics & Genomics, Duke University, Durham, NC, USA.
Brian Yu	brian.yu@czbiohub.org	CZ Biohub	Chan Zuckerberg Biohub, San Francisco, CA, USA.
Andrea R. Yung	andreay@stanford.edu	Mark Krasnow	Department of Biochemistry, Stanford University School of Medicine, Stanford, CA, USA.; Howard Hughes Medical Institute, USA.
Yue Zhang	helen18@stanford.edu	Mark Krasnow	Department of Biology, Stanford University, Stanford, CA, USA.; Howard Hughes Medical Institute, USA.
Jia Zhao	jzhaoaz@connect.ust.hk	Can Yang	Department of Mathematics, Hong Kong University of Science and Technology, Hong Kong SAR, China.
Zicheng Zhao	zczhao@stanford.edu; rezczhao@gmail.com	Megan Albertelli; Mark Krasnow	Department of Comparative Medicine, Stanford University School of Medicine, Stanford, CA, USA.; Howard Hughes Medical Institute, USA.

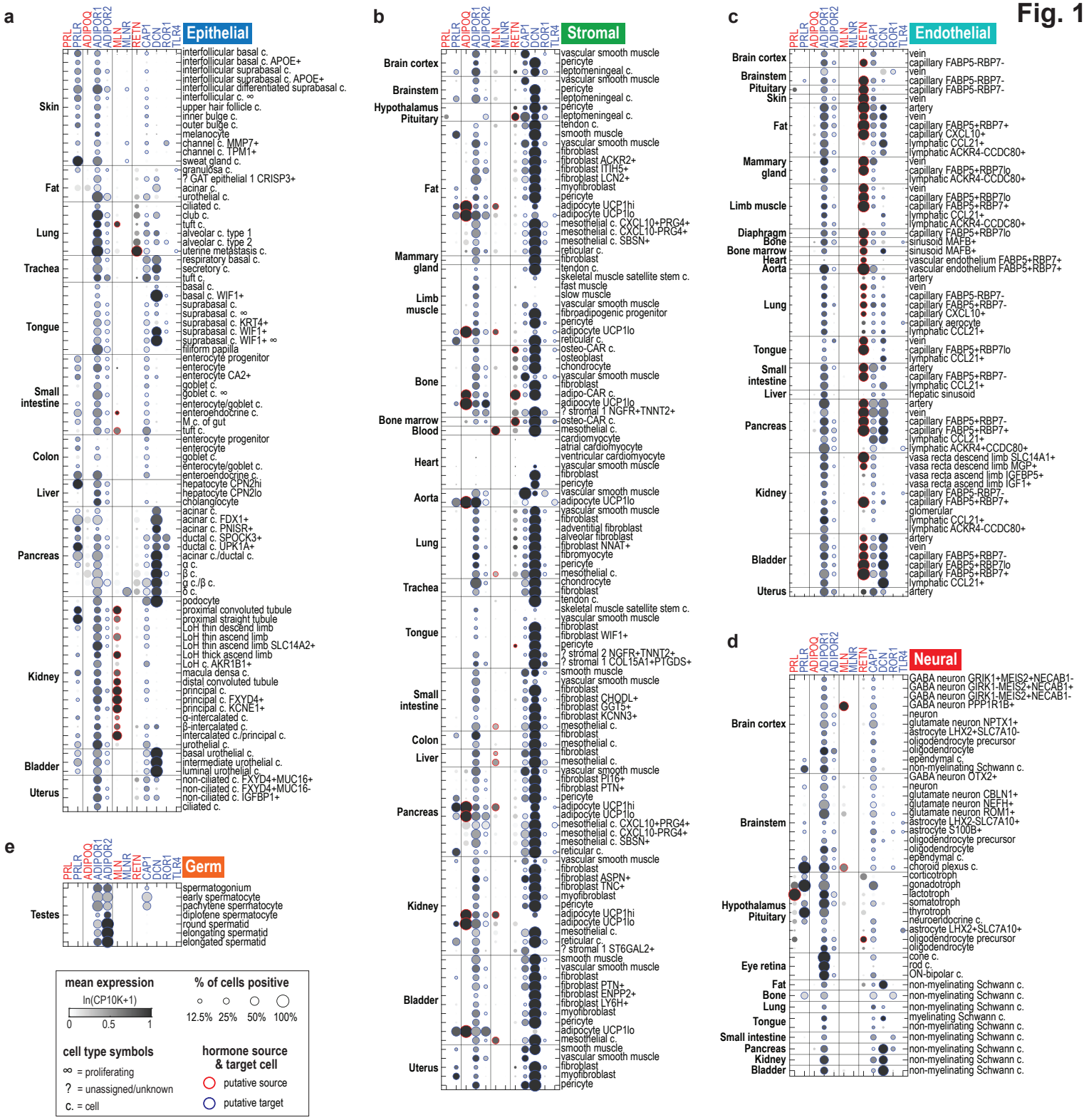
Fig. 1
a
Epithelial
PRL
PRLR
ADIPOQ
ADIPOR1
ADIPOR2
MLN
MLNR
RETN
CAP1
DCN
ROR1
TLR4
Skin
interfollicular basal c.
interfollicular basal c. APOE+
interfollicular suprabasal c.
interfollicular suprabasal c. APOE+
interfollicular differentiated suprabasal c.
interfollicular c. ∞
upper hair follicle c.
inner bulge c.
outer bulge c.
melanocyte
channel c. MMP7+
channel c. TPM1+
sweat gland c.
Fat
granulosa c.
? GAT epithelial 1 CRISP3+
acinar c.
urothelial c.
Lung
ciliated c.
club c.
tuft c.
alveolar c. type 1
alveolar c. type 2
uterine metastasis c.
Trachea
respiratory basal c.
secretory c.
tuft c.
Tongue
basal c.
basal c. WIF1+
suprabasal c.
suprabasal c. ∞
suprabasal c. KRT4+
suprabasal c. WIF1+
suprabasal c. WIF1+ ∞
filiform papilla
Small intestine
enterocyte progenitor
enterocyte
enterocyte CA2+
goblet c.
goblet c. ∞
enterocyte/goblet c.
enteroendocrine c.
M c. of gut
tuft c.
Colon
enterocyte progenitor
enterocyte
goblet c.
enterocyte/goblet c.
enteroendocrine c.
Liver
hepatocyte CPN2hi
hepatocyte CPN2lo
cholangiocyte
Pancreas
acinar c.
acinar c. FDX1+
acinar c. PNISR+
ductal c. SPOCK3+
ductal c. UPK1A+
acinar c./ductal c.
α c.
β c.
α c./β c.
δ c.
Kidney
podocyte
proximal convoluted tubule
proximal straight tubule
LoH thin descend limb
LoH thin ascend limb
LoH thin ascend limb SLC14A2+
LoH thick ascend limb
LoH c. AKR1B1+
macula densa c.
distal convoluted tubule
principal c.
principal c. FXYD4+
principal c. KCNE1+
α-intercalated c.
β-intercalated c.
intercalated c./principal c.
urothelial c.
Bladder
basal urothelial c.
intermediate urothelial c.
luminal urothelial c.
Uterus
non-ciliated c. FXYD4+MUC16+
non-ciliated c. FXYD4+MUC16-
non-ciliated c. IGFBP1+
ciliated c.
b
Stromal
Brain cortex
vascular smooth muscle
pericyte
leptomeningeal c.
Brainstem
vascular smooth muscle
pericyte
leptomeningeal c.
Hypothalamus
pericyte
Pituitary
leptomeningeal c.
tendon c.
smooth muscle
vascular smooth muscle
fibroblast
fibroblast ACKR2+
fibroblast ITIH5+
fibroblast LCN2+
Fat
myofibroblast
pericyte
adipocyte UCP1hi
adipocyte UCP1lo
mesothelial c. CXCL10+PRG4+
mesothelial c. CXCL10-PRG4+
mesothelial c. SBSN+
reticular c.
Mammary gland
fibroblast
tendon c.
skeletal muscle satellite stem c.
Limb muscle
fast muscle
slow muscle
vascular smooth muscle
fibroadipogenic progenitor
pericyte
adipocyte UCP1lo
reticular c.
Bone
osteo-CAR c.
osteoblast
chondrocyte
vascular smooth muscle
fibroblast
adipo-CAR c.
adipocyte UCP1lo
? stromal 1 NGFR+TNNT2+
Bone marrow
osteo-CAR c.
Blood
mesothelial c.
cardiomyocyte
Heart
atrial cardiomyocyte
ventricular cardiomyocyte
vascular smooth muscle
fibroblast
pericyte
Aorta
vascular smooth muscle
adipocyte UCP1lo
vascular smooth muscle
Lung
fibroblast
adventitial fibroblast
alveolar fibroblast
fibroblast NNAT+
fibromyocyte
pericyte
mesothelial c.
Trachea
chondrocyte
fibroblast
tendon c.
Tongue
skeletal muscle satellite stem c.
vascular smooth muscle
fibroblast
fibroblast WIF1+
pericyte
? stromal 2 NGFR+TNNT2+
? stromal 1 COL15A1+PTGDS+
Small intestine
smooth muscle
vascular smooth muscle
fibroblast
fibroblast CHODL+
fibroblast GGT5+
fibroblast KCNN3+
mesothelial c.
Colon
fibroblast
mesothelial c.
Liver
fibroblast
mesothelial c.
Pancreas
vascular smooth muscle
fibroblast
fibroblast PI16+
fibroblast PTN+
pericyte
adipocyte UCP1hi
adipocyte UCP1lo
mesothelial c. CXCL10+PRG4+
mesothelial c. CXCL10-PRG4+
mesothelial c. SBSN+
reticular c.
Kidney
vascular smooth muscle
fibroblast
fibroblast ASPN+
fibroblast TNC+
myofibroblast
pericyte
adipocyte UCP1hi
adipocyte UCP1lo
mesothelial c.
reticular c.
? stromal 1 ST6GAL2+
Bladder
smooth muscle
vascular smooth muscle
fibroblast
fibroblast PTN+
fibroblast ENPP2+
fibroblast LY6H+
myofibroblast
pericyte
adipocyte UCP1lo
mesothelial c.
Uterus
smooth muscle
vascular smooth muscle
fibroblast
myofibroblast
pericyte
c
Endothelial
Brain cortex
vein
capillary FABP5-RBP7-
Brainstem
vein
capillary FABP5-RBP7-
Pituitary
capillary FABP5-RBP7-
Skin
vein
artery
Fat
vein
capillary FABP5+RBP7+
capillary CXCL10+
lymphatic CCL21+
lymphatic ACKR4-CCDC80+
Mammary gland
vein
capillary FABP5+RBP7lo
lymphatic ACKR4-CCDC80+
Limb muscle
vein
capillary FABP5+RBP7lo
capillary FABP5+RBP7+
lymphatic CCL21+
lymphatic ACKR4-CCDC80+
Diaphragm
capillary FABP5+RBP7lo
Bone
sinusoid MAFB+
Bone marrow
sinusoid MAFB+
Heart
vascular endothelium FABP5+RBP7+
Aorta
vascular endothelium FABP5+RBP7+
artery
vein
Lung
capillary FABP5-RBP7-
capillary FABP5+RBP7-
capillary CXCL10+
capillary aerocyte
lymphatic CCL21+
Tongue
vein
capillary FABP5+RBP7lo
lymphatic CCL21+
Small intestine
artery
capillary FABP5+RBP7-
lymphatic CCL21+
Liver
hepatic sinusoid
Pancreas
artery
vein
capillary FABP5+RBP7-
capillary FABP5+RBP7+
lymphatic CCL21+
lymphatic ACKR4+CCDC80+
Kidney
vasa recta descend limb SLC14A1+
vasa recta descend limb MGP+
vasa recta ascend limb IGFBP5+
vasa recta ascend limb IGF1+
capillary FABP5-RBP7-
capillary FABP5+RBP7+
glomerular
lymphatic CCL21+
lymphatic ACKR4-CCDC80+
Bladder
artery
vein
capillary FABP5+RBP7-
capillary FABP5+RBP7lo
capillary FABP5+RBP7+
lymphatic CCL21+
Uterus
artery
d
Neural
Brain cortex
GABA neuron GRIK1+MEIS2+NECAB1-
GABA neuron GIRK1-MEIS2+NECAB1+
GABA neuron GIRK1-MEIS2+NECAB1-
GABA neuron PPP1R1B+
neuron
glutamate neuron NPTX1+
astrocyte LHX2+SLC7A10-
oligodendrocyte precursor
oligodendrocyte
ependymal c.
non-myelinating Schwann c.
Brainstem
GABA neuron OTX2+
neuron
glutamate neuron CBLN1+
glutamate neuron NEFH+
glutamate neuron ROM1+
astrocyte LHX2-SLC7A10+
astrocyte S100B+
oligodendrocyte precursor
oligodendrocyte
ependymal c.
choroid plexus c.
Hypothalamus
corticotroph
gonadotroph
Pituitary
lactotroph
somatotroph
thyrotroph
neuroendocrine c.
astrocyte LHX2+SLC7A10+
oligodendrocyte precursor
oligodendrocyte
Eye retina
cone c.
rod c.
ON-bipolar c.
Fat
non-myelinating Schwann c.
Bone
non-myelinating Schwann c.
Lung
non-myelinating Schwann c.
Tongue
myelinating Schwann c.
Small intestine
non-myelinating Schwann c.
Pancreas
non-myelinating Schwann c.
Kidney
non-myelinating Schwann c.
Bladder
non-myelinating Schwann c.
e
Germ
Testes
spermatogonium
early spermatocyte
pachytene spermatocyte
diplotene spermatocyte
round spermatid
elongating spermatid
elongated spermatid
mean expression
ln(CP10K+1)
0
0.5
1
% of cells positive
12.5%
25%
50%
100%
cell type symbols
∞ = proliferating
? = unassigned/unknown
c. = cell
hormone source & target cell
putative source
putative target

Fig. 1 - continued

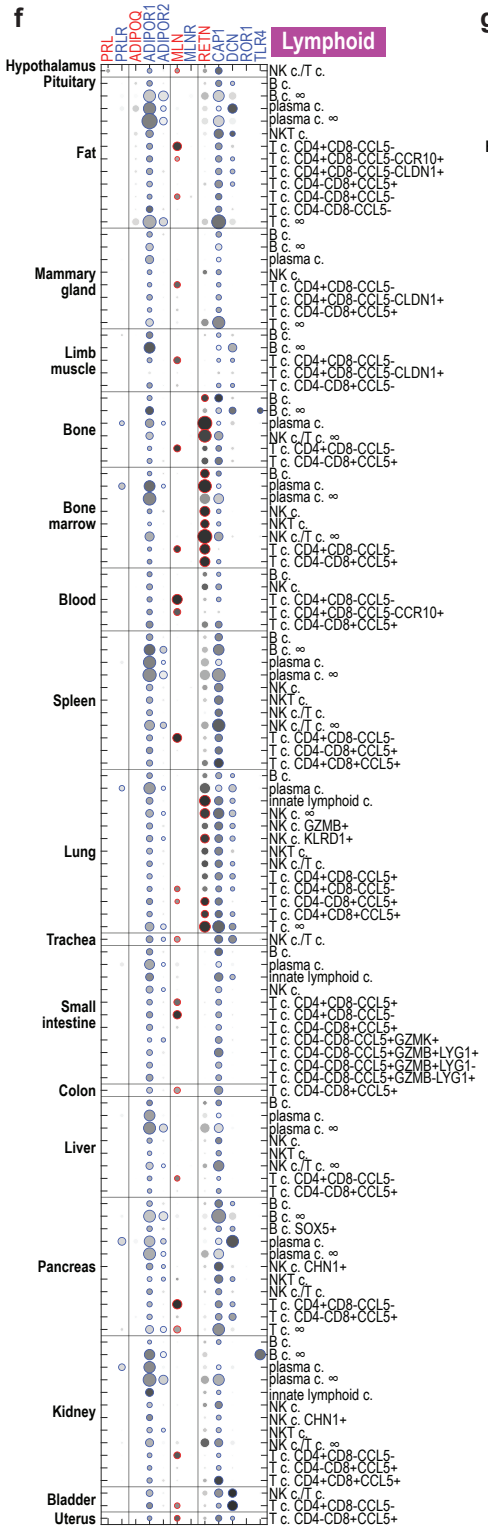

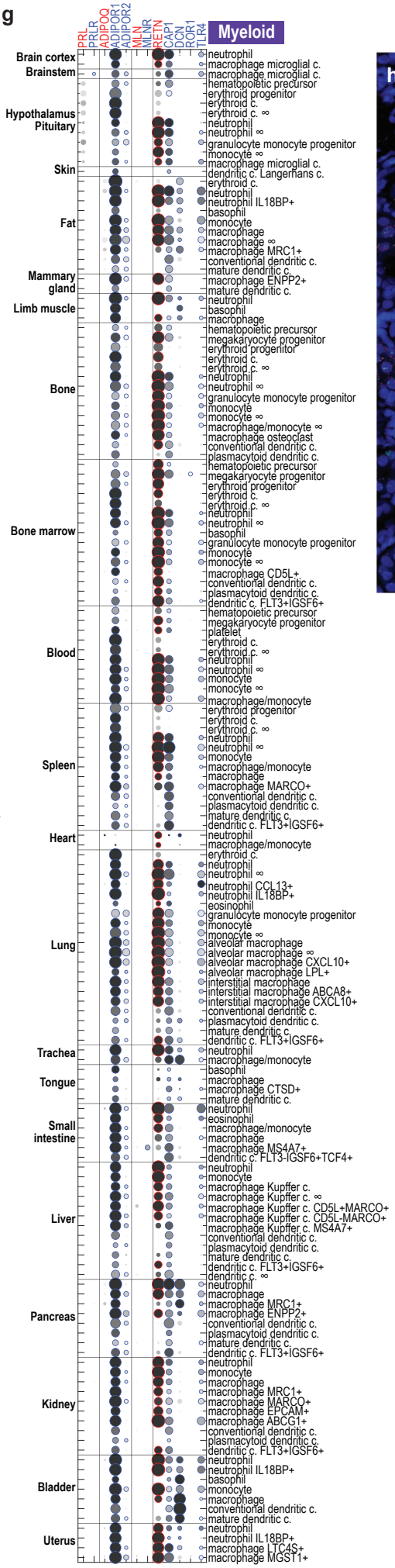

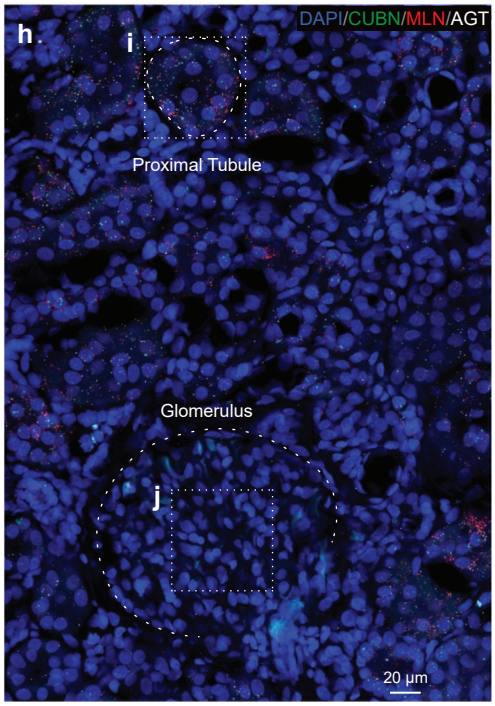

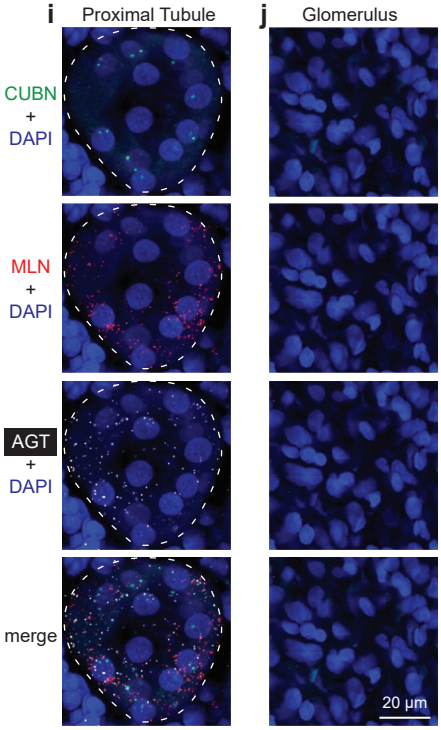

Fig. 2

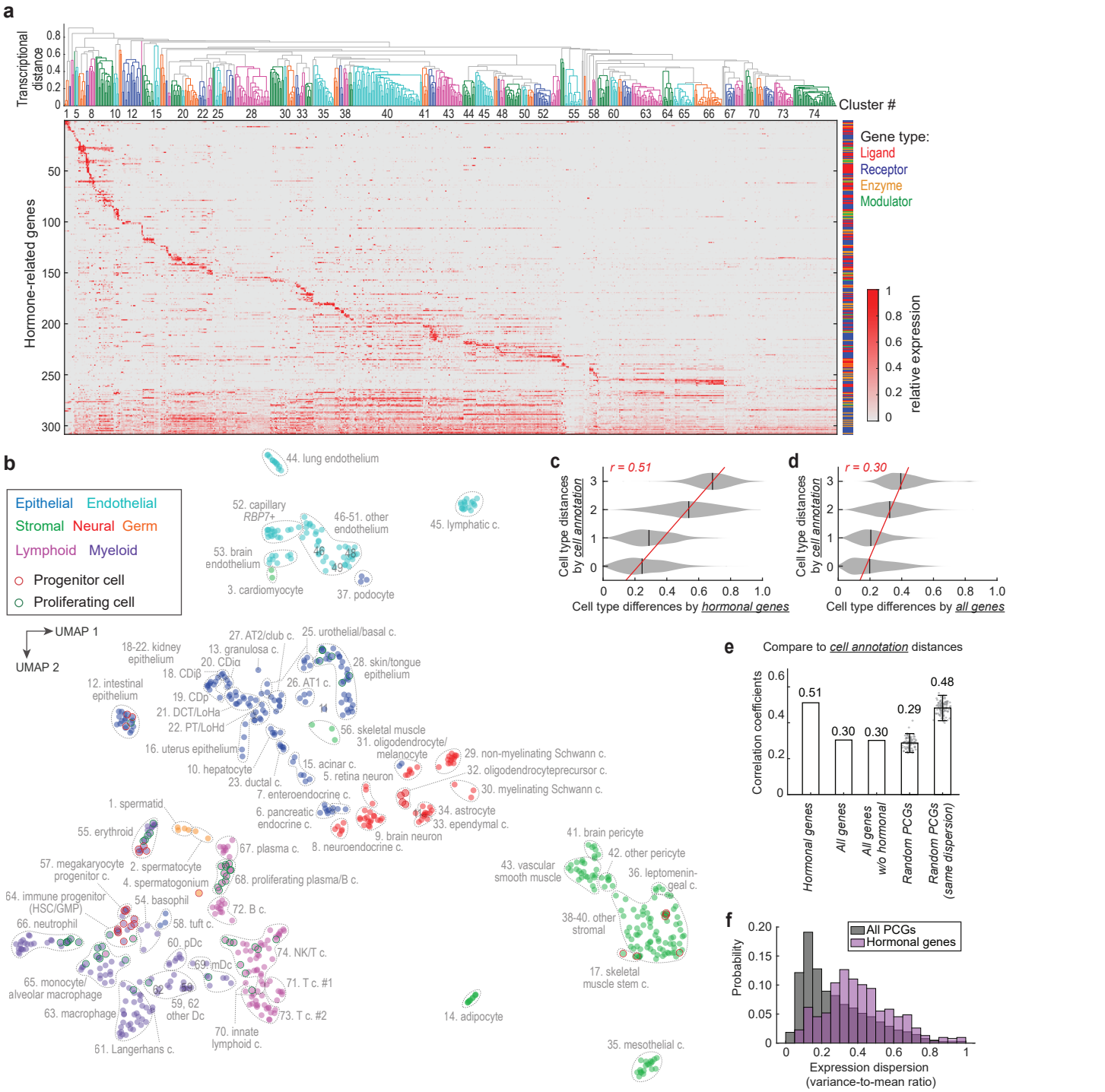
a
Transcriptional distance
Cluster #
Hormone-related genes
Gene type:
Ligand
Receptor
Enzyme
Modulator
relative expression
b
Epithelial
Endothelial
Stromal
Neural
Germ
Lymphoid
Myeloid
Progenitor cell
Proliferating cell
UMAP 1
UMAP 2
44. lung endothelium
52. capillary RBP7+
46-51. other endothelium
45. lymphatic c.
53. brain endothelium
3. cardiomyocyte
37. podocyte
27. AT2/club c.
25. urothelial/basal c.
13. granulosa c.
18-22. kidney epithelium
20. CDiα
28. skin/tongue epithelium
18. CDiβ
12. intestinal epithelium
26. AT1 c.
19. CDp
21. DCT/LoHa
22. PT/LoHd
56. skeletal muscle
16. uterus epithelium
31. oligodendrocyte/ melanocyte
29. non-myelinating Schwann c.
10. hepatocyte
15. acinar c.
32. oligodendrocyteprecursor c.
23. ductal c.
5. retina neuron
30. myelinating Schwann c.
7. enteroendocrine c.
1. spermatid
6. pancreatic endocrine c.
34. astrocyte
33. ependymal c.
55. erythroid
9. brain neuron
8. neuroendocrine c.
67. plasma c.
41. brain pericyte
57. megakaryocyte progenitor c.
2. spermatocyte
42. other pericyte
43. vascular smooth muscle
4. spermatogonium
68. proliferating plasma/B c.
36. leptomeningeal c.
64. immune progenitor (HSC/GMP)
54. basophil
72. B c.
66. neutrophil
58. tuft c.
38-40. other stromal
60. pDc
74. NK/T c.
69. mDc
17. skeletal muscle stem c.
65. monocyte/ alveolar macrophage
71. T c. #1
59, 62 other Dc
63. macrophage
73. T c. #2
14. adipocyte
70. innate lymphoid c.
61. Langerhans c.
35. mesothelial c.
c
r = 0.51
Cell type distances by cell annotation
Cell type differences by hormonal genes
d
r = 0.30
Cell type distances by cell annotation
Cell type differences by all genes
e
Compare to cell annotation distances
Correlation coefficients
0.51
0.30
0.30
0.29
0.48
Hormonal genes
All genes
All genes w/o hormonal
Random PCGs
Random PCGs (same dispersion)
f
All PCGs
Hormonal genes
Probability
Expression dispersion (variance-to-mean ratio)

Fig. 3

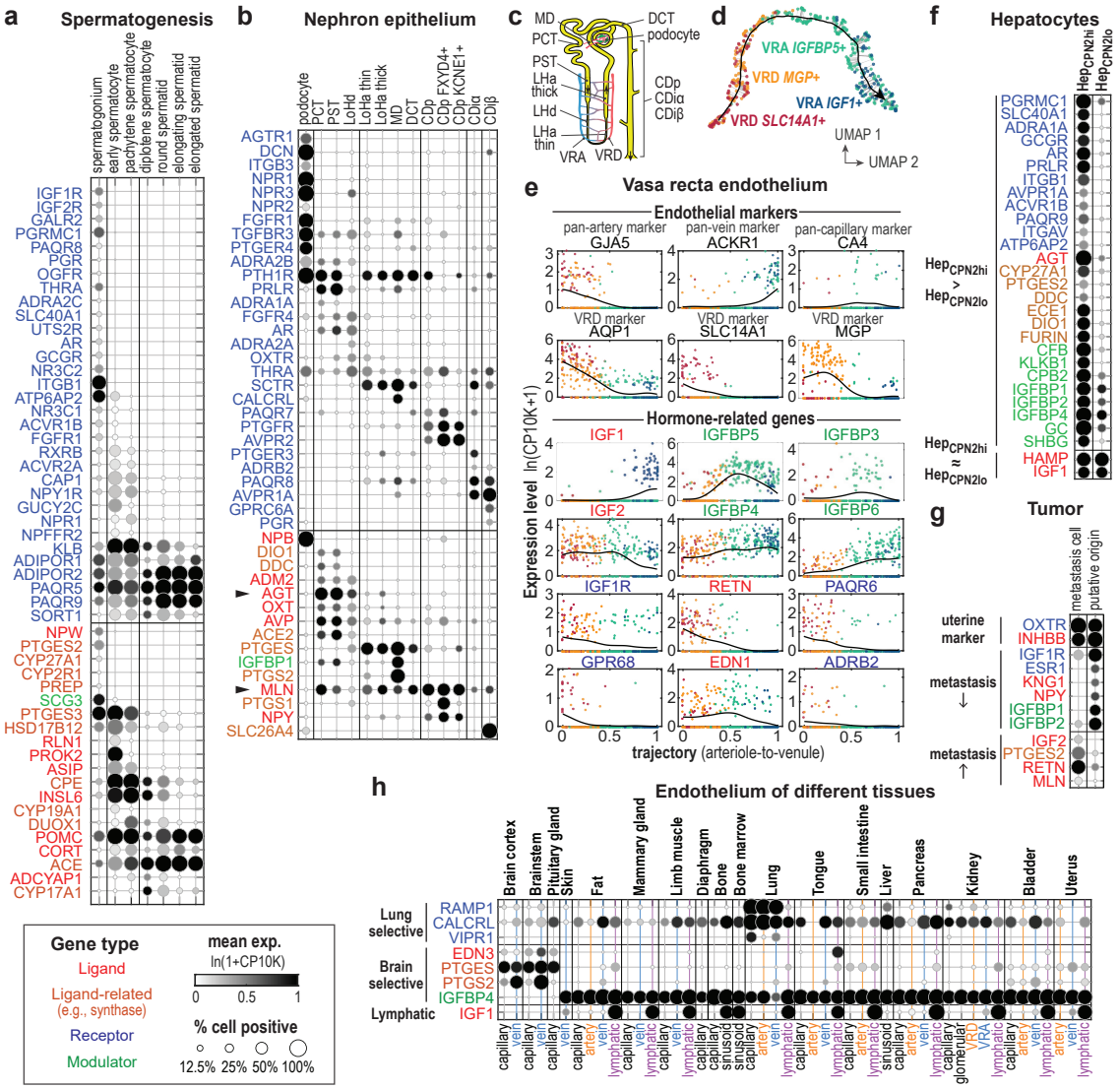
a
Spermatogenesis
spermatogonium
early spermatocyte
pachytene spermatocyte
diplotene spermatocyte
round spermatid
elongating spermatid
elongated spermatid
b
Nephron epithelium
podocyte
PCT
PST
LoHd
LoHa thin
LoHa thick
MD
DCT
CDp
CDp FXYD4+
CDp KONE1+
CDIα
CDIβ
c
MD
PCT
PST
LHa thick
LHd
LHa thin
VRA
VRD
DCT
podocyte
CDp
CDIα
CDIβ
d
VRA IGFBP5+
VRD MGP+
VRA IGF1+
VRD SLC14A1+
UMAP 1
UMAP 2
e
Vasa recta endothelium
Endothelial markers
pan-artery marker
pan-vein marker
pan-capillary marker
GJA5
ACKR1
CA4
VRD marker
AQP1
SLC14A1
MGP
Hormone-related genes
IGF1
IGFBP5
IGFBP3
IGF2
IGFBP4
IGFBP6
IGF1R
RETN
PAQR6
GPR68
EDN1
ADRB2
Expression level ln(CP10K+1)
trajectory (arteriole-to-venule)
f
Hepatocytes
Hep CPN2hi
Hep CPN2lo
g
Tumor
metastasis cell
putative origin
uterine marker
metastasis
h
Endothelium of different tissues
Brain cortex
Brainstem
Pituitary gland
Skin
Fat
Mammary gland
Limb muscle
Diaphragm
Bone
Bone marrow
Lung
Tongue
Small intestine
Liver
Pancreas
Kidney
Bladder
Uterus
Lung selective
Brain selective
Lymphatic
Gene type
Ligand
Ligand-related (e.g., synthase)
Receptor
Modulator
mean exp.
ln(1+CP10K)
% cell positive
12.5% 25% 50% 100%

Fig. 4

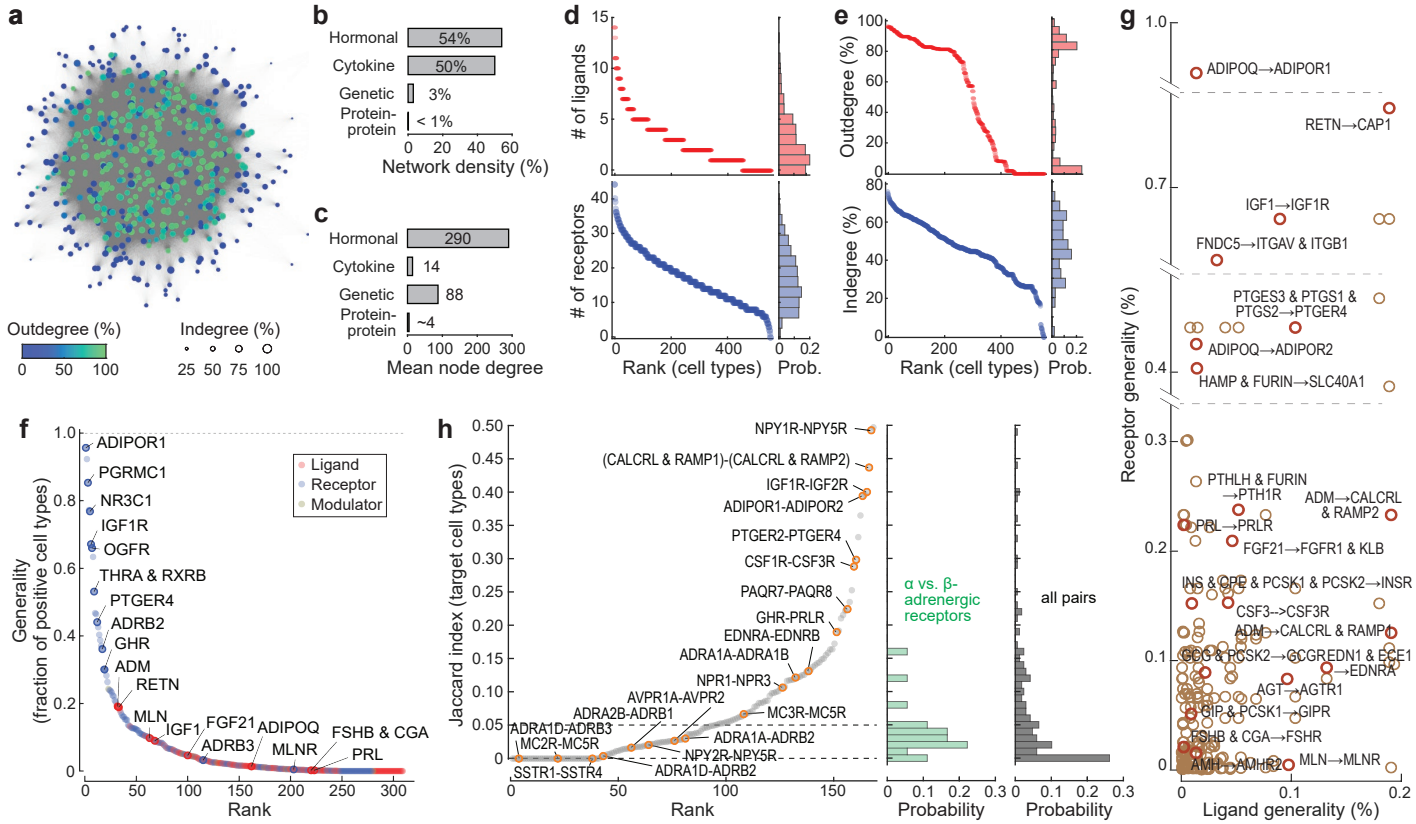
a
Outdegree (%)
0 50 100
Indegree (%)
25 50 75 100
b
Hormonal 54%
Cytokine 50%
Genetic 3%
Protein-protein < 1%
0 20 40 60
Network density (%)
c
Hormonal 290
Cytokine 14
Genetic 88
Protein-protein ~4
0 100 200 300
Mean node degree
d
# of ligands
# of receptors
Rank (cell types)
Prob.
e
Outdegree (%)
Indegree (%)
Rank (cell types)
Prob.
f
Generality (fraction of positive cell types)
Ligand
Receptor
Modulator
ADIPOR1
PGRMC1
NR3C1
IGF1R
OGFR
THRA & RXRB
PTGER4
ADRB2
GHR
ADM
RETN
MLN
IGF1
FGF21
ADIPOQ
ADRB3
MLNR
FSHB & CGA
PRL
Rank
g
Receptor generality (%)
ADIPOQ→ADIPOR1
RETN→CAP1
IGF1→IGF1R
FNDC5→ITGAV & ITGB1
PTGES3 & PTGS1 & PTGS2→PTGER4
ADIPOQ→ADIPOR2
HAMP & FURIN→SLC40A1
PTHLH & FURIN →PTH1R
ADM→CALCRL & RAMP2
PRL→PRLR
FGF21→FGFR1 & KLB
CSF3→CSF3R
AGT→AGTR1
GIP & PCSK1→GIPR
FSHB & CGA→FSHR
MLN→MLNR
Ligand generality (%)
h
Jaccard index (target cell types)
NPY1R-NPY5R
(CALCRL & RAMP1)-(CALCRL & RAMP2)
IGF1R-IGF2R
ADIPOR1-ADIPOR2
PTGER2-PTGER4
CSF1R-CSF3R
PAQR7-PAQR8
GHR-PRLR
EDNRA-EDNRB
ADRA1A-ADRA1B
NPR1-NPR3
AVPR1A-AVPR2
ADRA2B-ADRB1
MC3R-MC5R
ADRA1D-ADRB3
ADRA1A-ADRB2
MC2R-MC5R
NPY2R-NPY5R
SSTR1-SSTR4
ADRA1D-ADRB2
Rank
α vs. β-adrenergic receptors
all pairs
Probability
Probability

Fig. 5

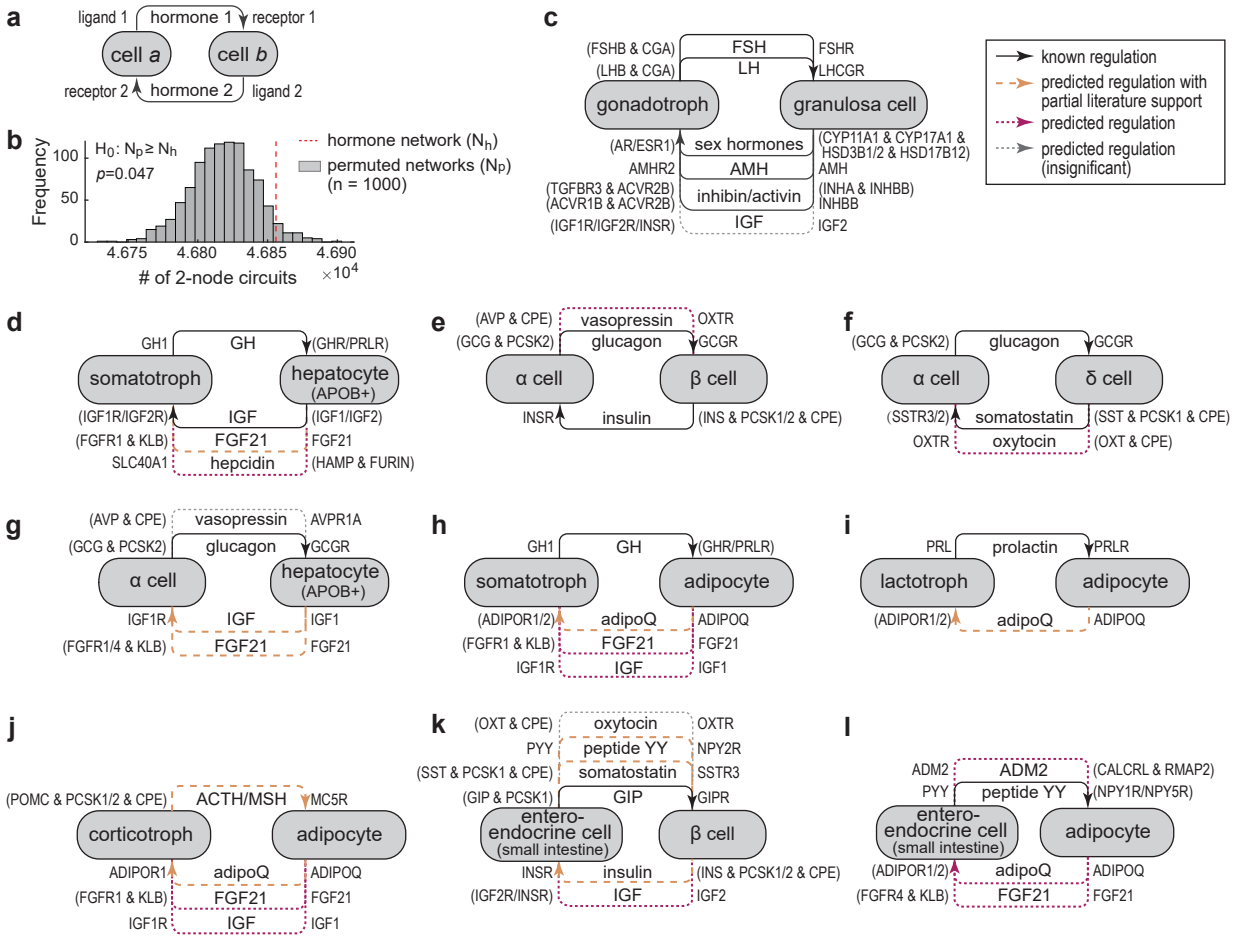
a
ligand 1
hormone 1
receptor 1
cell a
cell b
receptor 2
hormone 2
ligand 2
b
Frequency
100
50
0
H0: Np ≥ Nh
p=0.047
hormone network (Nh)
permuted networks (Np)
(n = 1000)
4.675
4.680
4.685
4.690
# of 2-node circuits
×10^4
c
(FSHB & CGA)
(LHB & CGA)
FSH
LH
FSHR
LHCGR
gonadotroph
granulosa cell
(AR/ESR1)
sex hormones
(CYP11A1 & CYP17A1 & HSD3B1/2 & HSD17B12)
AMHR2
AMH
AMH
(TGFBR3 & ACVR2B)
(ACVR1B & ACVR2B)
inhibin/activin
(INHA & INHBB)
INHBB
(IGF1R/IGF2R/INSR)
IGF
IGF2
known regulation
predicted regulation with partial literature support
predicted regulation
predicted regulation (insignificant)
d
GH1
GH
(GHR/PRLR)
somatotroph
hepatocyte (APOB+)
(IGF1R/IGF2R)
IGF
(IGF1/IGF2)
(FGFR1 & KLB)
FGF21
FGF21
SLC40A1
hepcidin
(HAMP & FURIN)
e
(AVP & CPE)
vasopressin
OXTR
(GCG & PCSK2)
glucagon
GCGR
α cell
β cell
INSR
insulin
(INS & PCSK1/2 & CPE)
f
(GCG & PCSK2)
glucagon
GCGR
α cell
δ cell
(SSTR3/2)
somatostatin
(SST & PCSK1 & CPE)
OXTR
oxytocin
(OXT & CPE)
g
(AVP & CPE)
vasopressin
AVPR1A
(GCG & PCSK2)
glucagon
GCGR
α cell
hepatocyte (APOB+)
IGF1R
IGF
IGF1
(FGFR1/4 & KLB)
FGF21
FGF21
h
GH1
GH
(GHR/PRLR)
somatotroph
adipocyte
(ADIPOR1/2)
adipoQ
ADIPOQ
(FGFR1 & KLB)
FGF21
FGF21
IGF1R
IGF
IGF1
i
PRL
prolactin
PRLR
lactotroph
adipocyte
(ADIPOR1/2)
adipoQ
ADIPOQ
j
(POMC & PCSK1/2 & CPE)
ACTH/MSH
MC5R
corticotroph
adipocyte
ADIPOR1
adipoQ
ADIPOQ
(FGFR1 & KLB)
FGF21
FGF21
IGF1R
IGF
IGF1
k
(OXT & CPE)
oxytocin
OXTR
PYY
peptide YY
NPY2R
(SST & PCSK1 & CPE)
somatostatin
SSTR3
(GIP & PCSK1)
GIP
GIPR
entero-endocrine cell (small intestine)
β cell
INSR
insulin
(INS & PCSK1/2 & CPE)
(IGF2R/INSR)
IGF
IGF2
l
ADM2
ADM2
(CALCRL & RMAP2)
PYY
peptide YY
(NPY1R/NPY5R)
entero-endocrine cell (small intestine)
adipocyte
(ADIPOR1/2)
adipoQ
ADIPOQ
(FGFR4 & KLB)
FGF21
FGF21

Fig. 6

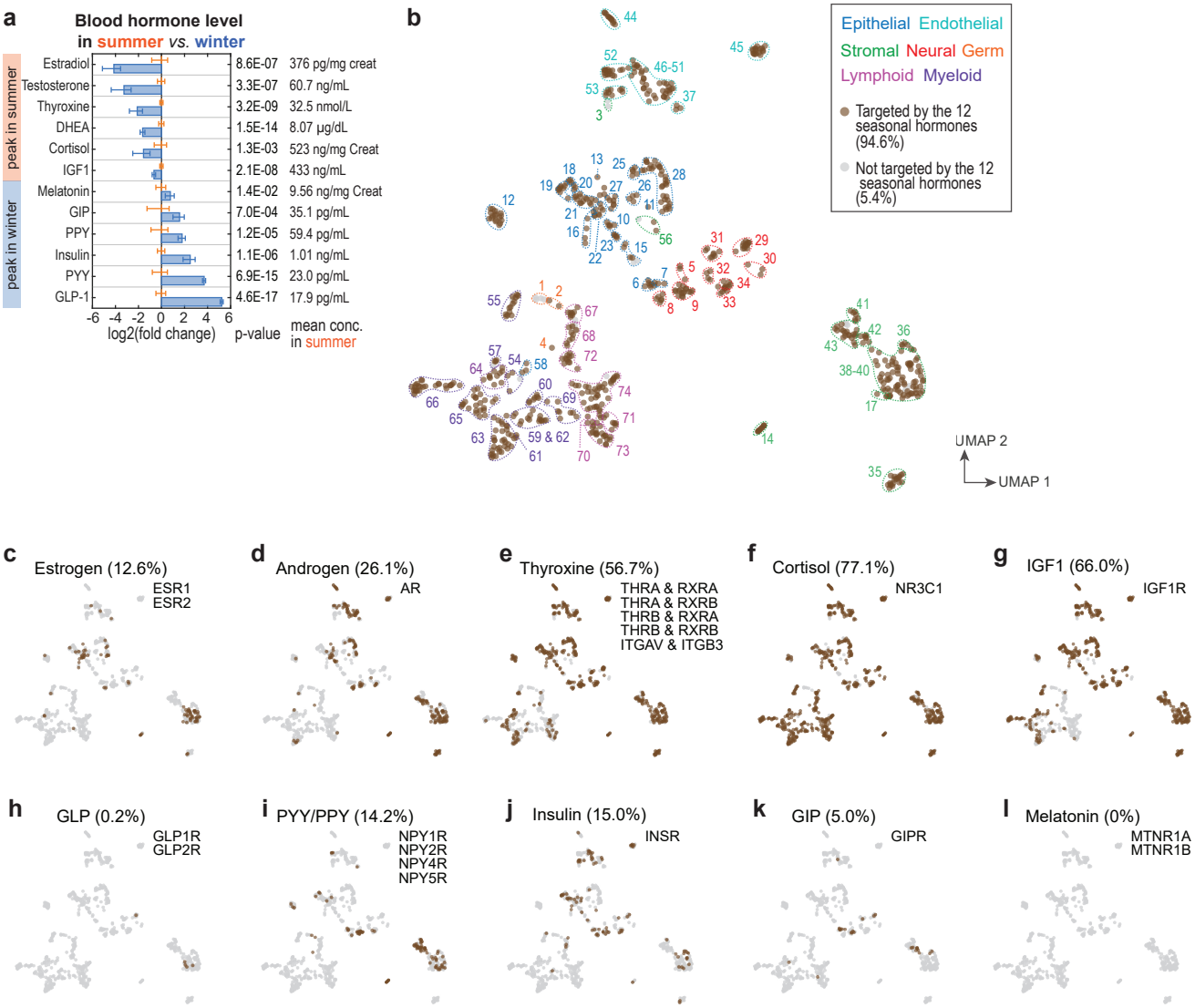
a
Blood hormone level
in summer vs. winter
peak in summer
peak in winter
Estradiol 8.6E-07 376 pg/mg creat
Testosterone 3.3E-07 60.7 ng/mL
Thyroxine 3.2E-09 32.5 nmol/L
DHEA 1.5E-14 8.07 µg/dL
Cortisol 1.3E-03 523 ng/mg Creat
IGF1 2.1E-08 433 ng/mL
Melatonin 1.4E-02 9.56 ng/mg Creat
GIP 7.0E-04 35.1 pg/mL
PPY 1.2E-05 59.4 pg/mL
Insulin 1.1E-06 1.01 ng/mL
PYY 6.9E-15 23.0 pg/mL
GLP-1 4.6E-17 17.9 pg/mL
-6 -4 -2 0 2 4 6
log2(fold change)
p-value
mean conc. in summer
b
Epithelial Endothelial
Stromal Neural Germ
Lymphoid Myeloid
Targeted by the 12 seasonal hormones (94.6%)
Not targeted by the 12 seasonal hormones (5.4%)
UMAP 2
UMAP 1
c Estrogen (12.6%)
ESR1
ESR2
d Androgen (26.1%)
AR
e Thyroxine (56.7%)
THRA & RXRA
THRA & RXRB
THRB & RXRA
THRB & RXRB
ITGAV & ITGB3
f Cortisol (77.1%)
NR3C1
g IGF1 (66.0%)
IGF1R
h GLP (0.2%)
GLP1R
GLP2R
i PYY/PPY (14.2%)
NPY1R
NPY2R
NPY4R
NPY5R
j Insulin (15.0%)
INSR
k GIP (5.0%)
GIPR
l Melatonin (0%)
MTNR1A
MTNR1B

Fig. 7

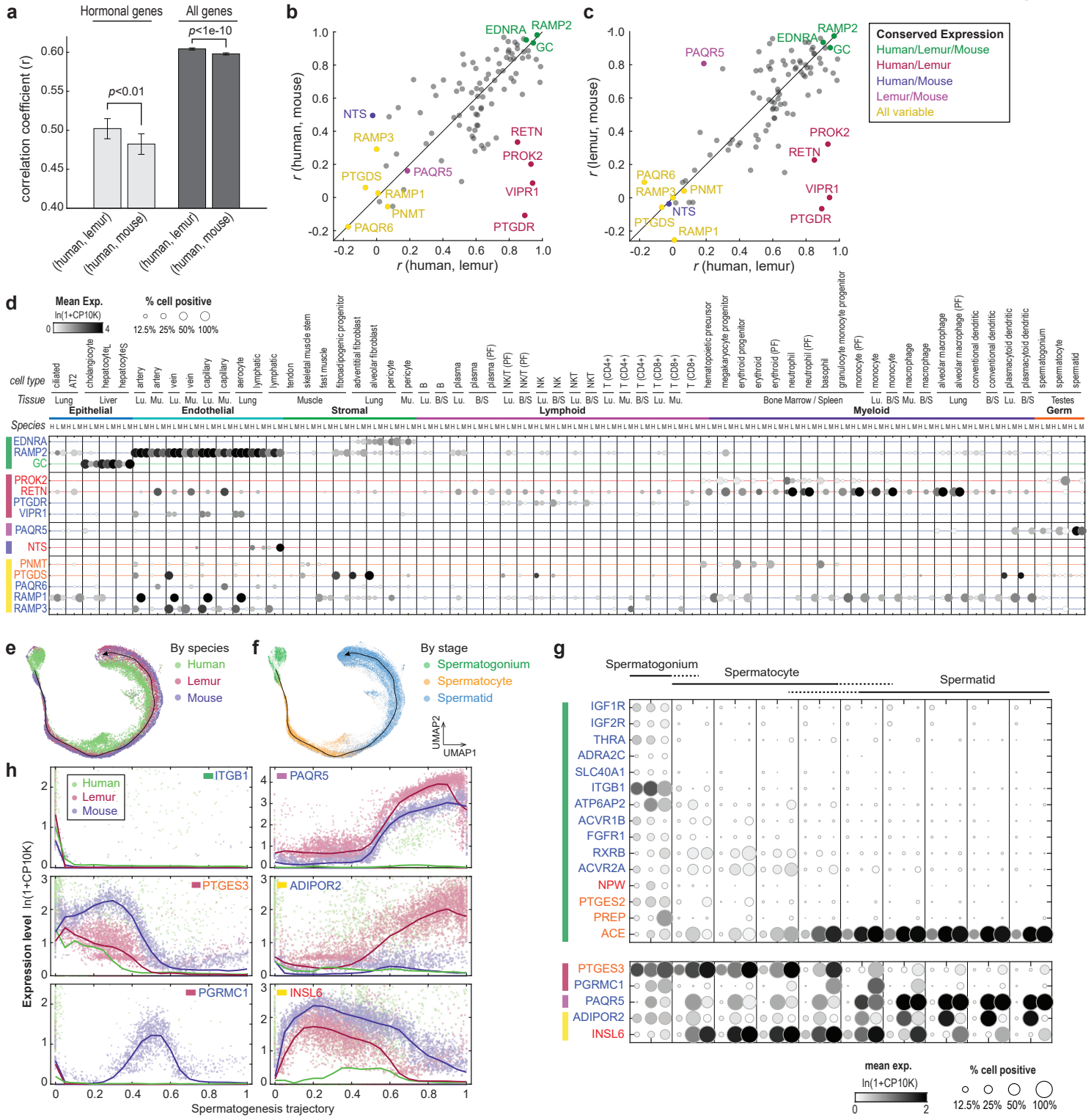
a
Hormonal genes
All genes
p<1e-10
p<0.01
correlation coefficient (r)
(human, lemur)
(human, mouse)
b
r (human, mouse)
r (human, lemur)
EDNRA
RAMP2
GC
NTS
RAMP3
RETN
PROK2
PAQR5
PTGDS
RAMP1
VIPR1
PNMT
PTGDR
PAQR6
c
r (lemur, mouse)
Conserved Expression
Human/Lemur/Mouse
Human/Lemur
Human/Mouse
Lemur/Mouse
All variable
d
Mean Exp.
ln(1+CP10K)
% cell positive
12.5% 25% 50% 100%
cell type
Tissue
Species
Epithelial
Endothelial
Stromal
Lymphoid
Myeloid
Germ
e
By species
Human
Lemur
Mouse
f
By stage
Spermatogonium
Spermatocyte
Spermatid
UMAP2
UMAP1
g
Spermatogonium
Spermatocyte
Spermatid
IGF1R
IGF2R
THRA
ADRA2C
SLC40A1
ITGB1
ATP6AP2
ACVR1B
FGFR1
RXRB
ACVR2A
NPW
PTGES2
PREP
ACE
PTGES3
PGRMC1
PAQR5
ADIPOR2
INSL6
mean exp.
ln(1+CP10K)
% cell positive
12.5% 25% 50% 100%
h
Human
Lemur
Mouse
ITGB1
PAQR5
PTGES3
ADIPOR2
PGRMC1
INSL6
Expression level ln(1+CP10K)
Spermatogenesis trajectory

Fig. S2

a

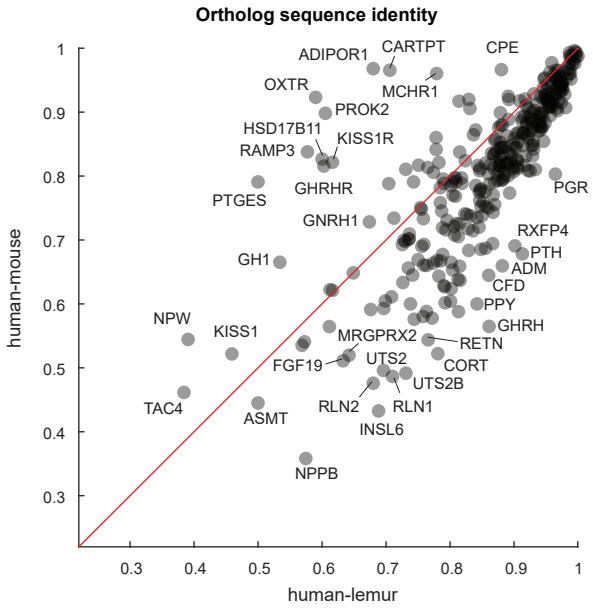
Ortholog sequence identity
human-mouse
human-lemur
ADIPOR1
CARTPT
CPE
OXTR
MCHR1
PROK2
HSD17B11
KISS1R
RAMP3
PTGES
GHRHR
PGR
GNRH1
RXFP4
PTH
GH1
ADM
CFD
PPY
NPW
GHRH
KISS1
MRGPRX2
RETN
FGF19
UTS2
CORT
UTS2B
TAC4
ASMT
RLN2
RLN1
INSL6
NPPB

b

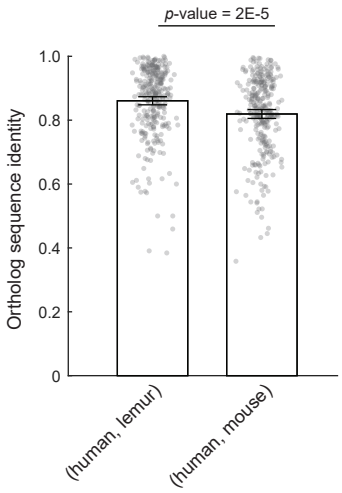
p-value = 2E-5
Ortholog sequence identity
(human, lemur)
(human, mouse)

Fig. S3

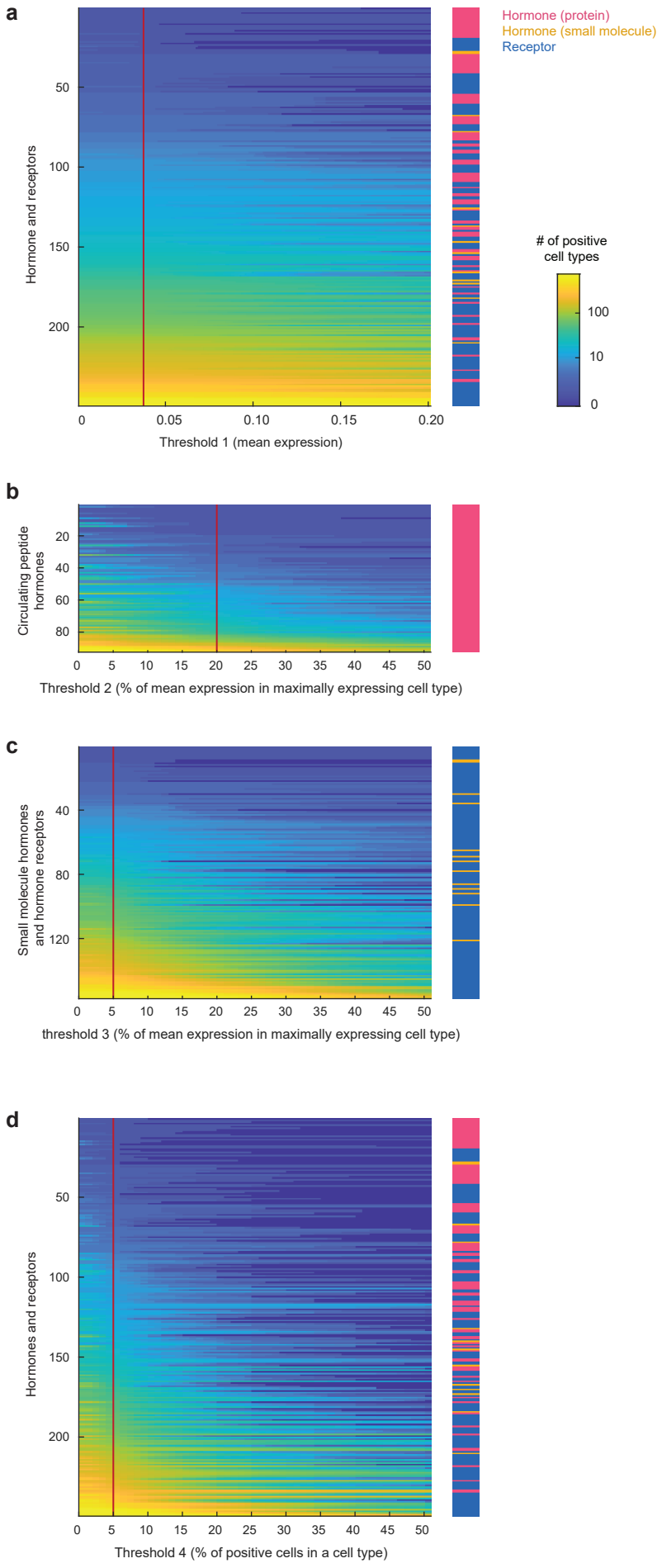
a
Hormone (protein)
Hormone (small molecule)
Receptor
Hormone and receptors
50
100
150
200
0
0.05
0.10
0.15
0.20
Threshold 1 (mean expression)
# of positive cell types
100
10
0
b
Circulating peptide hormones
20
40
60
80
0 5 10 15 20 25 30 35 40 45 50
Threshold 2 (% of mean expression in maximally expressing cell type)
c
Small molecule hormones and hormone receptors
40
80
120
0 5 10 15 20 25 30 35 40 45 50
threshold 3 (% of mean expression in maximally expressing cell type)
d
Hormones and receptors
50
100
150
200
0 5 10 15 20 25 30 35 40 45 50
Threshold 4 (% of positive cells in a cell type)

Fig. S4

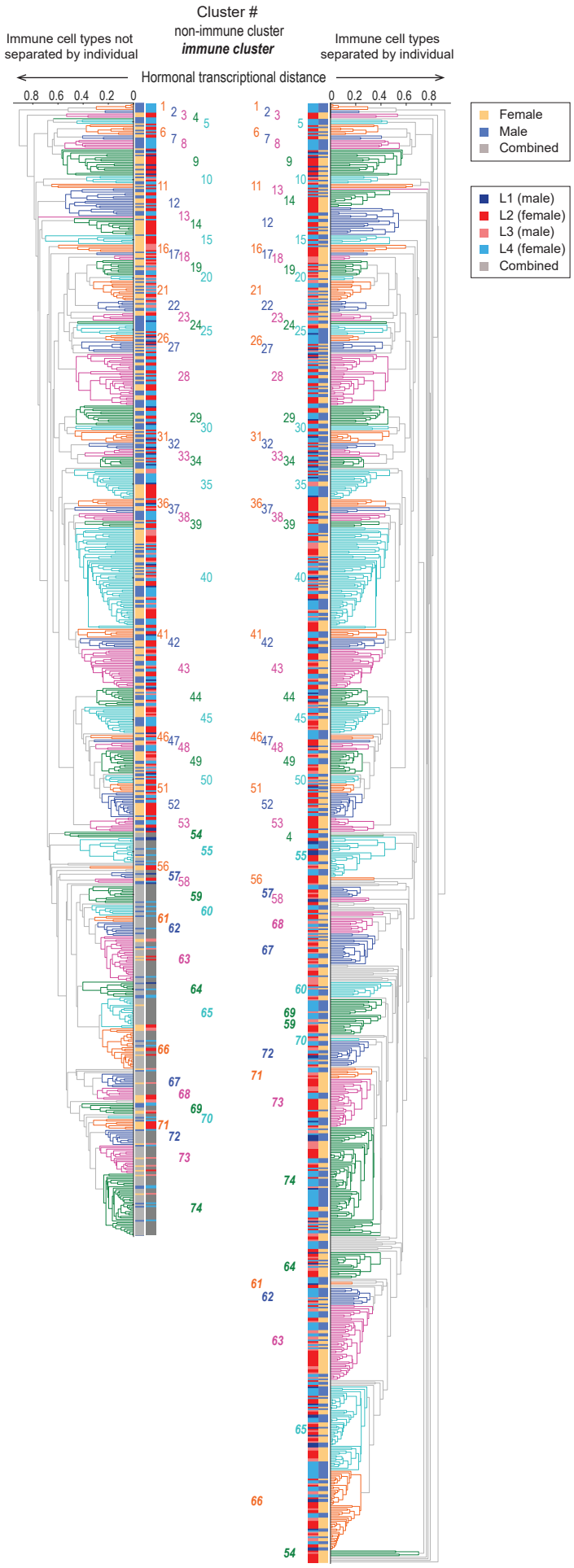
Cluster #
non-immune cluster
immune cluster
Immune cell types not separated by individual
Immune cell types separated by individual
Hormonal transcriptional distance
0.8 0.6 0.4 0.2 0
0 0.2 0.4 0.6 0.8
Female
Male
Combined
L1 (male)
L2 (female)
L3 (male)
L4 (female)
Combined

Fig. S5

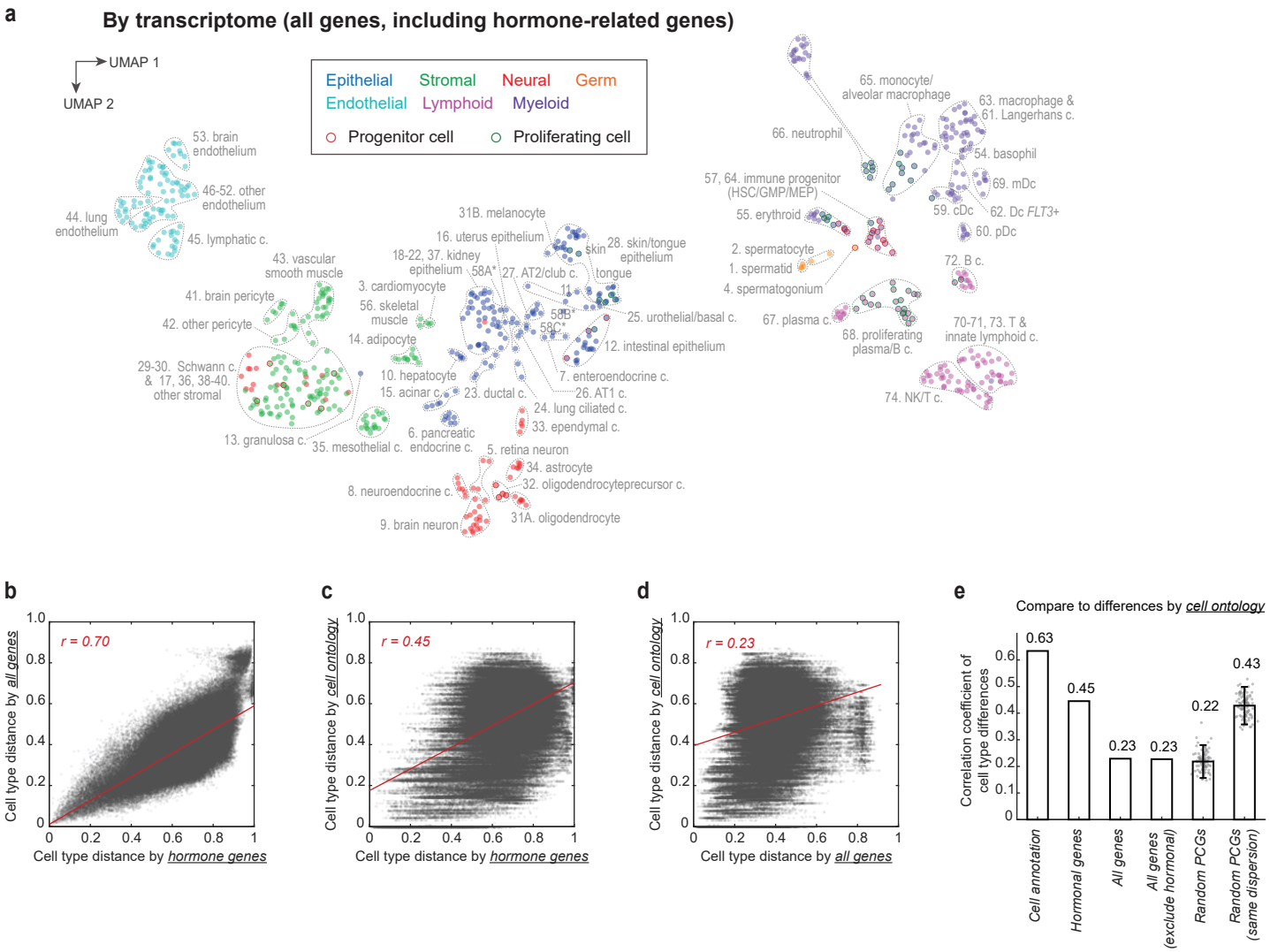
a
By transcriptome (all genes, including hormone-related genes)
UMAP 1
UMAP 2
Epithelial
Stromal
Neural
Germ
Endothelial
Lymphoid
Myeloid
Progenitor cell
Proliferating cell
53. brain endothelium
46-52. other endothelium
44. lung endothelium
45. lymphatic c.
43. vascular smooth muscle
41. brain pericyte
42. other pericyte
29-30. Schwann c. & 17, 36, 38-40. other stromal
13. granulosa c.
35. mesothelial c.
31B. melanocyte
16. uterus epithelium
18-22, 37. kidney epithelium
3. cardiomyocyte
56. skeletal muscle
14. adipocyte
10. hepatocyte
15. acinar c.
6. pancreatic endocrine c.
58A*
27. AT2/club c.
11
58B*
58C*
skin
28. skin/tongue epithelium
tongue
25. urothelial/basal c.
12. intestinal epithelium
7. enteroendocrine c.
26. AT1 c.
23. ductal c.
24. lung ciliated c.
33. ependymal c.
5. retina neuron
34. astrocyte
32. oligodendrocyteprecursor c.
8. neuroendocrine c.
9. brain neuron
31A. oligodendrocyte
65. monocyte/ alveolar macrophage
63. macrophage & 61. Langerhans c.
66. neutrophil
54. basophil
57, 64. immune progenitor (HSC/GMP/MEP)
69. mDc
55. erythroid
59. cDc
62. Dc FLT3+
60. pDc
2. spermatocyte
1. spermatid
4. spermatogonium
72. B c.
67. plasma c.
68. proliferating plasma/B c.
70-71, 73. T & innate lymphoid c.
74. NK/T c.
b
r = 0.70
Cell type distance by all genes
Cell type distance by hormone genes
c
r = 0.45
Cell type distance by cell ontology
Cell type distance by hormone genes
d
r = 0.23
Cell type distance by cell ontology
Cell type distance by all genes
e
Compare to differences by cell ontology
Correlation coefficient of cell type differences
0.63
0.45
0.23
0.23
0.22
0.43
Cell annotation
Hormonal genes
All genes
All genes (exclude hormonal)
Random PCGs
Random PCGs (same dispersion)

Fig. S6

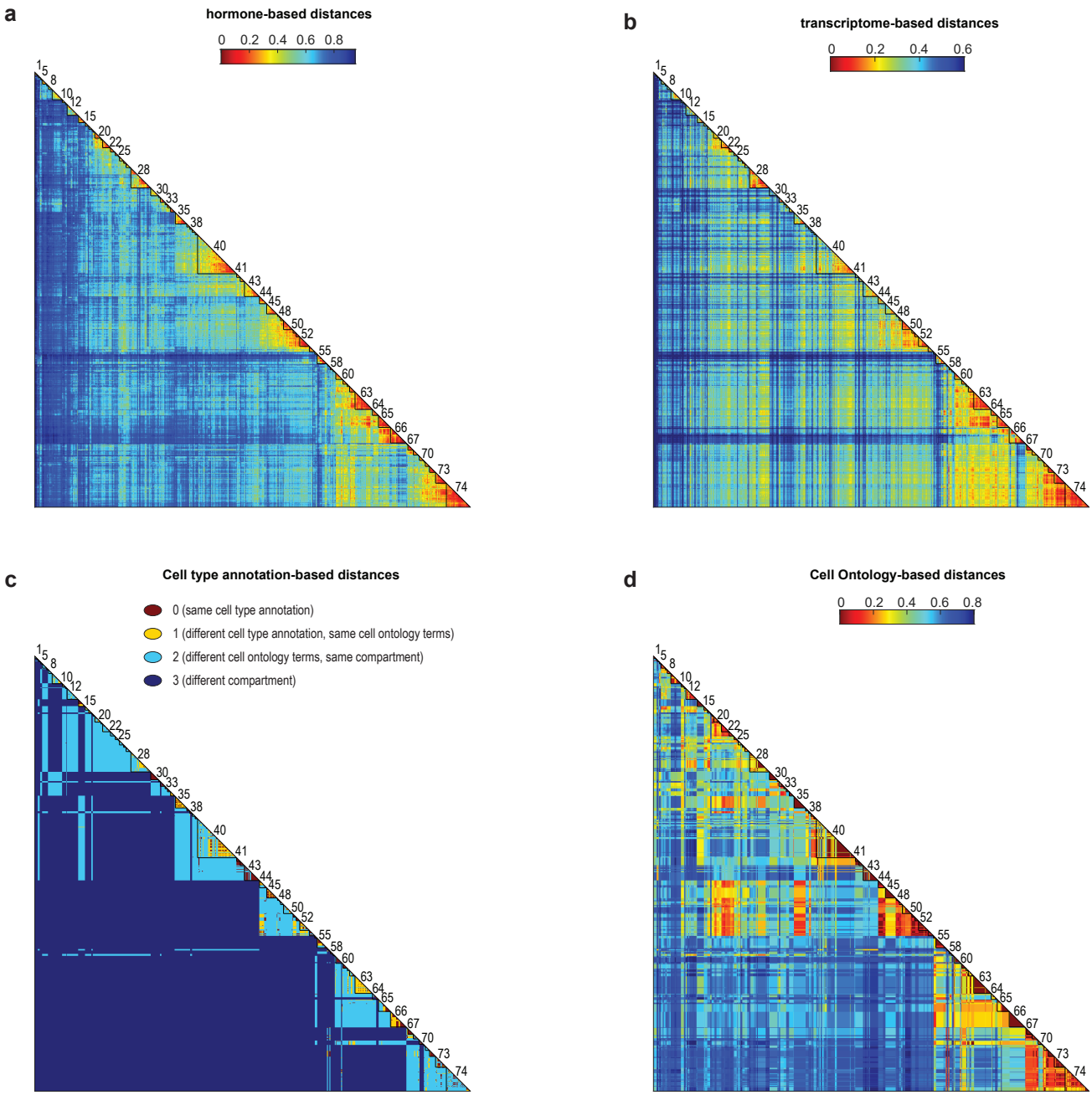
a
hormone-based distances
0 0.2 0.4 0.6 0.8
b
transcriptome-based distances
0 0.2 0.4 0.6
c
Cell type annotation-based distances
0 (same cell type annotation)
1 (different cell type annotation, same cell ontology terms)
2 (different cell ontology terms, same compartment)
3 (different compartment)
d
Cell Ontology-based distances
0 0.2 0.4 0.6 0.8
1 5 8 10 12 15 20 22 25 28 30 33 35 38 40 41 43 44 45 48 50 52 55 58 60 63 64 65 66 67 70 73 74

Fig. S7

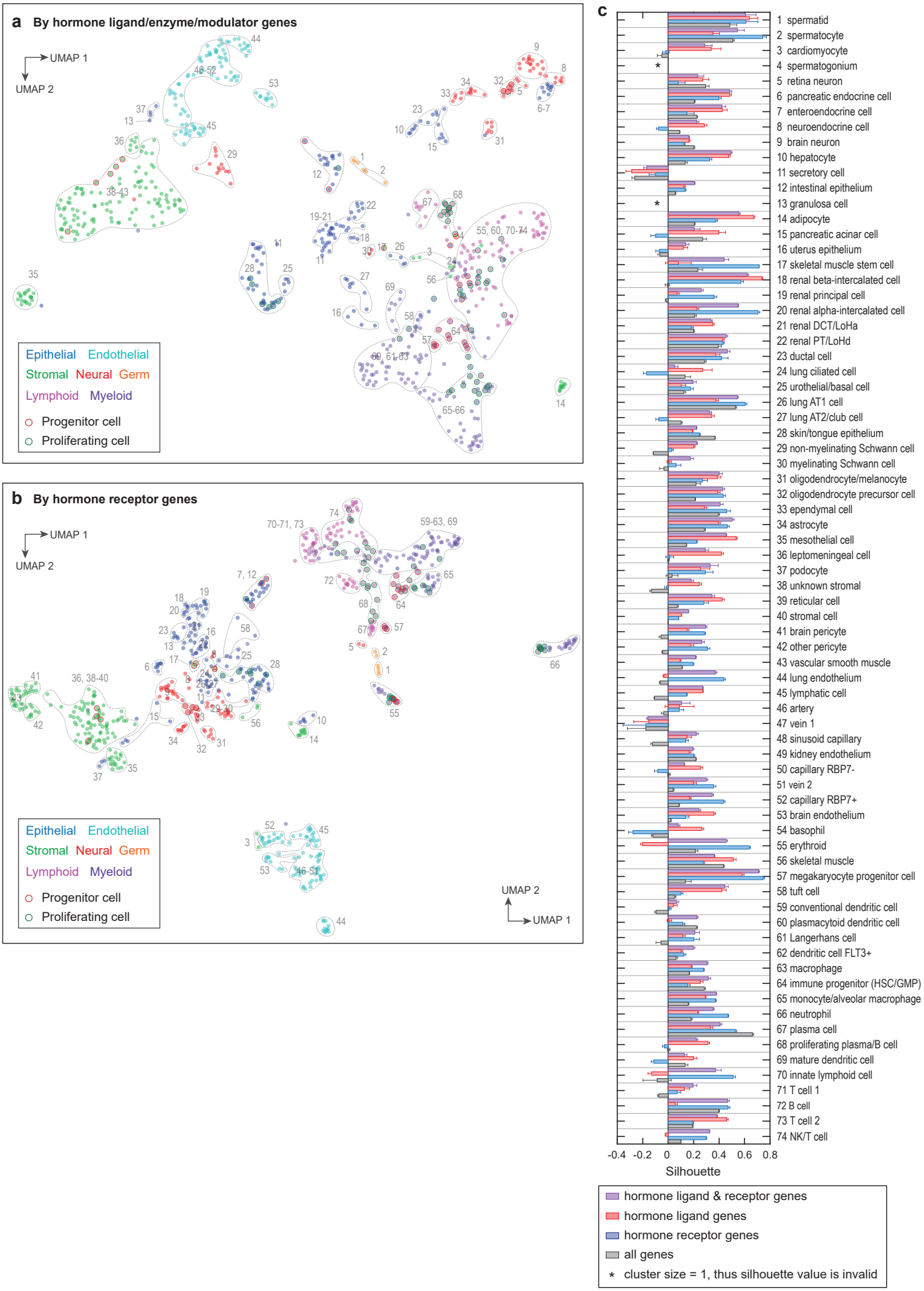
a By hormone ligand/enzyme/modulator genes
UMAP 1
UMAP 2
Epithelial Endothelial
Stromal Neural Germ
Lymphoid Myeloid
Progenitor cell
Proliferating cell
b By hormone receptor genes
UMAP 1
UMAP 2
Epithelial Endothelial
Stromal Neural Germ
Lymphoid Myeloid
Progenitor cell
Proliferating cell
UMAP 2
UMAP 1
c
1 spermatid
2 spermatocyte
3 cardiomyocyte
4 spermatogonium
5 retina neuron
6 pancreatic endocrine cell
7 enteroendocrine cell
8 neuroendocrine cell
9 brain neuron
10 hepatocyte
11 secretory cell
12 intestinal epithelium
13 granulosa cell
14 adipocyte
15 pancreatic acinar cell
16 uterus epithelium
17 skeletal muscle stem cell
18 renal beta-intercalated cell
19 renal principal cell
20 renal alpha-intercalated cell
21 renal DCT/LoHa
22 renal PT/LoHd
23 ductal cell
24 lung ciliated cell
25 urothelial/basal cell
26 lung AT1 cell
27 lung AT2/club cell
28 skin/tongue epithelium
29 non-myelinating Schwann cell
30 myelinating Schwann cell
31 oligodendrocyte/melanocyte
32 oligodendrocyte precursor cell
33 ependymal cell
34 astrocyte
35 mesothelial cell
36 leptomeningeal cell
37 podocyte
38 unknown stromal
39 reticular cell
40 stromal cell
41 brain pericyte
42 other pericyte
43 vascular smooth muscle
44 lung endothelium
45 lymphatic cell
46 artery
47 vein 1
48 sinusoid capillary
49 kidney endothelium
50 capillary RBP7-
51 vein 2
52 capillary RBP7+
53 brain endothelium
54 basophil
55 erythroid
56 skeletal muscle
57 megakaryocyte progenitor cell
58 tuft cell
59 conventional dendritic cell
60 plasmacytoid dendritic cell
61 Langerhans cell
62 dendritic cell FLT3+
63 macrophage
64 immune progenitor (HSC/GMP)
65 monocyte/alveolar macrophage
66 neutrophil
67 plasma cell
68 proliferating plasma/B cell
69 mature dendritic cell
70 innate lymphoid cell
71 T cell 1
72 B cell
73 T cell 2
74 NK/T cell
-0.4 -0.2 0 0.2 0.4 0.6 0.8
Silhouette
hormone ligand & receptor genes
hormone ligand genes
hormone receptor genes
all genes
* cluster size = 1, thus silhouette value is invalid

Fig. S8

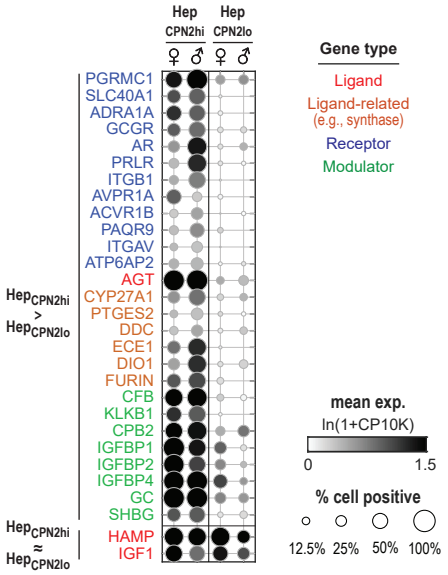
Hep CPN2hi
Hep CPN2lo
♀ ♂ ♀ ♂
PGRMC1
SLC40A1
ADRA1A
GCGR
AR
PRLR
ITGB1
AVPR1A
ACVR1B
PAQR9
ITGAV
ATP6AP2
AGT
CYP27A1
PTGES2
DDC
ECE1
DIO1
FURIN
CFB
KLKB1
CPB2
IGFBP1
IGFBP2
IGFBP4
GC
SHBG
HAMP
IGF1
Hep CPN2hi > Hep CPN2lo
Hep CPN2hi ≈ Hep CPN2lo
Gene type
Ligand
Ligand-related
(e.g., synthase)
Receptor
Modulator
mean exp.
ln(1+CP10K)
0
1.5
% cell positive
12.5%
25%
50%
100%

Fig. S9

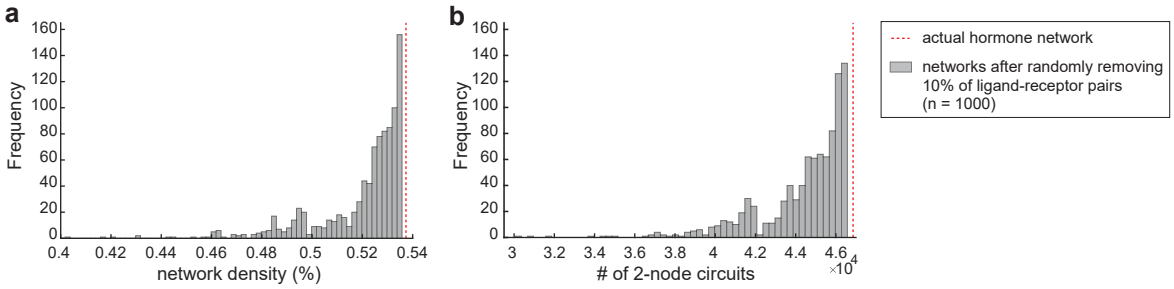
a
Frequency
network density (%)
b
Frequency
# of 2-node circuits
×10^4
actual hormone network
networks after randomly removing 10% of ligand-receptor pairs (n = 1000)

Fig. S10

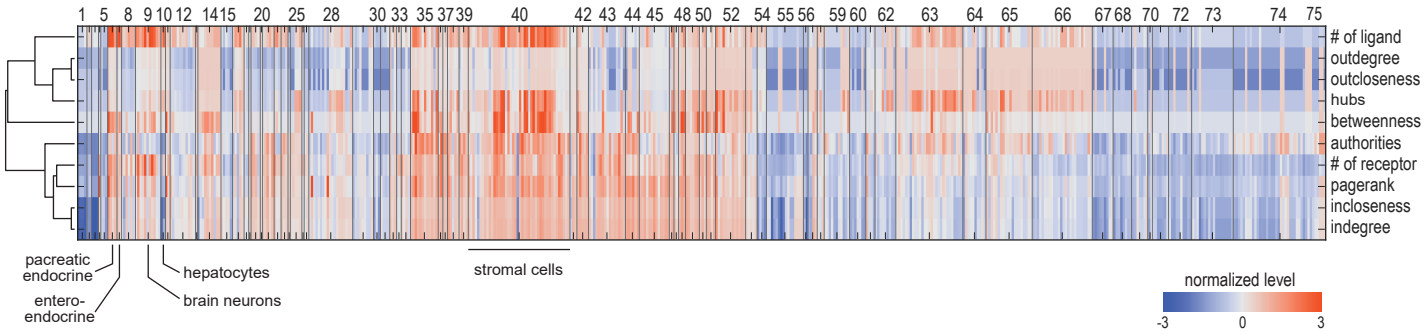
1 5 8 9 10 12 14 15 20 25 28 30 33 35 37 39 40 42 43 44 45 48 50 52 54 55 56 59 60 62 63 64 65 66 67 68 70 72 73 74 75
# of ligand
outdegree
outcloseness
hubs
betweenness
authorities
# of receptor
pagerank
incloseness
indegree
pacreatic endocrine
entero-endocrine
hepatocytes
brain neurons
stromal cells
normalized level
-3
0
3

Fig. S11

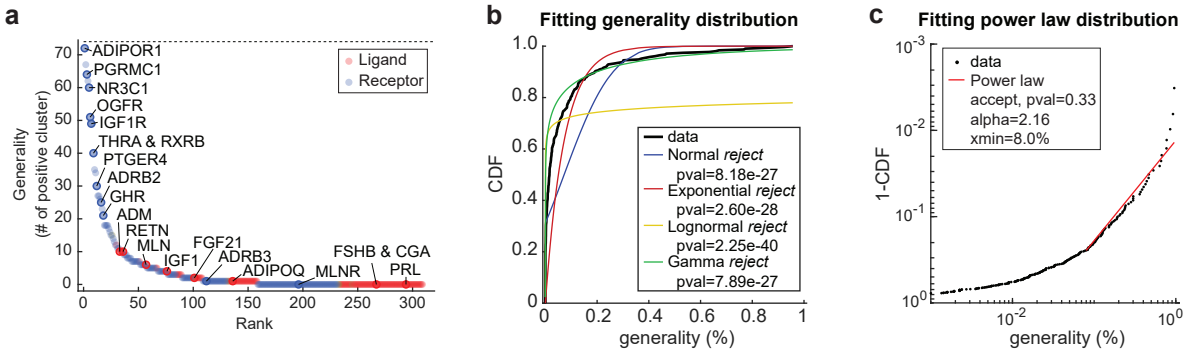
a
Generality
(# of positive cluster)
Rank
Ligand
Receptor
ADIPOR1
PGRMC1
NR3C1
OGFR
IGF1R
THRA & RXRB
PTGER4
ADRB2
GHR
ADM
RETN
MLN
IGF1
FGF21
ADRB3
ADIPOQ
MLNR
FSHB & CGA
PRL
b
Fitting generality distribution
CDF
generality (%)
data
Normal reject
pval=8.18e-27
Exponential reject
pval=2.60e-28
Lognormal reject
pval=2.25e-40
Gamma reject
pval=7.89e-27
c
Fitting power law distribution
1-CDF
generality (%)
data
Power law
accept, pval=0.33
alpha=2.16
xmin=8.0%

Fig. S12

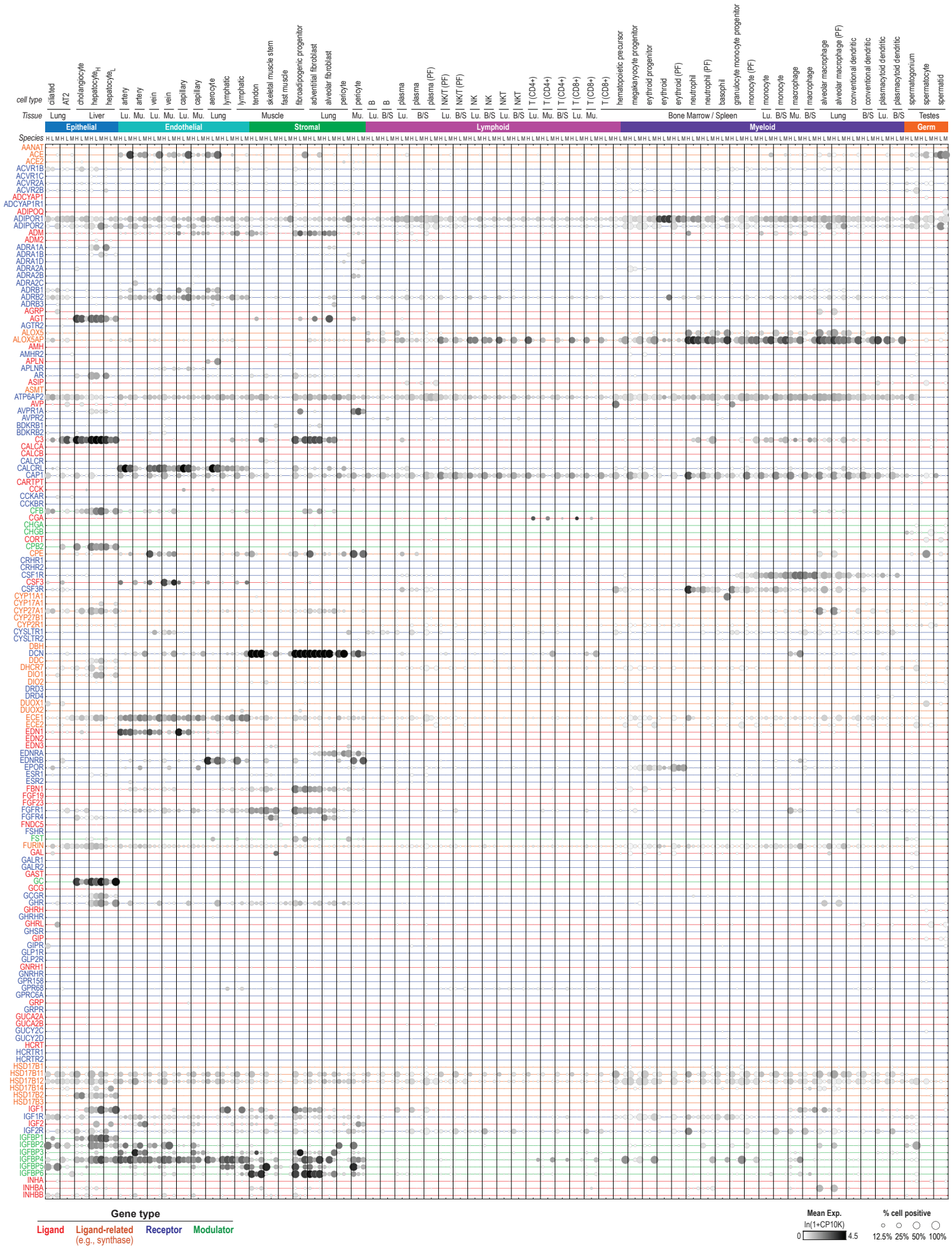
cell type
Tissue
Species
ciliated
AT2
cholangiocyte
hepatocyte
hepatocyte
artery
artery
vein
vein
capillary
capillary
aerocyte
lymphatic
lymphatic
tendon
skeletal muscle stem
fast muscle
fibroadipogenic progenitor
adventitial fibroblast
alveolar fibroblast
pericyte
pericyte
B
B
plasma
plasma
plasma (PF)
NKT (PF)
NKT (PF)
NK
NK
NKT
NKT
T (CD4+)
T (CD4+)
T (CD4+)
T (CD8+)
T (CD8+)
T (CD8+)
hematopoietic precursor
megakaryocyte progenitor
erythroid progenitor
erythroid
erythroid (PF)
neutrophil
neutrophil (PF)
basophil
granulocyte monocyte progenitor
monocyte (PF)
monocyte
monocyte
macrophage
macrophage
alveolar macrophage
alveolar macrophage (PF)
conventional dendritic
conventional dendritic
plasmacytoid dendritic
plasmacytoid dendritic
spermatogonium
spermatocyte
spermatid
Lung
Liver
Lu.
Mu.
Lung
Muscle
Lung
Mu.
Lu.
B/S
Lu.
B/S
Lu.
B/S
Lu.
B/S
Lu.
Mu.
B/S
Lu.
Mu.
Bone Marrow / Spleen
Lu.
B/S
Mu.
B/S
Lung
B/S
Lu.
B/S
Testes
Epithelial
Endothelial
Stromal
Lymphoid
Myeloid
Germ
AANAT
ACE
ACE2
ACVR1B
ACVR1C
ACVR2A
ACVR2B
ADCYAP1
ADCYAP1R1
ADIPOQ
ADIPOR1
ADIPOR2
ADM
ADM2
ADRA1A
ADRA1B
ADRA1D
ADRA2A
ADRA2B
ADRA2C
ADRB1
ADRB2
ADRB3
AGRP
AGT
AGTR2
ALOX5
ALOX5AP
AMH
AMHR2
APLN
APLNR
AR
ASIP
ASMT
ATP6AP2
AVP
AVPR1A
AVPR2
BDKRB1
BDKRB2
C3
CALCA
CALCB
CALCR
CALCRL
CAP1
CARTPT
CCK
CCKAR
CCKBR
CFB
CGA
CHGA
CHGB
CORT
CPB2
CPE
CRHR1
CRHR2
CSF1R
CSF3
CSF3R
CYP11A1
CYP17A1
CYP27A1
CYP27B1
CYP2R1
CYSLTR1
CYSLTR2
DBH
DCN
DDC
DHCR7
DIO1
DIO2
DRD3
DRD4
DUOX1
DUOX2
ECE1
ECE2
EDN1
EDN2
EDN3
EDNRA
EDNRB
EPOR
ESR1
ESR2
FBN1
FGF19
FGF23
FGFR1
FGFR4
FNDC5
FSHR
FST
FURIN
GAL
GALR1
GALR2
GAST
GC
GCG
GCGR
GHR
GHRH
GHRHR
GHRL
GHSR
GIP
GIPR
GLP1R
GLP2R
GNRH1
GNRHR
GPR156
GPR68
GPRC6A
GRP
GRPR
GUCA2A
GUCA2B
GUCY2C
GUCY2D
HCRT
HCRTR1
HCRTR2
HSD17B1
HSD17B11
HSD17B12
HSD17B14
HSD17B2
HSD17B3
IGF1
IGF1R
IGF2
IGF2R
IGFBP1
IGFBP2
IGFBP3
IGFBP4
IGFBP5
IGFBP6
INHA
INHBA
INHBB
Gene type
Ligand
Ligand-related
(e.g., synthase)
Receptor
Modulator
Mean Exp.
ln(1+CP10K)
0
4.5
% cell positive
12.5%
25%
50%
100%

Fig. S12 - continued

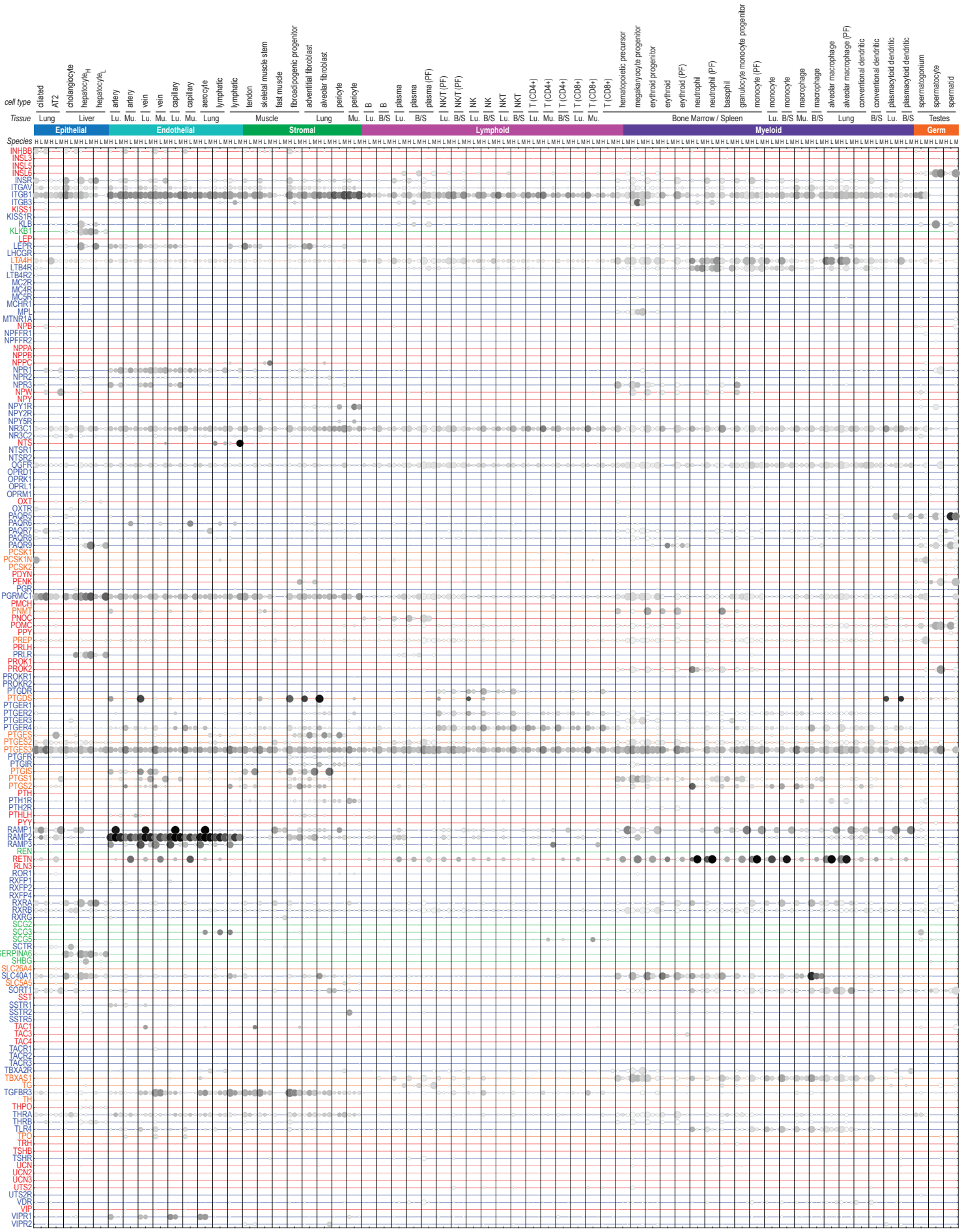
cell type
ciliated
AT2
cholangiocyte
hepatocyte H
hepatocyte L
artery
artery
vein
vein
capillary
capillary
aerocyte
lymphatic
lymphatic
tendon
skeletal muscle stem
fast muscle
fibroadipogenic progenitor
adventitial fibroblast
alveolar fibroblast
pericyte
pericyte
B
B
plasma
plasma
plasma (PF)
NKT (PF)
NKT (PF)
NK
NK
NKT
NKT
T (CD4+)
T (CD4+)
T (CD4+)
T (CD8+)
T (CD8+)
T (CD8+)
hematopoietic precursor
megakaryocyte progenitor
erythroid progenitor
erythroid
erythroid (PF)
neutrophil
neutrophil (PF)
basophil
granulocyte monocyte progenitor
monocyte (PF)
monocyte
monocyte
macrophage
macrophage
alveolar macrophage
alveolar macrophage (PF)
conventional dendritic
conventional dendritic
plasmacytoid dendritic
plasmacytoid dendritic
spermatogonium
spermatocyte
spermatid
Tissue
Lung
Liver
Lu.
Mu.
Lu.
Mu.
Lu.
Mu.
Lung
Muscle
Lung
Mu.
Lu.
B/S
Lu.
B/S
Lu.
B/S
Lu.
B/S
Lu.
Mu.
B/S
Lu.
Mu.
Bone Marrow / Spleen
Lu.
B/S
Mu.
B/S
Lung
B/S
Lu.
B/S
Testes
Epithelial
Endothelial
Stromal
Lymphoid
Myeloid
Germ
Species
H L M H L M H L M

Fig. S13

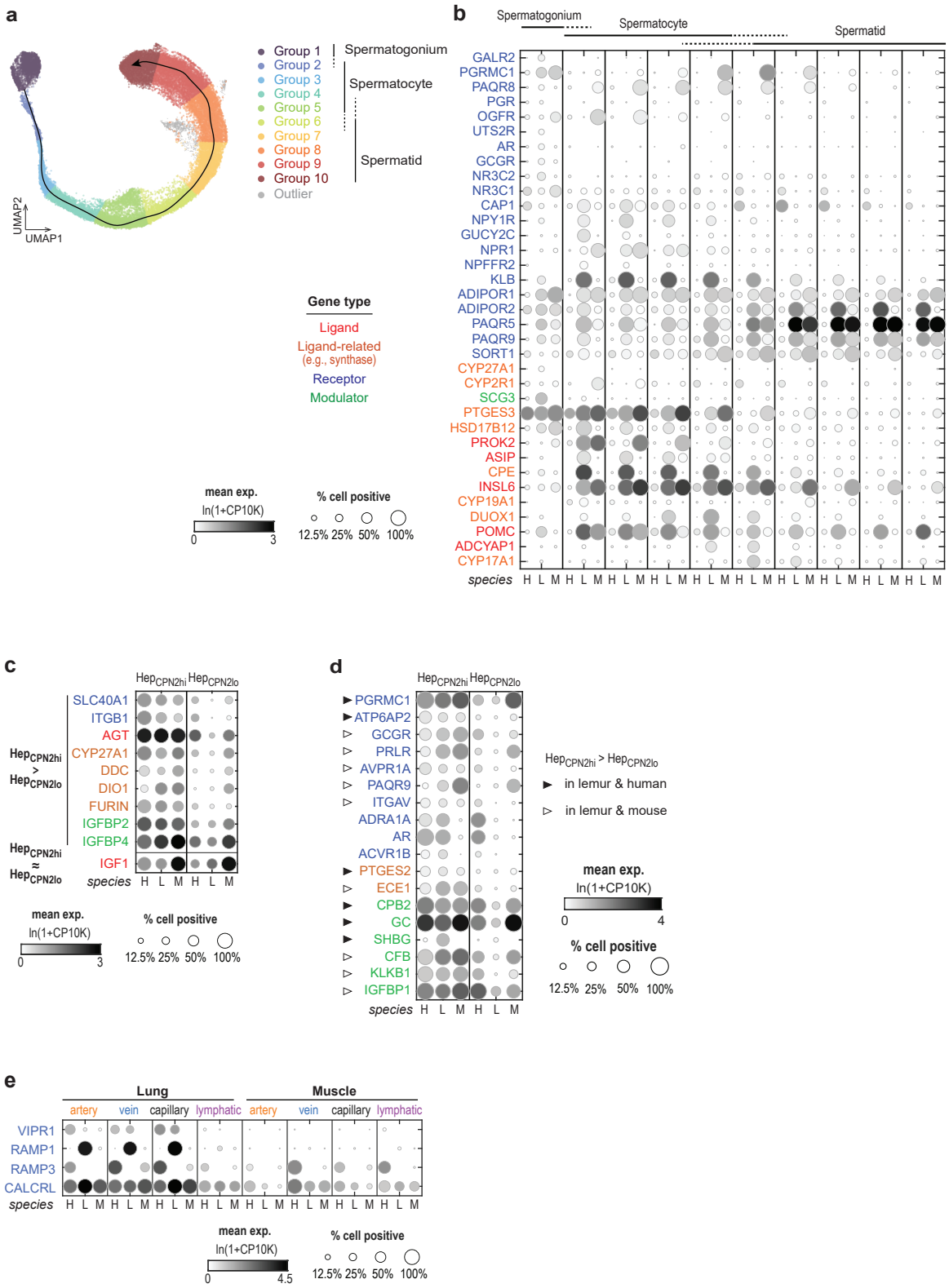
a
UMAP2
UMAP1
Group 1
Group 2
Group 3
Group 4
Group 5
Group 6
Group 7
Group 8
Group 9
Group 10
Outlier
Spermatogonium
Spermatocyte
Spermatid
Gene type
Ligand
Ligand-related (e.g., synthase)
Receptor
Modulator
mean exp.
ln(1+CP10K)
0
3
% cell positive
12.5% 25% 50% 100%
b
Spermatogonium
Spermatocyte
Spermatid
GALR2
PGRMC1
PAQR8
PGR
OGFR
UTS2R
AR
GCGR
NR3C2
NR3C1
CAP1
NPY1R
GUCY2C
NPR1
NPFFR2
KLB
ADIPOR1
ADIPOR2
PAQR5
PAQR9
SORT1
CYP27A1
CYP2R1
SCG3
PTGES3
HSD17B12
PROK2
ASIP
CPE
INSL6
CYP19A1
DUOX1
POMC
ADCYAP1
CYP17A1
species H L M H L M H L M H L M H L M H L M H L M H L M H L M H L M H L M
c
HepCPN2hi HepCPN2lo
SLC40A1
ITGB1
AGT
CYP27A1
DDC
DIO1
FURIN
IGFBP2
IGFBP4
IGF1
HepCPN2hi > HepCPN2lo
HepCPN2hi ≈ HepCPN2lo
species H L M H L M
mean exp.
ln(1+CP10K)
0
3
% cell positive
12.5% 25% 50% 100%
d
HepCPN2hi HepCPN2lo
PGRMC1
ATP6AP2
GCGR
PRLR
AVPR1A
PAQR9
ITGAV
ADRA1A
AR
ACVR1B
PTGES2
ECE1
CPB2
GC
SHBG
CFB
KLKB1
IGFBP1
species H L M H L M
HepCPN2hi > HepCPN2lo
in lemur & human
in lemur & mouse
mean exp.
ln(1+CP10K)
0
4
% cell positive
12.5% 25% 50% 100%
e
Lung
Muscle
artery vein capillary lymphatic artery vein capillary lymphatic
VIPR1
RAMP1
RAMP3
CALCRL
species H L M H L M H L M H L M H L M H L M H L M H L M H L M
mean exp.
ln(1+CP10K)
0
4.5
% cell positive
12.5% 25% 50% 100%